



PHD

**Adhesion of ethylene vinyl acetate copolymers to metals.**

Hatzinikolaou, Theodosios A.

*Award date:*  
1985

*Awarding institution:*  
University of Bath

[Link to publication](#)

## Alternative formats

If you require this document in an alternative format, please contact:  
[openaccess@bath.ac.uk](mailto:openaccess@bath.ac.uk)

### General rights

Copyright and moral rights for the publications made accessible in the public portal are retained by the authors and/or other copyright owners and it is a condition of accessing publications that users recognise and abide by the legal requirements associated with these rights.

- Users may download and print one copy of any publication from the public portal for the purpose of private study or research.
- You may not further distribute the material or use it for any profit-making activity or commercial gain
- You may freely distribute the URL identifying the publication in the public portal ?

### Take down policy

If you believe that this document breaches copyright please contact us providing details, and we will remove access to the work immediately and investigate your claim.

ADHESION OF ETHYLENE VINYL ACETATE

COPOLYMERS TO METALS

Submitted by:

THEODOSIOS A. HATZINIKOLAOU

for the Degree of Ph.D. of the  
University of Bath

JULY 1985

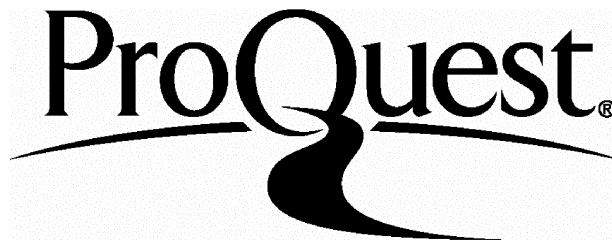
ProQuest Number: U365456

All rights reserved

INFORMATION TO ALL USERS

The quality of this reproduction is dependent upon the quality of the copy submitted.

In the unlikely event that the author did not send a complete manuscript and there are missing pages, these will be noted. Also, if material had to be removed, a note will indicate the deletion.



ProQuest U365456

Published by ProQuest LLC(2015). Copyright of the Dissertation is held by the Author.

All rights reserved.

This work is protected against unauthorized copying under Title 17, United States Code.  
Microform Edition © ProQuest LLC.

ProQuest LLC  
789 East Eisenhower Parkway  
P.O. Box 1346  
Ann Arbor, MI 48106-1346

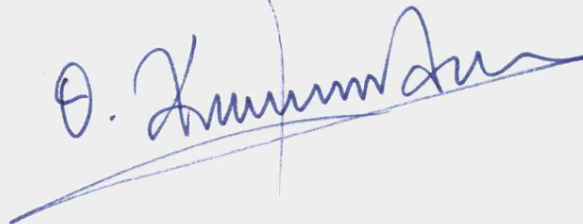
COPYRIGHT

"Attention is drawn to the fact that copyright of this thesis rests with its author. This copy of the thesis has been supplied on condition that anyone who consults it is understood to recognise that its copyright rests with its author and that no quotation from the thesis and no information derived from it may be published without the prior written consent of the author."

RESTRICTIONS

"This thesis may be made available for consultation within the University Library and may be photocopied or lent to other libraries for the purpose of consultation."

THE AUTHOR



## ACKNOWLEDGEMENTS

The author would like to thank Dr David E Packham for his support and many helpful discussions.

Thanks are also due to Miss S Gregory and Miss D Tzavella for their help and patience with the typing and the presentation of this thesis.

Finally, the author gratefully acknowledges the provision of a research studentship by the University of Bath Research Fund and of the electron optical facilities by the SERC.

To my parents .....

## SUMMARY

The 180° peel strength of four ethylene vinyl acetate copolymers with varying V.A. content was measured (Pol A: 28%, Pol B: 18%, Pol C: 12% and Pol D: 9.5% by weight). The polymers were applied as hot-melts with or without an inextensible fabric support on:

- (a) mild steel etched in hydrochloric acid;
- (b) chemically polished copper and;
- (c) oxidised copper with a fibrous topography.

The peel loads for a given polymer decreased from oxidised copper to etched steel to polished copper. For a given substrate the peel loads generally decreased from polymer A to polymer D with a peak for polymer C. This trend was correlated to similar trends obtained in mechanical tests like the tearing energy, strain energy density and tensile strength to failure.

The fractured parts of the bond were examined with a scanning electron microscope. There was microscopic evidence of an analogy between the peel load and the observed extent of polymer deformation in the fractured surfaces where the ductility of the particular polymer and the topography of the substrate were clearly depicted.

Contact angle measurement showed a cohesive type of failure in all cases. X-ray photo-electron spectroscopy and multiple internal reflection infra-red spectroscopy provided evidence of polymer oxidation by the substrate, mostly significant in the case of etched steel.

The energy balance approach was employed in order to analyse the peel test results further. The polymers response to the imposed mechanical deformations during peeling was shown to control the measured peel load. For the unbacked samples the major energy loss mechanism is the stretching of the freed strip. The much higher peel loads of the backed samples were attributed to energy losses around the peel front. Finally, plastic bending of the polymer was found to account for a relatively smaller part of the total input energy for both backed and unbacked samples.



## CONTENTS

	<u>Page</u>
<b><u>CHAPTER 1: INTRODUCTION</u></b>	
1.1	General introduction ..... 1
1.2	Theories of adhesion ..... 5
1.3	E.V.A. copolymers as hot-melt adhesives ..... 17
1.3.1	Hot-melt adhesives in general ..... 17
1.3.2	History and application of E.V.A. copolymers ..... 17
1.3.3	Structure and property relationships in E.V.A. copolymers ..... 19
1.3.4	Adhesion of E.V.A. coatings ..... 21
1.3.5	Objectives of the research project ..... 23
<b><u>CHAPTER 2: PEEL TESTING OF POLYMERIC COATINGS</u></b>	
2.1	Introduction ..... 26
2.2	Stress analysis of the peel test ..... 28
2.3	The energy balance approach to the peel test ..... 34
2.4	Conclusions ..... 48
<b><u>CHAPTER 3: MATERIALS AND METHODS</u></b>	
3.1	Polymers ..... 50
3.1.1	Quantitative determination of vinyl-acetate content in E.V.A. copolymer ..... 51
3.1.2	Crystallinity of E.V.A. copolymers ..... 63
3.1.3	Melt flow index of E.V.A. copolymers ..... 68
3.1.4	Molecular weight of E.V.A. copolymers ..... 70
3.2	Metals ..... 72
3.3	Preparation of test samples ..... 74
3.3.1	Metal preparation ..... 74
3.3.2	Preparation of coatings ..... 78
3.3.3	Adhesion test ..... 78

	<u>Page</u>
<b><u>CHAPTER 4: RESULTS OF THE PEEL TEST</u></b>	
4.1 Peel load of unbacked samples .....	79
4.2 Peel load of backed samples .....	79
4.3 Effect of polymer thickness .....	80
<b><u>CHAPTER 5: MECHANICAL TESTING OF E.V.A. COPOLYMERS</u></b>	
5.1 Introduction .....	91
5.2 Tensile properties .....	93
5.3 Tear strength of E.V.A. copolymers .....	105
5.4 One cycle loading .....	111
<b><u>CHAPTER 6: INTERFACIAL INVESTIGATIONS</u></b>	
6.1 Surface analytical techniques in adhesion .....	115
6.1.1 Introduction .....	115
6.1.2 Microscopic methods in fractography .....	116
6.1.3 Spectroscopic methods in fractography .....	121
6.1.4 Conclusions .....	128
6.2 Examination of fractured surfaces .....	130
6.2.1 Residual polymer after peeling .....	130
6.2.2 Scanning electron microscopy .....	142
6.2.3 Chemical changes at the interface .....	155
<b><u>CHAPTER 7: ENERGY DISSIPATION</u></b>	
7.1 The energy of separation .....	164
7.2 Thermodynamic work of cohesion $W_c$ .....	168
7.3 Energy losses in stretching the peeling strip .....	171
7.4 Energy losses due to plastic bending .....	179
7.5 Independent measurement of $W_b$ .....	187
7.6 Other loss mechanisms .....	190

	<u>Page</u>
7.7	Synthesis of the energy dissipation terms ..... 194

CHAPTER 8: DISCUSSION AND CONCLUSIONS

8.1	Effect of substrate on the peel load ..... 199
8.2	Effect of backing on the peel load ..... 206
8.3	Effect of polymer on the peel load ..... 207
8.4	Conclusions ..... 212

REFERENCES

## CHAPTER 1

### INTRODUCTION

#### 1.1 GENERAL INTRODUCTION:

An adhesive is a substance capable of holding two materials together and adhesion as a phenomenon has been noted by man very early.

Since a few decades ago our understanding of adhesion was limited and the application and use of adhesives was based on art rather than science. That is reflected in the relatively sparse literature until the 1950's which indicates little interest in the field. The massive growth in the production of synthetic polymers together with the increasing demand from technologists for stronger adhesives focused interest on the phenomenon of adhesion.

To understand the process of sticking things together is not simple. Any real surface is usually covered by sorbed moisture. In addition to that, a metal surface may be covered by a weak oxide layer and other contaminants eg rolling lubricants. To achieve good adhesion these layers must be removed. The adhesive is then applied, usually in liquid state. The requirement now is good wetting which ensures the maximum contact area between the adhesive and the substrate together with the appropriate flow properties so that it fills pores and irregularities on the substrate. When the adhesive is setting by cooling, solvent evaporation or chemical reaction, the chemical

and mechanical properties of the adhesive close to the interface may become different from those in the bulk. That change could weaken or strengthen the adhesive bond by processes close to the interface like orientation of polar molecules, formation of crystal structure or precipitation of additives.

To understand the above phenomena adequately the adhesives scientist is required to be familiar with such diverse subjects as metallurgy, physical chemistry, rheology and polymer science.

After the formation of the bond follows the evaluation of the adhesive. That is usually done by pulling the two parts of the bond apart by force. Destructive testing of an adhesive joint is expected to give directly its strength and that involves spending all the measured energy in fracturing its members. It is found in practice that part of that energy deforms the substrate or the bulk of the adhesive and so is not truly the adhesional failure energy. So, processes that consume part of this energy must be taken into account and be eliminated. Understanding the fracture mechanisms during any destructive adhesive testing becomes therefore vital and that is an area where an engineer can contribute.

Another fundamental question which must be answered in order to establish the mechanism of adhesion is the path that the fracture plane is following. Failure may occur through or between any of the phases shown schematically in fig (1-1). The fractured parts

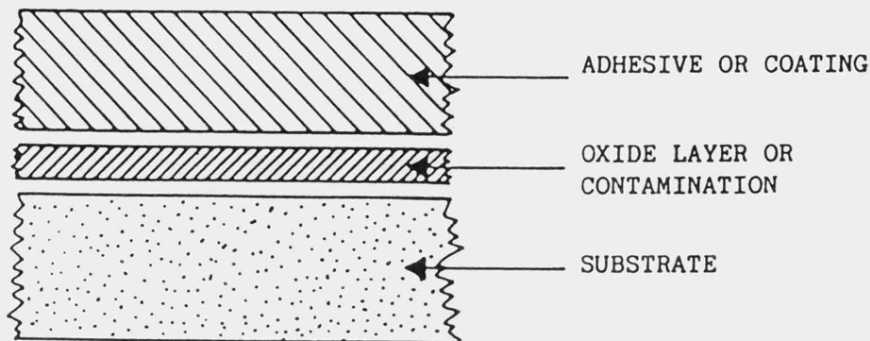


FIGURE 1-1: Phases commonly found in an adhesive bond.

of a bond can be examined after debonding by a variety of surface analytical techniques. Each one of these techniques provides different kind of information about the locus of failure, the chemical composition, morphology and structure of the fractured surfaces. In addition to determining the elements that exist on these surfaces it is useful to look at them using optical microscopy and scanning electron microscopy. When failure is cohesive the plastic or brittle mechanism can be distinguished and understood, especially for polymeric adherends. Also, the existence of voids, flaws or other features at the interface can be observed and related to the bond strength.

One system providing a suitable model to investigate the above mentioned problems is a polymeric coating bonded to a metal

substrate. Such systems have been studied extensively not only as theoretical models but also for their practical applications. To understand the prime cause of adhesion in a polymer/metal system the origin of the forces across the interface must be defined. Therefore, the current views about the adhesional forces that hold the two materials together in such a system are discussed in the following section.

## 1.2 THEORIES OF ADHESION

There is still some controversy about the cause of the adhesional forces across an interface. Many theories can be found in the literature but a universal theory of adhesion is not yet available. This is mainly due to our inability to measure interfacial interactions directly, so the need arises for a test method. Consequently, some imposed experimental factors like the test geometry and loading mode are introduced and the analysis becomes more complex. So, it seems that we can obtain information about the magnitude of interfacial forces only indirectly ie by analysing results from adhesive tests, and that could lead to confusion.

However, four main mechanisms of adhesion have been proposed and accepted contributing to a better understanding of the phenomenon; diffusion theory, electrical theory, absorption theory and mechanical theory.

The diffusion theory of adhesion was proposed by Voyutskii (1) and Vasenin (2) and is essentially applied to high polymers. The concept of the theory is that almost all cases of adhesion arise from mutual interdiffusion of macromolecules across the interface. If two polymers have similar solubility parameters and are brought to contact for sufficient time interpenetration of molecules or molecular segments can occur giving rise to adhesional forces. The diffusion theory therefore is the generally accepted mechanism



in adhesion processes like autohesion, heat sealing of thermoplastics, solvent welding and formation of films from latices. It is however unlikely that this theory can explain the adhesion of polymers to metals.

The electrostatic theory of adhesion was developed by Deryaguin and his co-workers (3) (4). According to the electrostatic theory, adhesion between the adhesive and the substrate is due to electrostatic forces arising from a double layer of electrical charge formed at the interface when the two materials come in contact (fig 1-2).

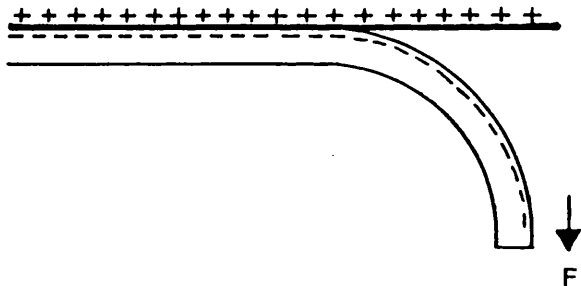


FIGURE 1-2: Electrostatic double layer formed when peeling polymer films from solids.

The electrostatic theory in effect treats the adhesive/substrate system as a capacitor in which the separation of its two parts is

accompanied by discharge. There were cases where the contribution of the electrostatic double layer forces to adhesion was clearly demonstrated (5) (6). It is difficult however for this theory to explain adequately the primary cause of adhesion between a polymer and a metal; Roberts (7) studied such a system and provided evidence showing an enormous difference between the measured peel energy and the maximum calculated electrostatic energy. In addition, the rate dependence of the peel test cannot be related to the electrical energy of the capacitor calculated by Deryaguin (8).

The mechanical theory proposes that adhesion is achieved by the penetration of the liquid or viscous adhesive into the pores or irregularities of the substrate followed by hardening of the adhesive. This phenomenon of "mechanical interlocking" was first reported by McBain and Hopkins (9) many years ago. Since then, the contribution of this mechanism to adhesive bonding has been demonstrated in certain cases like the adhesion of polymers to textiles (10), leather (11) and in metal plating of acrylonitrile-butadiene-styrene polymer. In all the above cases improved adhesion was observed after the substrates were roughened. Generally if a surface treatment increases the roughness, extra contact area becomes available which ought to improve adhesion. Furthermore, stress concentrations around unfilled voids at the interface may have a beneficial effect. Roughening may also look effective because it removes surface impurities, or because it improves the wetting kinetics of the adhesive.

The importance of surface rugosity in the resulting joint strength of a polymer/metal system has been demonstrated by various workers. Recently, Evans and Packham (12) studied the adhesion of polyethylene applied in a molten state to metallic substrates with various surface topographies. When the rough fibrous oxide developed on copper was damaged without any chemical modification of the substrate, the peel strength dropped significantly. Jennings (13) attributed an increase in the strength of butt joints to the alteration of the stress distribution at the interface caused by roughening the substrate. Finally, Allen (14) concluded that to obtain optimum joint strength with a Ti-6Al-4V alloy, "a surface coated with a stable oxide in a coherent and rough form is <sup>e</sup>necessary".

The most generally accepted theory of adhesion yet is the absorption theory because it takes into account the nature of the adherents and explains theoretically the strength of interfacial forces. The essence of the theory is that provided there is good interfacial contact, secondary and/or primary interactions are sufficient to account for the observed adhesion. The adsorption of a liquid adhesive applied on a substrate can be envisaged as a three-stage process. In the first stage the Brownian movement of the polymeric adhesive molecules causes a migration towards the interface. Possible polar groups of the adhesive are oriented relative to polar groups of the substrate and contact points at the interface are established. In the second stage the migration is intensified, the density of the contact points is increased and intermolecular

forces start to operate. These forces may produce secondary interactions, ie van der Waals type of bonds or even covalent and ionic bonds. Finally, at the third stage the polymeric adhesive is reinforced by solvent expulsion, crosslinking, cooling etc.

As it is clear from these processes the ability of the polymer to wet the substrate becomes very important. If that is achieved there is theoretical evidence (15) (16) based on thermodynamic considerations that the attraction forces developed at the interface account for the observed joint strengths. A review of intermolecular and interatomic forces has been published by Good (17). Many types of bonds may exist across an interface. Dipole - dipole interactions are likely between two polar molecules. The electric field of a polar molecule can induce a dipole moment to a neighboring non-polar molecule. Also, the definite electron configuration of a molecule at one instant produces an instantaneous dipole moment inducing a dipole to a neighboring molecule. Thus the two molecules are attracted by such dispersion forces. Hydrogen bonds are possible where a hydrogen atom is attached to a highly electronegative atom. Strong ionic bonds can exist between a positive and a negative ion. When the electrons are shared between the nuclei of two atoms covalent bonds are formed. Pauling (18) gives the approximate bond energy of common chemical bonds (table 1-1).

To accept absorption as the most important mechanism in adhesion, the existence and role of the above mentioned interactions across

TABLE 1-1

Bond energies of typical types of chemical bonds (18).

Bond type	Bond energy (KJ. mole <sup>-1</sup> )
Ionic	590 - 1050
Covalent	63 - 710
H-bonds	10 - 26
Dipole - induced dipole	Very small
Dispersion forces	0.08 - 42

the interface must also be proved experimentally. The discrepancy between the calculated joint strength and the much lower measured experimental value is attributed to cracks, air voids and defects at the interface which cause premature fracture of the joint. There is some direct evidence of interactions across the interface. Owens (19) reported that corona-treated polyethylene films exhibit strong self-adhesion under heat and pressure compared to no adhesion between untreated films. He attributed that increase solely to hydrogen bonding between ketone and enol groups produced on the polymer surface by the corona treatment. Later he observed the same effect on polyethylene terephthalate (20). The existence of the above groups and the importance of hydrogen bonding were later verified by Blythe et al (21) by using x-ray photoelectron spectroscopy.

Another possible interaction at the interface is when an acid (proton acceptor) base (proton donor) situation occurs. Fowkes suggested (22) that good adhesion between polystyrene - water and polyvinylchloride-formamide may be explained by such interactions.

The polar and dispersion interactions across the interface can also be evaluated indirectly. The technique is discussed by Owens and Wendt (23) and it involves measuring the dispersion  $\gamma_s^d$  and polar  $\gamma_s^p$  contributions to the surface tension of a solid by measuring the contact angle  $\theta$  of a series of liquids of known dispersion and polar characteristics. Although there was some

criticism about the theoretical basis of this method (22) there seems to be general agreement that the free energy change on separating (or forming) two surfaces is the reversible thermodynamic work of adhesion  $W_A$  is composed of a variety of interactions:

$$W_A = W_A^d + W_A^p + W_A^h + W_A^{ab} + W_A^i + \dots$$

where d stands for dispersion, p for polar, h for hydrogen bonding, ab for acid-base interaction, and i for induced dipole-dipole interactions.

In addition to secondary forces the absorption theory allows that covalent or ionic bonds may be formed across an interface. Their contribution to specific adhesion as well as their role in the durability of the joint have been studied. With the aid of modern sensitive surface analytical techniques there is direct evidence about their presence under certain conditions. The relevant literature is rapidly expanding. Koenig et al (24) used Raman spectroscopy to show that vinyl - polysiloxane is chemically bonded to glass fibres when applied as an aqueous solution. Bailey et al (25) used x-ray photoelectron spectroscopy to prove that vinyl-triethoxysilane in a solution was chemisorbed onto an iron surface. The presence of  $FeSiO^+$  radicals was detected in a similar system by Gettings et al (26) using secondary ion mass spectroscopy (SIMS). Inelastic electron tunneling spectroscopy provides a useful method of detecting absorbed molecules on the

surface of a metal. White et al (27) discussed its potential while Simonsen et al (28) detected ionic bonding of organic molecules onto metal oxides.

In spite of extensive experimental evidence about the occurrence of physical and chemical absorption of molecules in contact, the exact nature and magnitude of the corresponding interactions across the interface are still uncertain. However, the absorption theory is the most widely accepted mechanism of intrinsic adhesion except in the USSR. The fact that it cannot explain experimental data like for example the temperature or rate dependence of adhesive joint strength, should not be considered as inadequacy of the theory; any destructive testing of an adhesive bond is greatly influenced by the response of the members of the bond and does not necessarily measure directly the interactions across the interface.

Concluding this brief review of the four main theories of adhesion is clear that adhesion is not a simple phenomenon explicable by only one model. For the formation of a real bond it is common that more than one mechanism operate at the same time. Absorption has been proposed as the prevailing mechanism when a polymeric adhesive is applied on a high energy substrate. That is the case in the present work, where ethylene vinyl-acetate copolymers are applied as hot-melts on steel and copper. Therefore absorption is suggested as the most likely mechanism for the polymer/metal system studied. The mechanical factor due to irregularities or a



prepared surface topography on the metals was found to enhance the peel strength via failure mechanisms described in a later chapter.

Finally, it is useful to consider the hypothesis that weak boundary layers formed at the interface exert a decisive influence on adhesion, since it has been the subject of considerable controversy.

This hypothesis is mainly concerned with the forces in the destruction of the joints rather than with those causing the unstressed components to adhere.

Bikerman has suggested (29) that practically always rupture in an adhesive joint occurs in a material and not between two materials. He attributed that to a weak boundary layer close to the interface which determines the breaking load.

Although this is not a theory proposing a mechanism of adhesion but an explanation of why joints fail, Bikerman insisted (30) that all the theories connecting the strength of a joint with intermolecular interactions, wetting and surface tension cannot be trusted. He calculated that the probability of a crack propagating along the interface is very small. His second theoretical argument was that intermolecular energies between two dissimilar gas molecules A and B follow the relation:

$$U_{AA} > U_{AB} > U_{BB}$$

so by analogy to adhesive systems cohesive failure is energetically favoured. Finally, he argued, it is very improbable that a crack can follow the exact contour of any real surface given that microscopically even the polished surfaces appear rough.

Although Good (31) and others strongly criticised the W.B.L as a universal phenomenon occurring at any interface, there is some evidence that such a layer may be important in particular systems. It is well known that absorbed water, contamination of the surface, grease or a weak cohesively metal oxide decrease adhesion significantly. In other cases however an interfacial layer of stearic acid onto aluminium (32) or silane onto glass (33) can enhance the adhesion on these substrates.

More recently experimental data have been accumulating to indicate that interfacial failure can occur. Huntsberger (34) used interferometry to show that poly-isobutylene and a crosslinked alkyd resin exhibited purely interfacial separation. Briggs et al (35) employed x-ray photoelectron spectroscopy to study the surface of polyethylene and polypropylene adherent to an epoxy resin. After failure they detected no polyolefine remains, not at least thicker than the detection limit of  $20\text{\AA}$ . In some cases (36) the crack appears to propagate close to the interface but that does not prove the existence of a weak boundary layer. Bascom et al (37) point out to the importance of the stress field around the tip of the crack causing a "mechanical focusing" of failure into the

interfacial region. The importance of boundary layer phenomena with properties different from the bulk material is emphasized by Sharpe (38). He makes the distinction that these boundary layers may be potentially, but not necessarily weak. The mechanical properties of the materials and stress concentration close to the interface must also be examined.

Much of the controversy about the WBL hypothesis may arise from the difficulty to compare experimental data of adhesive tests for various materials and probably the inadequacy of the surface analytical techniques available. Although Bikerman's arguments are not generally accepted - at least in their original form - more evidence is needed about the role that, undoubtedly, changes at or close to the interface have on adhesion.

Concluding this brief review of the theories of adhesion it is suggested that for the polymer/metal system studied in the present project, adsorption is the most likely mechanism. The surface roughness of the substrate will be altered by changing its topography and that contributes also to the measured adhesion.

### 1.3 E.V.A. COPOLYMERS AS HOT-MELT ADHESIVES

#### 1.3.1 HOT-MELT ADHESIVES IN GENERAL

Hot-melt adhesives are based upon thermoplastics and are solid at normal temperatures becoming a mobile liquid when heated to temperatures over approximately 100° C. The adhesive can then be applied to the adherents to form the bond and is left to solidify.

The main advantages of hot-melt adhesive formulations are that they are solvent-free (and hence not a health or fire hazard), they have good wetting characteristics and can provide rapid adhesion. Their disadvantages are formation of joints with poor strength compared with other types of adhesives and also high heat sensitivity followed by loss of strength.

Areas where hot-melt adhesives are employed include among others the packaging and footwear industries, bookbinding, coating, woodworking, and pressure sensitive tapes.

#### 1.3.2 HISTORY AND APPLICATIONS OF E.V.A COPOLYMERS

In 1946 Hanford (39) at Dupont copolymerised ethylene and vinyl acetate by using a high pressure and temperature technique. Ethylene vinyl acetate copolymers became commercially available in 1961 (40) and since then they have been accepted as the resin base

of many hot-melt adhesive and other formulations. The main reason for that is the compatibility of E.V.A. copolymers with chemicals necessary for adhesive compositions like wax, tackifying or wetting agent, flexibilizer, antioxidant, filling powder and plasticizer. Markets for E.V.A. copolymers have also been expanding in replacement of plasticized P.V.C., rubber and polyethylene. The material is rubbery without the use of plasticizer, so "blooming" or migrating of the plasticizer do not occur.

It has been claimed that E.V.A. copolymers can compete with rubber (41) and in a few cases they are actually being used for rubbery applications; syringes, billiard table cushions, air hose and some types of tubing, cable jacketing.

The implications of using ethylene vinyl acetate copolymers in emulsion paint formulations have been discussed by G E J Reynolds (42) and M H Edser (43). They conclude that they offer easy paint formulation, good stability and are economical. Compared with similar copolymers they suffer from limited pigment binding efficiency and poor alkali resistance. Similar conclusions are reached in a review by C A Finch (44) who also foresees great potential in E.V.A. emulsions and a lot of room for development.

Another area of application of E.V.A. copolymers is as the base elastomer for hot-melt pressure-sensitive adhesive formulations. The copolymer is chosen because it combines good specific adhesion,

adequate melt stability, and sufficiently low viscosity to allow compatibility with other ingredients at the compounding temperature (45).

However, the vast number of uses of ethylene vinyl acetate copolymers is as the basic ingredient in hot-melt adhesive or coating formulations. The packaging industry takes advantage of their excellent compatibility with paraffin wax to yield a low-cost, easily applied flexible coating (46). An E.V.A. coating exhibits good specific adhesive properties and is capable of high water barrier performance (40).

A list of applications of E.V.A. copolymers as adhesives and coatings can be found in the literature (47) (48). In his review of E.V.A. copolymers G W Gilby (49) concludes that "E.V.A. has now come of age but in spite of this, many new, as yet unthought of, outlets will undoubtedly be developed in the future. A stimulating prospect for an exciting range of materials".

### 1.3.3 STRUCTURE AND PROPERTY RELATIONSHIPS IN E.V.A. COPOLYMERS

The basic parameters which determine the physical properties of an E.V.A. copolymer are the vinyl acetate content and the average molecular weight. At very low vinyl acetate content the polymers resemble low density polyethylene. Over a range of 5 to

40% they become progressively more flexible and rubbery. From 40 to 70% vinyl acetate content they are amorphous mechanically weak rubbery materials. As the amount of vinyl acetate is increased the properties of E.V.A. copolymers change predictably considering that a bulky polar acetoxy group is incorporated in the polymer as side chain. Thus, as the V.A. content increases so does the polarity of the copolymer and properties connected to the polarity like compatibility with polar resins and specific adhesion in adhesive formulations.

The effects of V.A. content on crystallinity of E.V.A. copolymers were investigated by Salyer et al (50). The crystallinity was measured by x-ray and differential thermal analysis and was found to decrease with increasing V.A. content. That was accompanied by a decrease in mechanical properties as tensile yield strength, stiffness modulus and surface hardness.

As with all polymers, the average molecular weight has a major influence on their properties. Increasing the number average molecular weight of E.V.A. copolymers has the same effect on their melt viscosity which is usually measured and quoted as the Melt Flow Index (M.F.I). The influence of Molecular Weight Distribution (M.W.D) on the flow properties of E.V.A. copolymers was studied by Fujiki et al (51). They found that generally, the broader the (M.W.D) of the polymer the higher its melt viscosity.

The physical properties of E.V.A. copolymers are also influenced by short hydrocarbon chain branches (52). These branches disrupt the crystallinity of the copolymer, increase the flexibility and generally decrease the stiffness.

It must be emphasized that the above mentioned structural features do not determine the physical properties exclusively. Vinyl acetate distribution and long chain branching must also be considered although they have a lesser effect on properties (49).

#### 1.3.4 ADHESION OF E.V.A. COATINGS

In the majority of the adhesive applications of E.V.A. copolymers outlined before the resin is mixed with various ingredients. There is a large amount of literature, mainly patent, about adhesive formulations based on E.V.A. copolymers and their properties.

In contrast to that there is very little work reported about pure E.V.A. resins used as coatings. Smarook et al (53) studied the adhesion of carboxyl containing ethylene copolymers to copper, aluminium and steel. The peel strength increased with acrylic acid content. When the polar carboxyl groups are neutralized by metallic association, adhesion falls. Better adhesion to grit-blasted aluminium over non-blasted is attributed to mechanical bonding resulting from an increased surface area.



Both the above observations are consistent with the suggestion of adsorption as the prime cause of adhesion between E.V.A. copolymers and metals as well as the significance of the surface topography. Experimental evidence about the contribution of the polar groups to adhesion is provided in a later chapter where the influence of the metal topography on the mechanism of debonding is also discussed.

Nobuhiro et al (54) focused their attention to the flow properties rather than the carboxyl content. Studying the peel strength of ethylene vinyl acetate based hot-melt adhesives they report an adhesion maximum at a melt flow index of 170 (gr/10 minutes) and 28% vinyl acetate content. Although there is no explanation for these values their results demonstrate the correlation between structural polymer parameters and adhesion.

Vaganov et al (55) extends this correlation to include the tensile strength at break ( $\sigma_t$ ), internal failing stress ( $\sigma_i$ ), crystallinity (C) and elongation at break (E). They prepared coatings by dipping hot metal plates into fluidized beds containing ethylene vinyl acetate powder. As the vinyl acetate content increases so does the adhesion and that is ascribed to an increase in (E) and a decrease in ( $\sigma_t$ ), ( $\sigma_i$ ) and (C). No detailed explanation is given for these observations. Further support for the correlation put forward by Vaganov comes from work reported by Lee et al (56). They related the 180° peel strength of P.V.C - plywood laminates bonded with ethylene vinyl acetate copolymers to their tensile

strength and elongation characteristics. They suggest that the ability of the polymer to flow or deform is associated with higher peel strength and generally a cohesive mode of failure. Inability of the polymer to flow, ie at high peel rates, leads to lower peel strength and "clean" delamination. They emphasize that if the failing zone is extended by polymer flow or at low peel rates more adhesive becomes available to absorb the work of peeling and as a result higher failing force is recorded.

Experimental results reported by Hiroshi et al (57) provide more evidence about the importance of polymer properties in peel testing E.V.A. adhesives. They bonded aluminium - aluminium laminates by pressing ethylene vinyl acetate films 0.5 mm thick at 180° C for 5 minutes. For resins with vinyl acetate content ranging from 10 to 87% by weight and for a variety of temperatures maximum adhesion was observed near the Tg of the polymers. This is contradicted by Smarook et al (53) who found relatively poor peel adhesion at -30° C, a temperature inside the transition region of -25 to -40° C reported in the literature. However, this discrepancy could be due to the different peel test set ups used by the two authors.

#### 1.3.5 OBJECTIVES OF THE RESEARCH PROJECT

The papers discussed above are only those with direct relevance

to peel adhesion of ethylene vinyl acetate copolymers. It is clear that different authors place their emphasis to different properties in order to explain the observed adhesion. Therefore the need arises for a better understanding of the adhesive performance of these materials as coatings.

E.V.A. copolymers are structurally related to polyethylenes the adhesion of which to metals has been studied extensively and explained in terms of their mechanical response to deformation. The four E.V.A. copolymers chosen for this project provide a series of materials where an increase in vinyl acetate content causes a progressive change in their mechanical response. It is expected that this change will be reflected in their performance as coatings. The increasing commercial interest in E.V.A. copolymers as coatings or as ingredients in hot-melt formulations justifies their choice for this project even more.

The critical influence of the metal topography upon the adhesive strength of coatings has been discussed in section 1.2. The effect that the surface preparation has on the adhesion of E.V.A. copolymers will also be investigated. To achieve that three different metal substrates will be used in this project, two with a conventional and one with a microfibrinous topography. So far, published adhesion studies for substrates identical to those in the present work involved tough epoxy resins (rubber modified or not) and various types of polyethylenes (12) (58). The more

rubbery ethylene vinyl acetate copolymers investigated here complete a group of materials with a wide range in ductility. The metal substrates used in this project are copper and steel because of their commercial importance for coating applications as well as available surface treatments for these metals which produce the required controlled topography.

Finally, the method employed in order to assess the adhesion of E.V.A. copolymers to the above metals will be the peel test. It appears that the peel test is the most popular method of evaluating the adhesion of flexible coatings to rigid substrates and that is mainly due to its simplicity. The two main analyses available for such a combination are:

- (a) A consideration of the static stress distribution in the bond and;
- (b) An interpretation based on the energy balance argument.

Both analyses are reviewed in the following chapter.

## CHAPTER 2

### PEEL TESTING OF POLYMERIC COATINGS

#### 2.1 INTRODUCTION

Over the years peel test has proved to be very useful in providing a measure of adhesion for practical and theoretical purposes.

Rivlin (59) appears to have been the first to analyse data obtained by the peel test. He was followed by Hata (60) who examined the relation of the peel angle with the force required for peeling during a "stripping test". It is interesting to note that in his analysis he mentioned two different approaches:

(a) the equilibrium of the moment produced by the load and the adhesive force and;

(b) the equilibrium of the work required for peeling.

Another early study of peel test data came from Deryaguin and Krotova (61). They argued that "almost all the work of detachment is spent to overcome electrostatic forces between opposite charges formed in the process of peeling". Their views are discussed in the electrostatic theory of adhesion.

Since then peel testing has been investigated by a number of

adhesion scientists. Results have been published about the effects on the peel strength of changing the peel angle, test temperature, rate of peeling, physical or chemical properties and surface topography of the adherents. Also, a flexible backing can be introduced, the joint environment may vary and so forth.

As it was mentioned in the previous chapter the two main approaches to interpret experimental peel results for a polymer coating/metal system are the stress analysis and the energy balance approach. Both analyses are discussed in the following sections.

## 2.2 STRESS ANALYSIS OF THE PEEL TEST

One of the ways that the peeling test may be analysed is by studying the static stresses set up when the flexible member is detached from the substrate. Spies (62) appears to be the first to analyse these stresses theoretically. He described a theoretical method of calculating the stresses set up in the peel joint recognizing also the importance of the mechanical response of the adhesive and its thickness. A discrepancy between the calculated and measured values of peel strength was attributed to lack of data for the adhesive's elastic and plastic behaviour. Bikerman (63) studied the peel adhesion of a ribbon bonded to a rigid plate with a Hookean solid and reported that the minimum force  $F_0$  to initiate 90° peeling was:

$$F_0 = 0.3799 \cdot b \cdot \sigma \cdot (E_a/E_b)^{1/4} t_a^{1/3} t_b \quad (2-1)$$

where  $b$  is the width of the ribbon,  $\sigma$  the tensile strength of the adhesive,  $(E_a, t_a)$  and  $(E_b, t_b)$  the moduli of elasticity and the thickness of the adhesive and of the ribbon respectively. Later he extended the theoretical treatment to include non-Hookean behaviour of both adhesive and backing (64). Kaelble (65) (66) developed Bikerman's analysis to include all possible peel angles. For a test piece shown in fig (2-1), he calculated that the cleavage stress,  $\sigma_c$ , at a distance  $-x$  into the bond is given by:

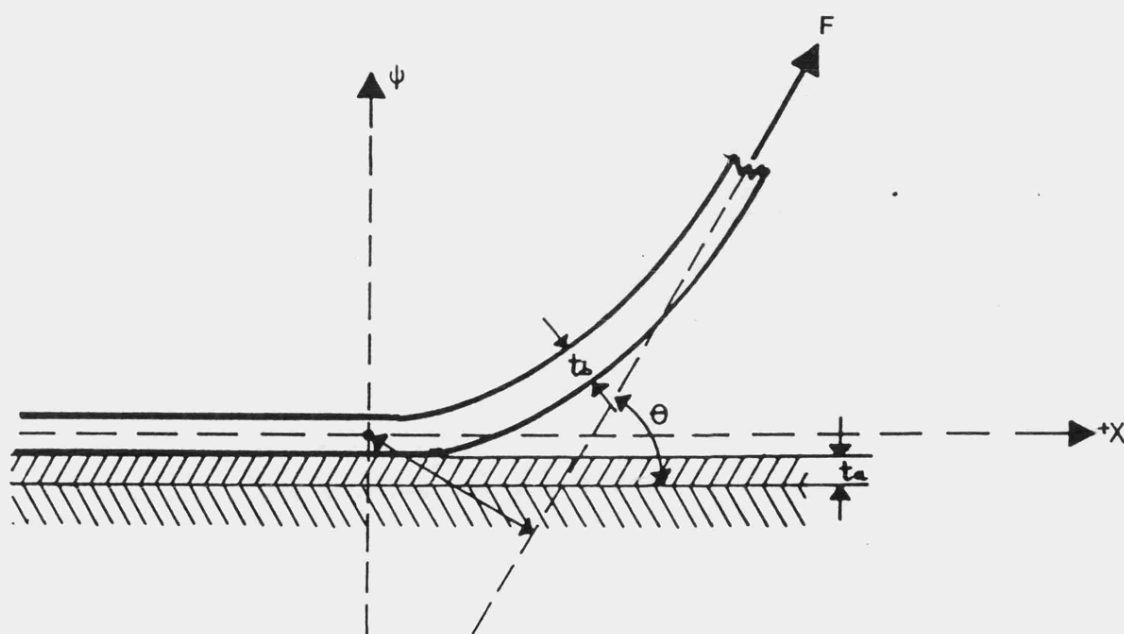


FIGURE 2-1 : Schematic diagram for the stress analysis of a flexible member peeled from a rigid substrate.(65)



$$\sigma_c = \sigma (\cos \beta x + K \sin \beta x) e^{x\beta} \quad (2-2)$$

Where:

$$\beta = \left[ \frac{E_a \cdot b}{4E_b I \cdot t_a} \right]^{1/4}$$

and

$$K = \frac{\beta m}{\beta m + \sin \theta}$$

$\sigma_c$  = cleavage stress at  $x = 0$ ,  $E_a$  = Young's modulus of the adhesive,  $E_b$  = Young's modulus of the flexible member,  $b$  = bond width,  $I$  = moment of inertia of flexible adherent,  $m$  = moment arm of the peel force  $F$ ,  $t_a$  = adhesive layer thickness and  $\theta$  = peel angle.

Later Gent and Hamed (67) criticised the assumptions that Kaelble made in developing his equations; the adherent and adhesive are assumed to be elastically deformed only; the cleavage stress  $\sigma_c$  is assumed constant through the thickness and across the width of the adhesive; failure is assumed to occur as a line propagation. Indeed, these assumptions do not hold for adhesives exhibiting plastic response or stresses behind the line of separation due to adhesive ligaments.

Gardon (68) (69) studied the variation of peel force with adhesive layer thickness. His experimental results came from peel testing

of cellophane sheets coated with acrylic polymers and pressed together at elevated temperature. He derived an equation predicting the peel force in terms of:

- (a) the moduli of the substrate and adhesive;
- (b) the maximum stress developed in the adhesive at the failure point and;
- (c) geometric considerations.

He disregarded shear stresses and again assumed Hookean behaviour of the adherents as well as that the failure stress was independent of the rate. The latter two assumptions are partially true only at high peeling rates, although as Jouwersma (70) points out, the restriction of lateral adhesive contraction and the high strain rate that a resting adhesive element experiences during peeling favour a more Hookean behaviour.

Both the analyses of Kaelble and Gordon predict correctly the existence of compressive stresses developing as the peel front proceeds prior to the detachment line. Evidence about that phenomenon was provided by Wong (71) who measured the half-wavelength of a pattern of waves running ahead of the line of separation. The treatment of Kaelble and Gordon assumed the flexible backing to peel from the adhesive whereas interfacial or cohesive failure

within the adhesive is frequently observed. In conclusion, experimental data seem to fit the predictions of their analyses (ie their assumptions hold) only when a relatively soft adhesive is peeled at an angle of  $90^\circ$  or more and at a high pulling rate.

In an effort to define the stress distribution in the peel test Crocombe and Adams (72) employed a finite element analysis approach. Considering only large displacement elastic response they concluded that failure is caused at a critical applied bending moment and that the principal stresses drive the crack towards the interface. Extending their analysis to include elasto-plastic behaviour (73) they found that plastic deformation accounts for about 50% of the total energy supplied during peeling. More significantly, they demonstrated from both analyses the non-linearity of the peel test, ie a small increase in the strength of their epoxy adhesive caused a much larger increase in the measured peel load.

The extension of the stress analysis approach to softer polymeric materials presents additional problems like the determination of the stress zone. Working towards that direction Wang et al (74) derived an equation to predict the peel force from the size of the plastic zone of a polyethylene-epoxy-oxidised copper system. For this particular situation that size was equal to the distance between two ridges observed at the peeled surfaces. Although their model fit the experimental results they admitted that "from

an analytical point of view it is preferable to determine the size of the plastic region from an elastic-plastic analysis. The subject is, however, very complicated."

### 2.3 THE ENERGY BALANCE APPROACH TO THE PEEL TEST

Griffith (75) was one of the first to apply energy considerations in a fracture process. He suggested that the formation of a crack of area  $A$  in glass needed energy  $2A\gamma$  where  $\gamma$  was the surface free energy. That energy was supplied by the external force and the stored elastic energy in the bulk of the sample.

The same energy balance concept was later extended by Rivlin and Thomas (76) to cross-linked elastomers. They reported that the measured values of tearing energy required for crack growth were much larger than the free surface energy because of extensive hysteresis losses experienced in rubbers at high strains.

The stress analysis in non-linear elastic or dissipative materials is generally difficult as a great deal of information can be obtained from considering the energy balance. This is certainly the case when a flexible strip is peeled from a rigid substrate.

For such a system, mechanisms by which the energy is dissipated have been studied by various authors. Lindley (77) was one of the first to examine the extension of the peeled leg. He considered the debonding of a length  $X$  of a flexible coating in a  $180^\circ$  peel test. For such a geometry the cross-head of the testing machine will move a distance of  $2X$ . For the case of an extensible coating there will be also an increase  $\Delta l$  in length due to stretching that

the peeling force  $F$  is exerting on the coating. If the final extension ratio is  $\lambda$  it follows that the total input work done by the machine in the peel test will be:

$$\begin{aligned}
 P_i &= F(X + X + \Delta l) \text{ or} \\
 P_i &= F(X + \lambda X) \text{ or finally} \\
 P_i &= FX (1 + \lambda) \qquad (2-3)
 \end{aligned}$$

Similar although not identical stress conditions apply when a strip of the same polymer is deformed in a tensile mode up to the same extension ratio  $\lambda$ . Then, the work of deformation per unit volume  $E_{e/p}$  done in stretching the strip will be given by the area of a stress-extension ratio curve up to  $\lambda$ . In the peel test situation the corresponding volume under stress is  $(X.t.b)$  where  $X$  is the previously described debonded length,  $t$  the thickness and  $b$  the width of the strip. So, the tensile work of elastic-plastic deformation for the peel test becomes:

$$E_{e/p} \cdot X.t.b \qquad (2-4)$$

Considering the energy balance in the system it is obvious that the input work  $P_i$  must be equal to work done in stretching plus the remaining work  $W_r'$  available for peeling. Thus, from equations (2-3) and (2-4) we have:

$$P_i = E_{e/p} \cdot X.t.b + W_r'$$

$$F.X. (1 + \lambda) = E_{e/p} .X.t.b + W_r'$$

or  $W_r = \frac{F}{b} (1 + \lambda) - E_{e/p} .t$  (2-5)

It must be emphasized that  $W_r$  should not be treated as a thermodynamic quantity like the surface energy or work of adhesion.  $W_r$  represents the fracture energy per area debonded which is available for peeling after the energy losses due to stretching are subtracted.

Lindley's experimental results confirmed the validity of equation (2-5). Later, Kendal (78) derived a similar equation based on the simple considerations outlined before. His experimental results for vulcanized rubber bonded to steel and crosslinked ethylene-propylene rubber bonded to glass also agreed with the theoretical predictions.

A backing is often used in order to avoid the stretching of the peeled strip. However, it has been noticed that in the absence of such a support the coating may yield under the imposed bending stresses. Duke (79) photographed the irreversible bending deformation of a cellulosic pressure sensitive tape after peeling and stated: "evidently, elastic peel mechanics can describe only a very limited number of types of peel of practical interest, these being chiefly in the field of cleavage of joints between thick, rigid adherents".

Therefore when plastic yielding occurs additional energy is dissipated resulting in higher peel force. This constitutes a second energy loss mechanism and must be considered in any energy balance analysis. By considering the peel energies predicted by equation (2-5) at 90° and 180° in the absence of any stretching, ie when  $E_{e/p} = 0$  and  $\lambda = 1$  it is expected that for geometrical reasons  $W_{r(90^\circ)} = 2 W_{r(180^\circ)}$ . However, there are experimental results (80) suggesting that  $W_{r(90^\circ)} < 2 W_{r(180^\circ)}$  and that was attributed by Gent and Hamed (81) to increased plastic deformation of the peeling member. (fig 2-2).

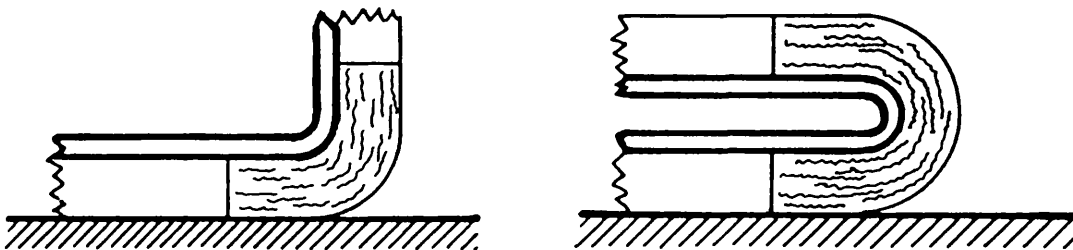


FIGURE 2-2: Representation of strains in the macromolecules of a polymer peeled at 90° and 180°.



Applying the energy balance approach to the T-peel test Yamamoto et al (82) studied the adhesion of hydrolysed and acrylic acid grafted ethylene-ethyl acrylate and ethylene-vinyl acetate copolymers. Considering only the energy dissipated inside a polymer volume confined by a fraction of the total thickness they concluded "that there are also some contributions to the measured peel strengths from energy dissipation due to bending and tensile deformation of the adherents".

Several other workers have recognized that in a peeling experiment sufficiently large bending stresses imposed on the stripping member can cause plastic yielding (83) (79) (73) (80). Gent et al (84) succeeded in measuring experimentally the energy dissipated by that mechanism for a Mylar strip. Their experimental results were compared with calculated values from an approximate theoretical treatment and the agreement was good. This treatment takes into account the elastic-plastic behaviour of the stripping member, its thickness and the radius of curvature and is based on elementary theory of bending.

When a polymer strip is bent back in a 180° peel experiment the regions of outer and inner curvature are subjected to the maximum tensile and compressive stress respectively (fig 2-3). So, the peeling force applied to overcome the adhesion of the strip to the rigid substrate introduces large bending moments and it is likely that the yield point of the polymer will be exceeded. That was

clearly the case for the ethylene vinyl acetate copolymers since the strips exhibited residual curvature after peeling, especially those without the fabric support.

Let us consider a strip of thickness  $t$  adhered to a rigid substrate and bent back after a peel force  $F$  is applied (fig 2-3). If we assume that the polymer's behaviour in tension (outer region of curvature) is the same as in compression (inner region of curvature) then there is a neutral axis  $OO'$  at the middle of the strips thickness. Let us consider now a section of the strip in the bent region (figure 2-4). For an ideal elastic-plastic material the total energy per unit area debonded  $W_b$  spent in plastic bending of the strip is equivalent to the sum of the energy represented by the two shaded areas in figure (2-4). Thus:

$$W_b = 2 \int_{BC}^{AC} \sigma_y (e_A - e_B) dx \quad (2-6)$$

The distance  $AC$  from the neutral axis can be replaced by  $t/2$ . The strain at point  $B$  is the yield strain  $e_y$ . For each particular radius of curvature  $R$  the strain imposed on any point on the  $xx'$  axis can be expressed as:

$$e = \frac{x}{R}$$

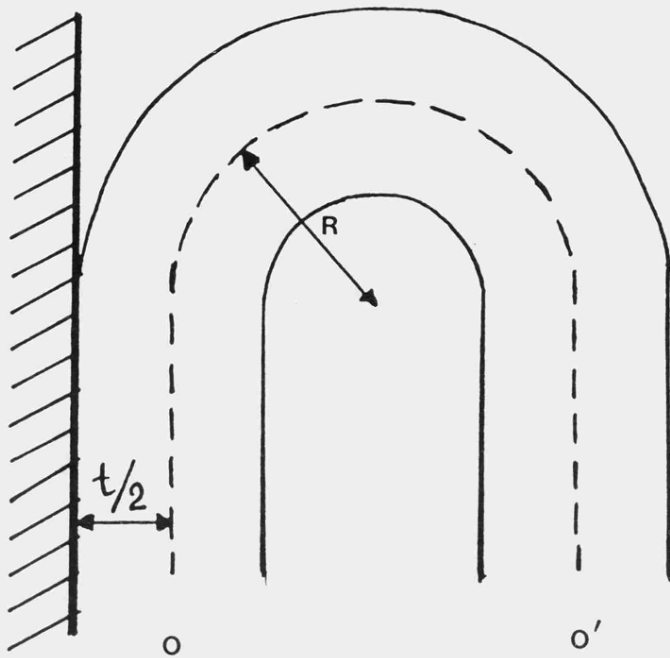


FIGURE 2-3 : Schematic diagram of a peeling strip.  $OO'$  is the neutral axis and  $R$  the radius of curvature.

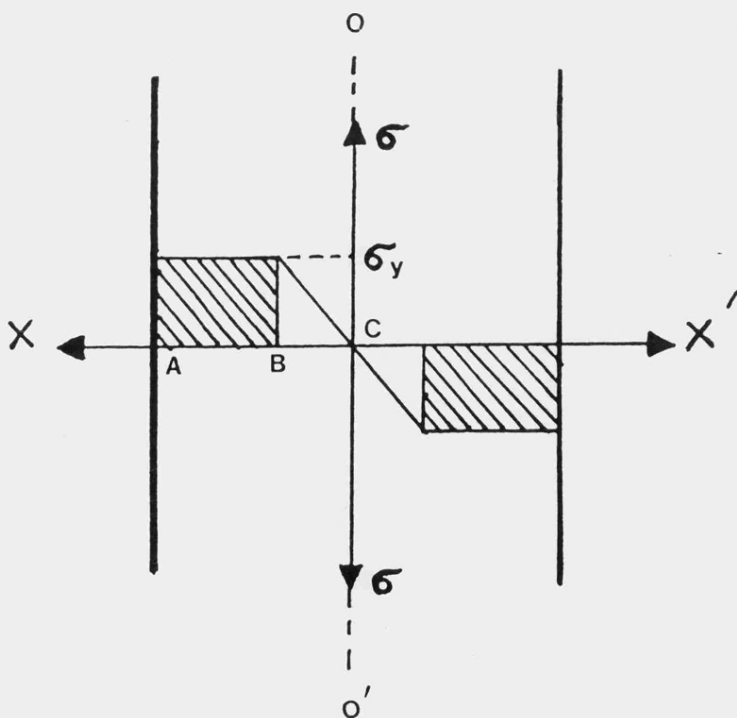


FIGURE 2-4 : Bending stresses developed in a section of an ideally elastic-plastic strip.

where  $x$  is its distance from the neutral axis. Thus, BC becomes  $e_y R$  and so equation (2-6) can be integrated from  $e_y R$  to  $t/2$ , two limits that for a particular polymer can be measured. Finally, the integration yields the energy per unit area debonded  $W_b$  which is expended in plastic deformation:

$$W_b = \frac{1}{2} (\sigma_y e_y t) \left[ \frac{t}{2Re_y} + \frac{2Re_y}{t} - 2 \right] \quad (2-7)$$

Equation (2-7) however, is derived using an approximate theory and that is so because of the assumptions involved:

- (a) The material behaves as an ideal elastic-plastic solid.
- (b) It responds to compression and tension identically.
- (c) The elastic energy is recovered when the strip is straightened and
- (d) Any plastic energy expended in stretching a section after it traverses through the bent region is smaller than the energy expended in plastic bending.

For the polymers and substrates investigated in this project the experimental observations suggested that the last two conditions

were met. The second condition, although not proved experimentally by conducting compression tests, can be accepted provided that the maximum bending stresses are relatively small. Finally, the first condition leads generally to an under-estimation of  $W_b$ . Again the extent of that discrepancy depends on the maximum bending stress that the material experiences as well as on the shape of the stress/strain curve.

A third energy dissipation mechanism can operate when a flexible coating is peeling from a rigid substrate. A distinct lip of highly extended polymer is sometimes observed following the advance of the peel front. This phenomenon is sometimes referred to as "legging" of the coating and it has not been investigated systematically. If the polymer undeformed thickness is  $t$  (fig. 2-5) when the peel front line approaches a vertical cross-section of the coating it is forcing a longitudinal stretching of that section at a very fast rate of deformation. The original thickness takes its maximum value  $t_1$  when the peel front reaches the cross-section considered. The peeling process continues by debonding at or close to the interface and then the polymer relaxes gradually. When an inextensible backing is used, the process approximately resembles a very fast tensile loading of the considered cross-section inside the coating up to a strain  $e_1$  equal to  $\frac{t_1-t}{t}$  followed by a sudden release of the tensile force. Therefore, it is suggested that the mechanical equivalent of that energy loss mechanism is a

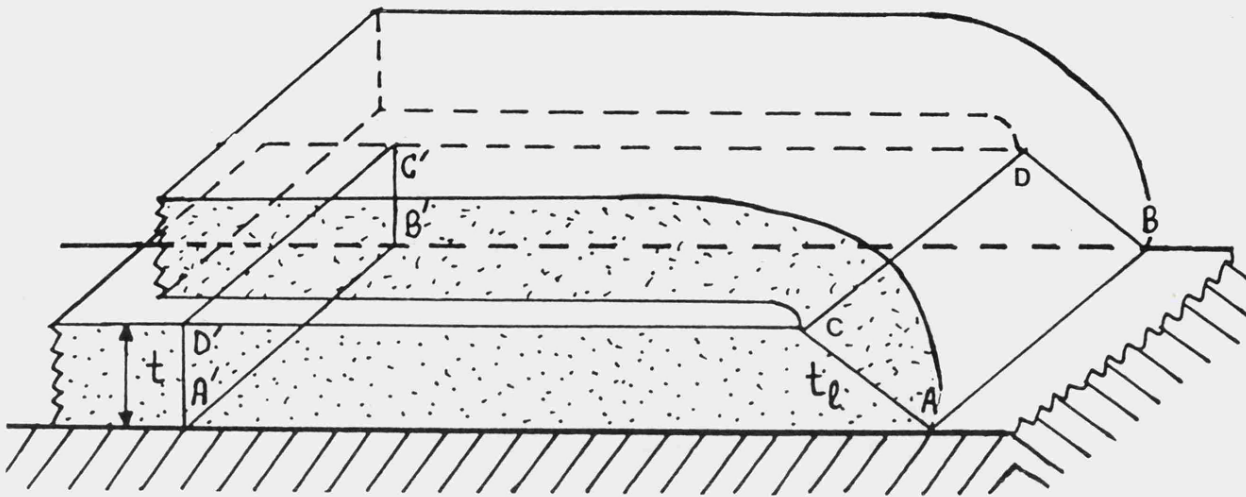


FIGURE 2-5: Schematic diagram of a strip peeling at 180° showing polymer extension at the peel front.

one cycle loading-unloading tensile test up to the same strain  $e_1$ . That of course is only a close approximation since it is obvious that the stress is not evenly distributed along the distance  $t_1$ ; close to the line of detachment AB the stress is very close to the failing stress and is gradually reduced as we move towards line CD at the top of the strip.

The energy dissipated by that mechanism can be considerable because of the large stresses experienced by a relatively small polymer volume. These losses are obviously enhanced by a substrate capable of holding back this polymer lip and/or polymers dissipating more energy per unit volume during a loading-unloading cycle.

A fourth energy loss mechanism present when a flexible coating is peeled from a rigid substrate is the viscoelastic energy lost during debonding very close to the advancing crack. If the fracture is cohesive a simple examination of the two detached parts of the bond with an electron microscope usually provides evidence to support the above mechanism. If the fracture is purely adhesive then obviously the signs of that large local deformation are clearer only in the polymer part.

The dependence of peel strength on the viscoelastic properties of polymeric adhesives was demonstrated by Aubrey et al (85). Peeling a pressure sensitive tape consisting of a polyester backing and polyacrylate adhesive from glass over a wide range of pulling rates, they correlated the observed peel force to the viscoelastic response of the adhesive at the particular rate. They also showed that the peel force at various pulling rates can be converted to a single master-curve by using the W.L.F transformation.

Finally, the thermodynamic work of adhesion (or cohesion in the case of cohesive failure) expended in creating two new surfaces must also be considered in an energy balance in a peeling test.

So, taking into account all the dissipation mechanisms outlined so far an energy balance equation for the peeling of a flexible coating from a rigid substrate can be described as:

$$P = W_a \text{ (or } W_c) + W_s + W_b + W_l + W_{v/e} + \dots \quad (2-8)$$

where P is the fracture energy of detachment per unit area due to the peel force,  $W_a$  (or  $W_c$ ) the thermodynamic work of adhesion (or cohesion depending on the failure mode),  $W_s$  the work done to extend the peeled strip longitudinally (without inextensible backing),  $W_b$  the work dissipated to initiate and maintain plastic bending of the peeling strip,  $W_l$  the losses at the advancing peeling front due to "legging" of the polymer and  $W_{v/e}$  the viscoelastic energy lost in deforming the polymer at the vicinity of the fracture plane.

It must be noted that the energy dissipation mechanisms represented in the right hand side of equation (2-8) do not define all the energy types that may be present.

For example, several workers detected small amounts of heat generated during peeling, probably due to friction of macromolecular chains under tension. Electrical discharge phenomena (see work by Deryaguin and co-workers) may also be of importance in some cases. It is generally accepted however that these forms of energy loss are small compared with the major dissipation mechanisms described before.

In an attempt to describe the viscoelastic energy losses in simpler terms, Andrews and Kinloch (86) developed a single failure



criterion for adhesive tests. They measured the input energy to fracture joints of three different geometries between a crosslinked amorphous styrene-butadiene rubber and rigid substrates. They showed both theoretically and experimentally that this energy could be separated to two contributions:

- (a) the intrinsic adhesive failure energy  $\Theta_0$  which gives a measure of the interfacial forces.  $\Theta_0$  can be represented as:

$$\Theta_0 = iI + rR + sS$$

Where I, R and S are the intrinsic failure energies for interfacial, adhesive or substrate fracture respectively and i, r and s are the area fractions of the corresponding failures. For completely interfacial failure  $i = 1$  and  $I = W_A$ , so  $\Theta_0 = W_A$ .

- (b) all the rate dependent energy losses within the adhesive are given by a function  $f(\dot{c}, T, \dots)$ .

Although the function  $f$  is not defined mathematically, Andrews and Kinloch demonstrated for their models that:

$$P = \Theta_0 f(\dot{c}, T, \dots)$$

They pointed out that the function  $f$  and the total of the visco-elastically dissipated energy losses are "intimately connected but not identical" (87).

Earlier than Andrews and Kinloch and peeling a lightly crosslinked rubbery adhesive from a Mylar strip, Gent and Schultz (88) studied the effect of various wetting liquids on the peel force over a range of rates and temperatures. They also reached the conclusion that the observed peel strength is a product of the thermodynamic work of adhesion and a numerical factor which represents the elastic imperfection of the adhesive.

Provided that the various energy loss mechanisms can be isolated and studied, the energy balance approach can be very useful in analysing peel test data. It may also provide information about failure mechanisms and thus contribute in predicting the joint strength.

## 2.4 CONCLUSIONS

The peeling test provides a useful method of assessing the strength of adhesive joints. It has found a lot of practical applications as a means of obtaining the work of detachment quickly. Furthermore, it has provided the basis of fundamental studies mainly because failure proceeds at a controlled rate. The results can be analysed either by considering the stresses set up in the adhesive layer or by looking at an energy balance during the test.

It is now widely recognized (89) (91) (90) (78) that the latter approach is more suitable in the case of peeling flexible polymers from rigid substrates and so it will be followed in the present project. Variables like the peel angle and peeling rate will be kept constant since the emphasis is placed on the effects of changing the mechanical properties of the coatings and the substrate topography.

The investigation of the adhesion of ethylene vinyl acetate copolymers begins with the characterisation of the polymers used in the present project. Their adhesion to copper and steel is then measured by a 180° peel test. As it has been discussed the energy balance approach will be adopted in order to analyse the peel test results. In attempting to assess the contribution of each of the different energy loss mechanisms outlined in this chapter, the mechanical properties of the polymers which are

connected to these mechanisms will be measured. The examination of the fractured surfaces by microscopic and spectroscopic techniques is also expected to assist to a better understanding of the fracture mechanisms and path. Finally, the various forms of energy lost will be determined quantitatively. It is hoped that the above course of investigation will provide an adequate explanation to the effects that vinyl acetate content and substrate topography are expected to have on the peel adhesion of the E.V.A. copolymers of this project.

## CHAPTER 3

### MATERIALS AND METHODS

#### 3.1 POLYMERS

Four commercially available ethylene vinyl acetate copolymers were used in the present project. Three were supplied by ICI Ltd from their Alkathene series; type 2805-042 (28% V.A. by weight) designated as polymer A, type 5401-041 (18% V.A. by weight) designated as polymer B and type 554-080 (12% V.A. by weight) designated as polymer C. All the above resins were supplied in powder form. The fourth resin was the Elvax 750 type manufactured by Du Pont (containing 9% V.A. by weight) designated as polymer D.

All resins according to the manufacturers were additive free and for the purposes of the present work all came from the same batch.

As discussed in the previous chapter the peel behaviour of these polymers was expected to depend on their mechanical and physical properties. It was therefore considered expedient to characterise certain of these properties for the particular materials used although in some cases nominal values were available in the manufacturers' literature. The parameters measured were the vinyl acetate content, melt viscosity, crystallinity, and molecular weights.

The methods used and the results are described in the following sections.

### 3.1.1 QUANTITATIVE DETERMINATION OF VINYL ACETATE CONTENT IN E.V.A. COPOLYMERS

The most important factor which characterises an E.V.A. copolymer is its content of V.A units. To check the values given by the manufacturers for the V.A content of the E.V.A. copolymers supplied for this project, three independent experimental techniques were used from all the methods available (92).

The first method is based on the thermal decomposition of E.V.A. copolymers at elevated temperatures liberating acetic acid which is then neutralized by a suitable base. Approximately 1 gr of copolymer powder was weighed accurately and then placed into a small porcelain boat. The porcelain was pushed inside a preheated ceramic tube at 395° C for twenty minutes (fig 3-1). At that temperature the E.V.A. copolymer decomposes and produces a gaseous mixture consisting mainly of acetic acid. (fig 3-2)

By using nitrogen as carrier gas at a flow rate of 2 lt per minute, the liberated acid was passed through 50 ml of 0.1N sodium hydroxide solution and the excess base was titrated with 0.1 N hydrochloric acid solution using phenol phthalein as indicator. The same procedure was repeated four times for each

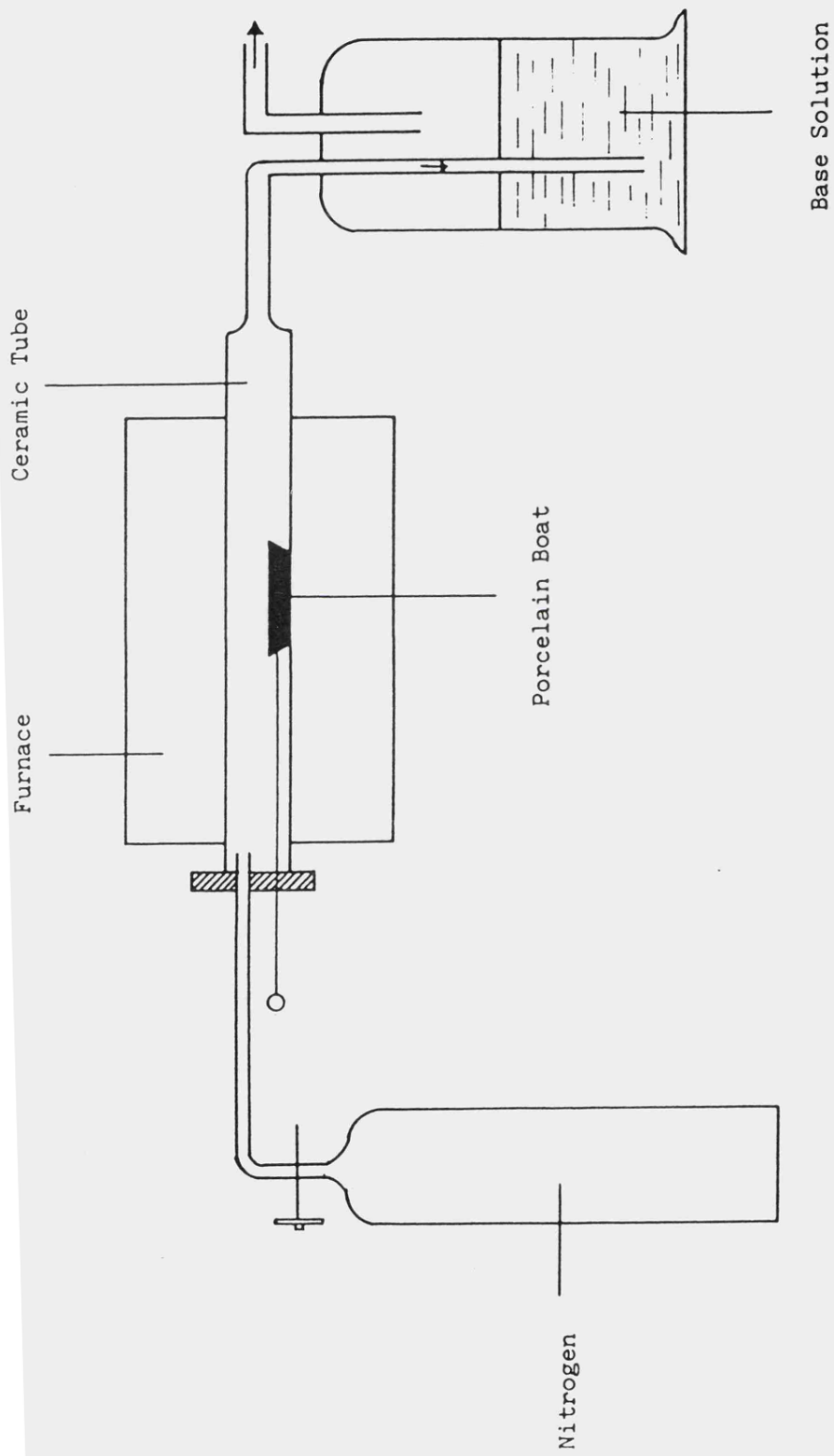


FIGURE 3-1: Experimental set up for vinyl acetate determination by thermal decomposition and titration.

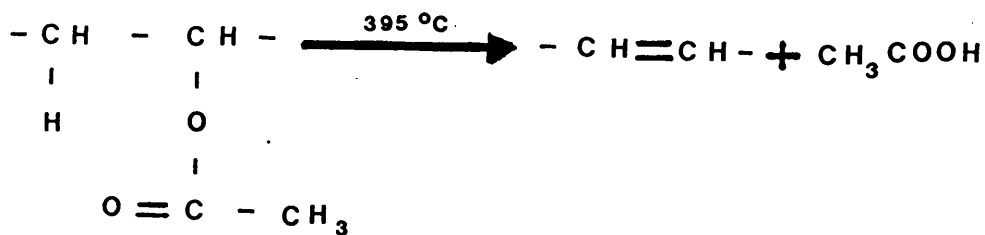


FIGURE 3-2: Decomposition mechanism of E.V.A. copolymers proposed by Grant and Grassie (93) (94).

copolymer. The vinyl acetate content was then deduced from a simple stoichiometric calculation, and the results are shown in table (3-1).

The second method employed to determine the V.A content was infra-red spectrometry. To use that method quantitatively the I.R spectrum of the polymer is initially obtained and the absorption intensity of a band characteristic of the acetoxy group is measured. Then the V.A content is deduced from standard I.R. spectra of E.V.A. copolymers. When no such standards are available, infra-red spectroscopy is used indirectly; the V.A. contents of a series of E.V.A. copolymers is determined by another method - which is more accurate - together with the corresponding ratios of



TABLE 3-1

Vinyl-acetate content of EVA copolymers measured by thermal decomposition and titration.

(95% confidence limits are indicated)

	Nominal % VA	% VA from Pyrolysis
Polymer A	28	27.5 $\pm$ 0.90
Polymer B	18	17.5 $\pm$ 0.87
Polymer C	12.5	12.0 $\pm$ 0.72
Polymer D	9	9.8 $\pm$ 0.69

characteristic infra-red absorptions; the combination of these data yields a calibration curve which can be then used for quantitative V.A. content determination for other E.V.A. copolymers.

From several infra-red peaks allowing quantitative determination the ones that have most successfully been used and gave accurate and reproducible results are the  $3460\text{ cm}^{-1}$  and  $2678\text{ cm}^{-1}$  bands (95). The former band is the first overtone of the carbonyl (C = O) stretching and the latter is due to the methylene group ( $\text{CH}_2$ ) stretching. Koopmans and co-workers measured first the V.A. content by pyrolysis and then the  $3460/2678\text{ cm}^{-1}$  peak ratios for the same polymers. They used these results to construct a calibration curve for determining the V.A. content directly from infra-red spectra. (96)

In order to obtain the I.R. spectra for the resins used in this project, a few grams of each polymer powder was pressed for 30 seconds between two 7 mm thick P.T.F.E plates heated at  $150^\circ\text{ C}$ . The resulting films were between 54 and 84  $\mu\text{m}$  thick and were used for transmission I.R spectra with a Perkin-Elmer 1420 Ratio Recording Infra-Red Spectrophotometer. One of these spectra is shown in fig (3-3). The baseline was established by extrapolating the almost horizontal shoulder in the spectrum, ie between approximately  $1900$  and  $2500\text{ cm}^{-1}$  and then the peak height ratios were measured. The resulting V.A. content values from the calibration curve in (96) are given in table (3-2). Also in table (3-2) are calculated

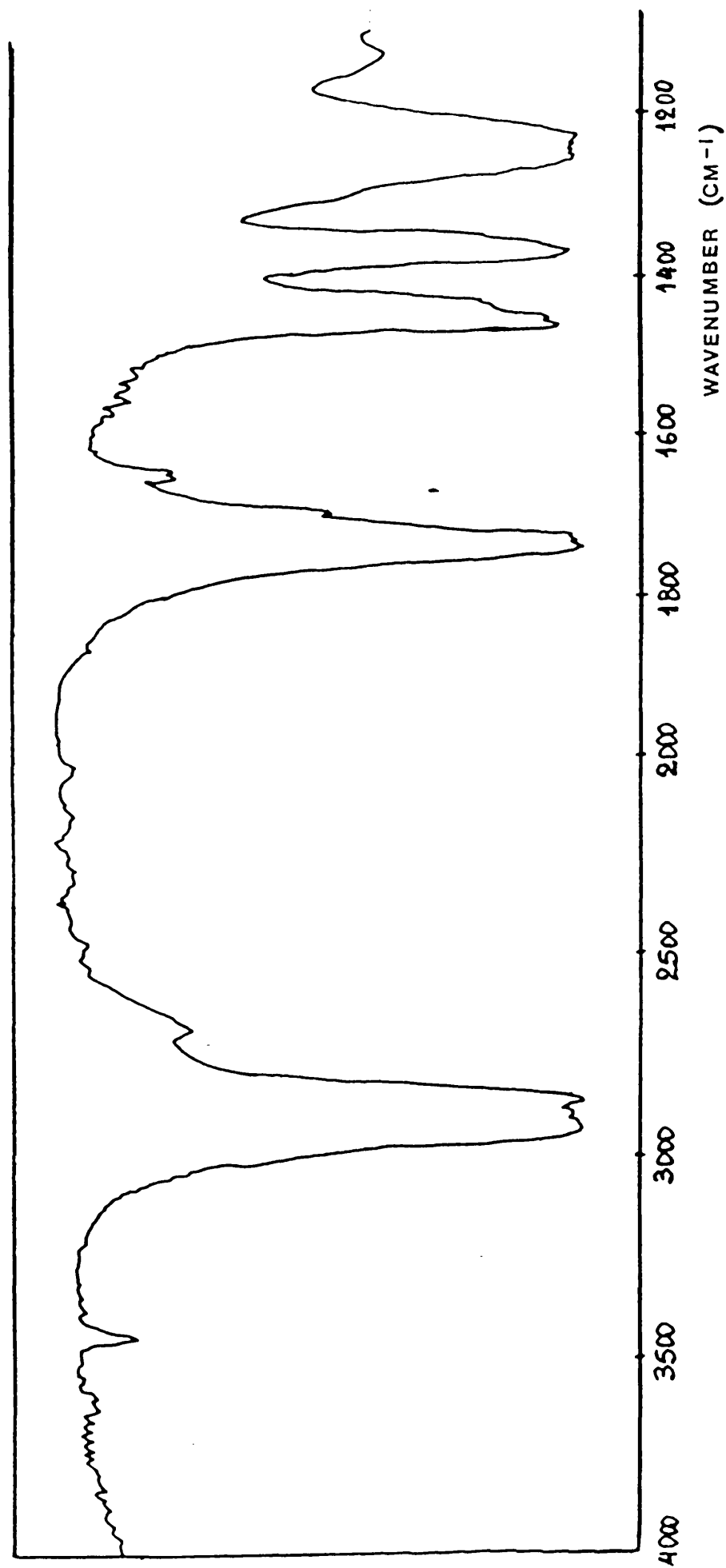


FIGURE 3-3: Transmission infra-red spectrum of an ethylene vinyl acetate copolymer. (Polymer A)

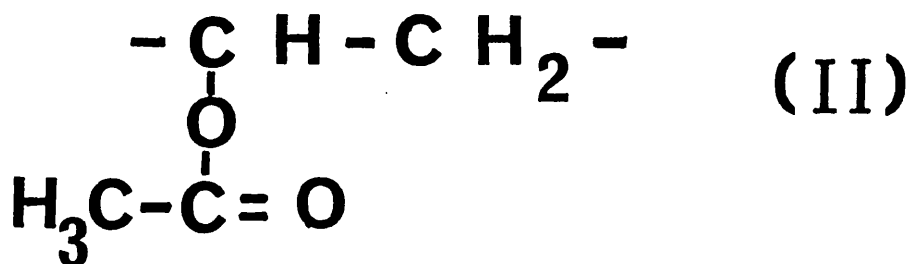
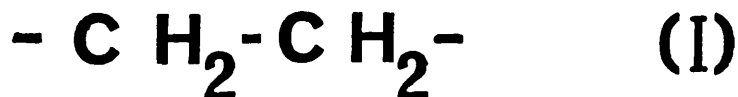
TABLE 3-2

Vinyl-acetate content of EVA copolymers measured by infra-red spectroscopy.

	Peak Height Ratio Calculated From Reference (95)	Experimental Peak Height Ratio	Nominal % VA Content	Experimental % VA Content From Infra- Red
Polymer A	0.467	0.482	28	27.9
Polymer B	0.285	0.279	18	16.9
Polymer C	0.221	0.200	12.5	10.8
Polymer D	0.173	0.166	9	8.7

peak ratios from the same calibration curve if the values of V.A. content determined previously by pyrolysis are considered. The agreement with the experimental ratios is satisfactory.

The third measuring technique was  $^1\text{H-NMR}$  spectrometry. Chen et al (97) have developed an attractive method for direct measurement of vinyl acetate content by using NMR spectra. The basis of the method is that the total area of a NMR peak consisting of overlapping peaks due to the various protons present in a molecule is proportional to the number of protons per unit weight. In ethylene vinyl acetate copolymers the following monomer units are present:



The spectral lines of such a NMR spectrum corresponding to the various protons are shown in fig (3-4). They are:

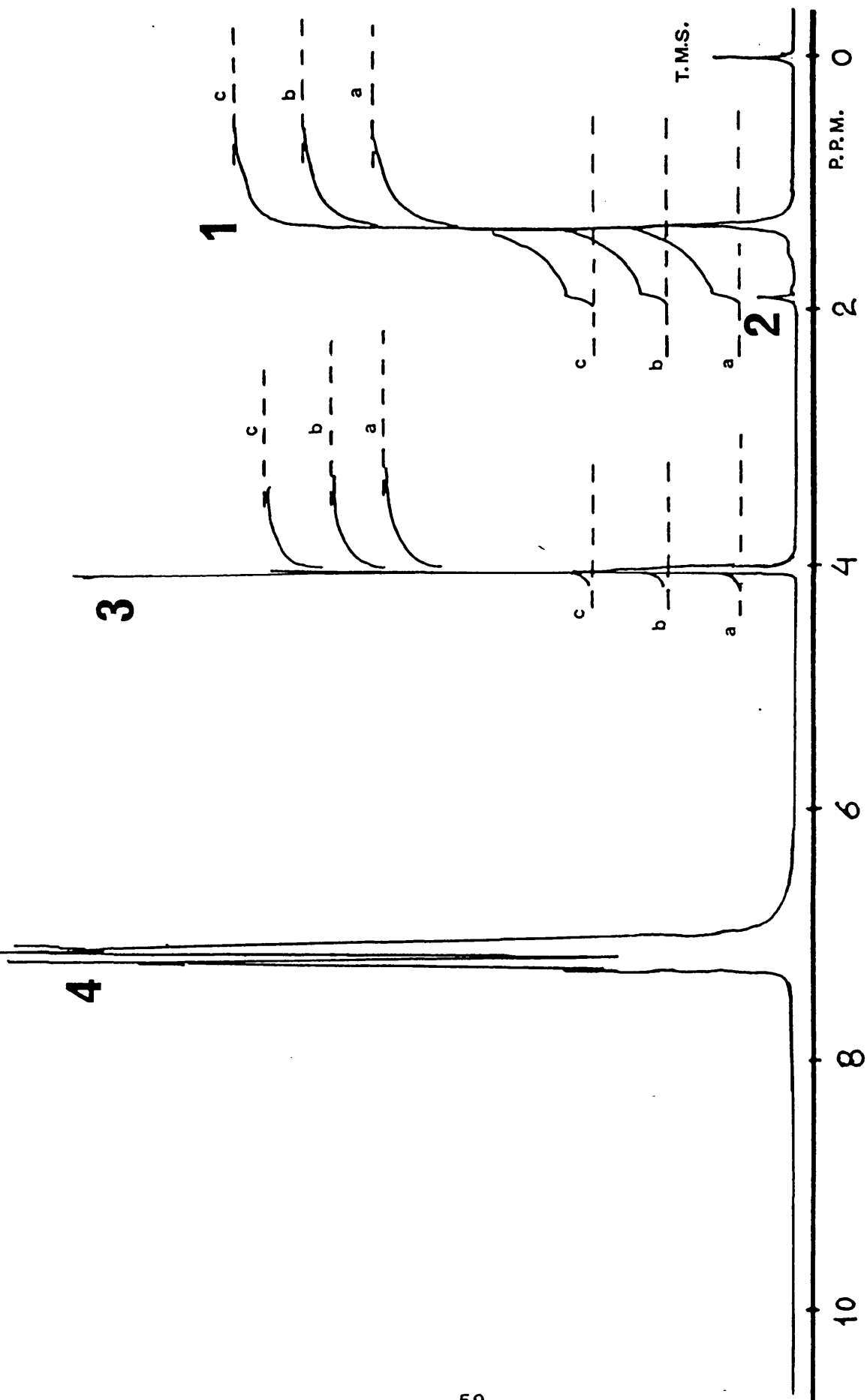
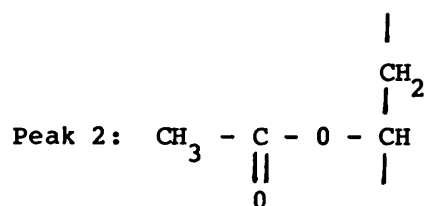


FIGURE 3-4: N.M.R. spectrum of an ethylene-vinyl acetate copolymer. (Polymer A)

Peak 1: - CH<sub>2</sub> - CH<sub>2</sub> -



Peak 4: Chlorobenzene (solvent)

If the weight fraction of vinyl acetate in the copolymer is (a) then for the total number of protons per unit weight (X) in the copolymer is:

$$X = \frac{4}{28.03} (1-a) + \frac{5}{86.05} \cdot a$$

where 4 and 5 is the number of protons contributed by monomer units (I) and (II) and 28.03 and 86.05 the corresponding molecular weights (the tertiary methylene proton in unit (II) is not included in the calculations).

A known amount of ferrocene  $W_f$  is added to the sample as an internal standard. Again the area  $I_f$  of the corresponding NMR peak (peak 3) will be proportional to the number of protons (10) per unit weight (185.92) of the ferrocene ie:

$$I_f = K \cdot \frac{10}{185.92} \cdot W_f$$

If the initial weight of E.V.A. copolymer is  $W_c$  the total area  $I_c$  of peaks 1 and 2 will by analogy be:  $I_c = K.(X).W_c$  where, as described before (X) is the number of protons per unit weight of the copolymer

The ratio of the peak areas  $I_f/I_c$  allows the calculation of (X) and hence of the weight fraction (a) of vinyl acetate in the copolymer.

To use this method small quantities of copolymer and ferrocene were accurately weighed and dissolved in monochlorobenzene. The  $^1\text{H-NMR}$  spectra were obtained with a JEOL P.S. 100 instrument operating at 100 MHz and at a temperature of  $120^\circ\text{C}$ . The peak areas were the average of three integrations represented by the distance between the horizontal parts of lines a, b and c. The integrations were done in the instrument's recorder. From the known weights of copolymer and ferrocene the value of X was calculated and finally the corresponding weight fraction of vinyl acetate (a). The results for the four polymers are given in table (3-3).

A comparison of the results of the above mentioned three methods and the values quoted by the manufacturers shows only small and rather insignificant differences. Generally, polymers A, B and C appear with an over-estimated vinyl acetate content whereas the opposite is true for polymer D.



TABLE 3-3

Vinyl-acetate content of EVA copolymers measured by  $^1\text{H}$  - NMR spectroscopy.

	Nominal % VA	NMR % VA
Polymer A	28	27.2
Polymer B	18	17.8
Polymer C	12.5	11.4
Polymer D	9	9.6

From the three different techniques used NMR allows a fast and reliable V.A. determination for resins with over 1% V.A. by weight (92). The infra red method can be equally fast, requires less expensive equipment than NMR and can also provide information about the structure of the E.V.A. copolymer. However, it relies upon the use of a calibration curve and that could introduce errors. The pyrolysis method was found to be reliable for E.V.A. copolymers having less than 50% V.A. by weight (95). The titration technique after pyrolysis can be replaced by more sophisticated methods like gas chromatography and thermogravimetry.

There is a number of different techniques available to determine the V.A. content in E.V.A. copolymers. Each technique is capable of producing results with good reproducibility. The V.A. values obtained by the three methods in this project are comparable. The choice of a particular method depends upon the available equipment and time as much as upon the additional information required from the analysis.

### 3.1.2 CRYSTALLINITY OF E.V.A. COPOLYMERS

The crystal structure of a polymer coating applied on a rigid substrate as a hot-melt can affect its adhesive properties to a great extent. The influence of the polymer crystallinity on these properties after solidification has been investigated by many authors (98) (99) (100) (32).

In E.V.A. copolymers the crystallinity is due to the polyethylene segments of the macro-molecule and therefore is progressively reduced by increasing the vinyl acetate content until the material becomes completely amorphous. And as with polyethylene, factors like short hydrocarbon chain branching can also influence the crystallinity and hence the structure and properties of E.V.A. copolymers (50).

The experimental technique employed to measure the crystallinity of the E.V.A. copolymers was X-ray diffraction. The diffraction diagrams were obtained according to the usual method used for polyethylene. Because ethylene vinyl acetate copolymers are largely amorphous the peaks in their diffraction diagrams are usually broad and dominated by a characteristic halo. Kamath et al (101) overcame this problem successfully and determined the crystallinity of these copolymers. Their approach is based on the shape and placement of the amorphous halo which has its maximum at around  $19.75^\circ$  ( $2\theta$ ).

In such a diffraction diagram in figure (3-5) the shape of the amorphous halo is represented by the dashed line. As the vinyl acetate content increases so does the area of the amorphous halo. Kamath et al (101) found that the line at  $19.75^\circ$  ( $2\theta$ ) divides the area of the halo in a constant ratio of 1.84/1.00 even as the vinyl acetate content increases. They also argued that the area  $A_1$  of the halo below  $19.75^\circ$  ( $2\theta$ ) can be considered, for all

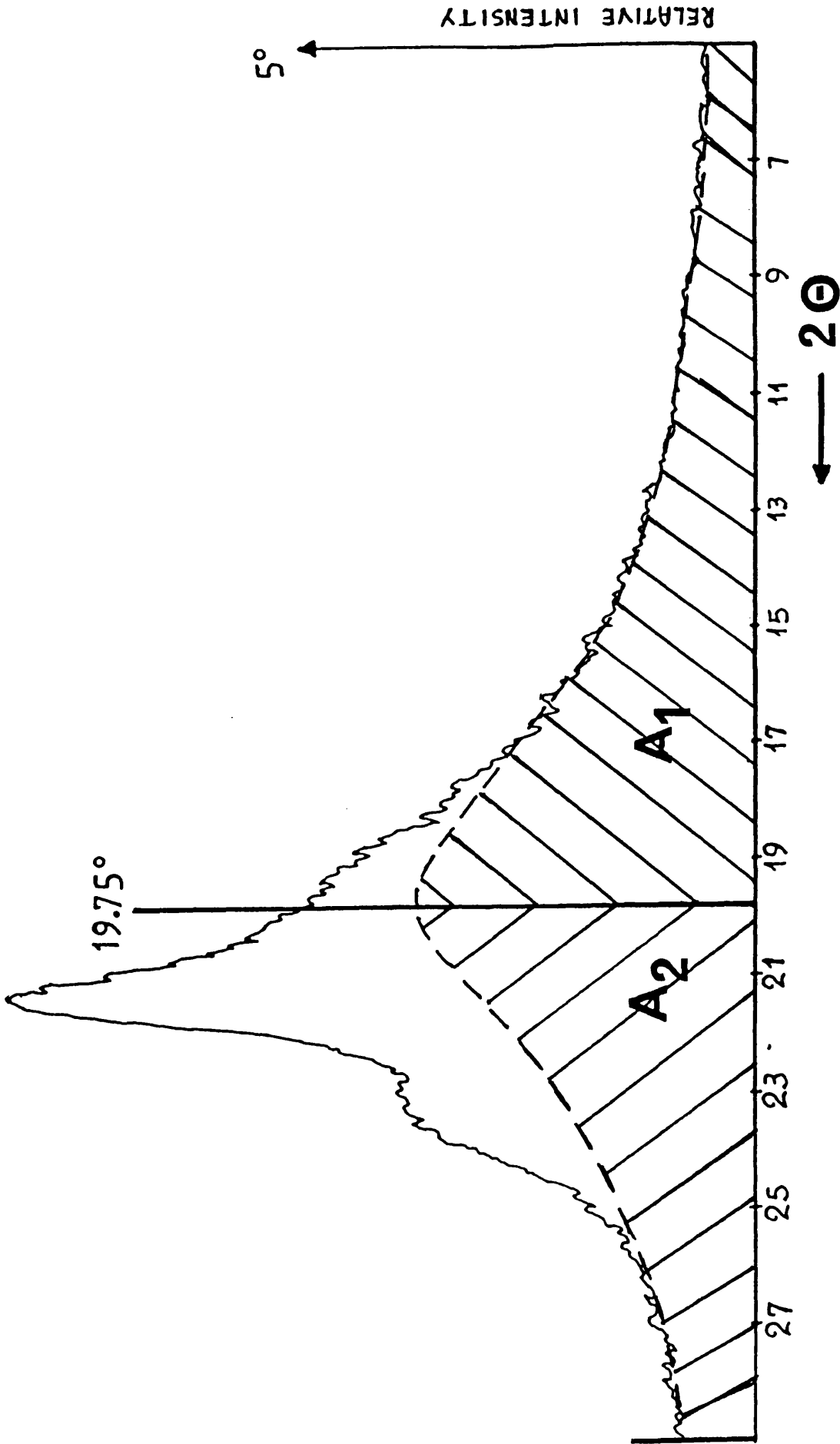


FIGURE 3-5: X-ray diffraction diagram of ethylene-vinyl acetate copolymers. (Polymer B).

practical purposes, as entirely due to the amorphous scattering alone. The above two observations allow the measurement of the amorphous fraction (a) from the areas  $A_1$  and  $A_2$  because the ratio  $A_2/A_1$  is 1.84 and proportional to (a). Hence:

$$a = K A_1 \frac{2.84}{A_1} + A_2$$

where K is a constant close to unity (101) and therefore:

$$\% \text{ Crystallinity} = 100 (1 - a)$$

For the present project the X-ray diagrams were taken with a Philips P.W. 1730 X-ray generator using a Cu target and operated at 40 KV and 20mAmps. The polymers were in powder form. The areas  $A_1$  and  $A_2$  were measured graphically and the resulting values of crystallinity are shown in table (3-4).

Kamath and Wakefield (101) found a straight line relationship between crystallinity and weight percent vinyl acetate content held for the E.V.A. copolymers they investigated:

$$\% \text{ Crystallinity} = 63.0 - 1.47 \times (\% \text{ V.A.})$$

Values of crystallinity calculated from the above equation agreed well with those determined by X-ray diffraction in this project (table 3-4).

TABLE 3-4

‡ Crystallinity of EVA copolymers measured by x-ray diffraction

	Manuf Data*	Calculated From Reference (101)**	Measured By X-Ray Diffraction
Pol A	25	21.8	22.0
Pol B	36	36.5	38.2
Pol C	48	44.6	45.9
Pol D	NA	49.0	47.3

\* The method of measuring is unspecified.

\*\* The values obtained by  $^1\text{H-NMR}$  were used to calculate the crystallinity.

### 3.1.3 MELT FLOW INDEX OF E.V.A. COPOLYMERS

Viscosity is an important factor in characterising a hot-melt adhesive. The spreading of a polymer melt across a metal surface depends strongly on its ability to flow. Cherry has directly associated joint strengths with melt viscosity (102). Schonhorn et al (103) have studied the kinetics of wetting of surfaces by polymer melts - including E.V.A. copolymers - and concluded that the rate of wetting correlates inversely with the melt viscosity.

A practical measure of a polymer's melt viscosity is its melt flow index (M.F.I). In an effort to keep the important wetting properties of the copolymers similar the four resins were chosen to have melt flow indices as close as possible. To confirm that, the melt flow indices were measured according to B.S. 2781 Part 1 Method 105C.

The conditions used were identical with those used for polyethylene M.F.I determinations, ie a temperature of 190° and a load of 2.16 kg. The results expressed as grams of polymer extruded in 10 minutes are shown in table (3-5).

For an E.V.A. copolymer of a standard vinyl acetate content there are commercially available grades with melt flow indices ranging from 1 to 400. Therefore the M.F. indices of table (3-5) for the four polymers can be considered reasonably close. These results justified the choice of the 4 resins for the purposes of

TABLE 3-5

Melt-flow index of the EVA copolymers (95% confidence limits are indicated)

	MFI Measured	MFI Quoted By Manuf.
Polymer A	7.18 $\pm$ 0.43	5.5
Polymer B	7.20 $\pm$ 0.24	10
Polymer C	3.14 $\pm$ 0.11	4
Polymer D	6.20 $\pm$ 0.08	6.3 - 7.7



the present work after considering the melt flow indices of E.V.A. copolymers available in the manufacturer's literature.

#### 3.1.4 MOLECULAR WEIGHT OF E.V.A. COPOLYMERS

The molecular weights of the E.V.A. copolymers in the present project were measured by gel permeation chromatography. The determination was conducted by the Rubber and Plastics Research Laboratories. The Mark-Houwink parameters for low density polyethylene were used as the best approximation in the calculations. The results are shown in table (3-6). The variation in both the number and weight average molecular weights in table (3-6) is clear. The number average molecular weight ( $M_n$ ) is generally inversely proportional to the melt flow index (49). For the M.F.I values measured and shown in table (3-5) this correlation yields calculated values of ( $M_n$ ) which should follow the trend of those measured. This is partially true, with polymer C having a smaller value for ( $M_n$ ) than the M.F.I suggested. This discrepancy can be due to the effect that other structural properties like short or long chain branching have on the M.F.I (49). Also, in the case of molecular weights the values are only approximate.

TABLE 3-6

Molecular weights of EVA copolymers measured by GPC. (The Mark-Houwink parameters for Low Density Polyethylene were used in the calculation).

	Mw x 10 <sup>5</sup>	Mn x 10 <sup>4</sup>	Mw/Mn
Polymer A	1.38	4.19	3.29
Polymer B	1.25	3.09	4.04
Polymer C	1.89	3.53	5.53
Polymer D	2.36	3.80	6.21

### 3.2 METALS

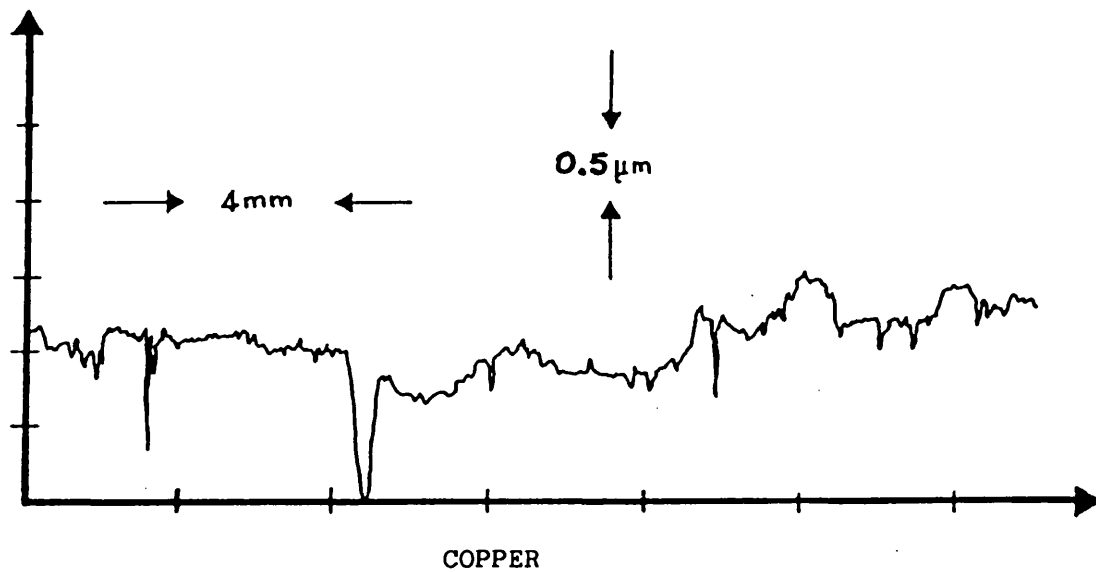
The metal substrates used in the project were as mentioned before, copper and steel.

Both metals were cut into panels 10 x 15 cm.

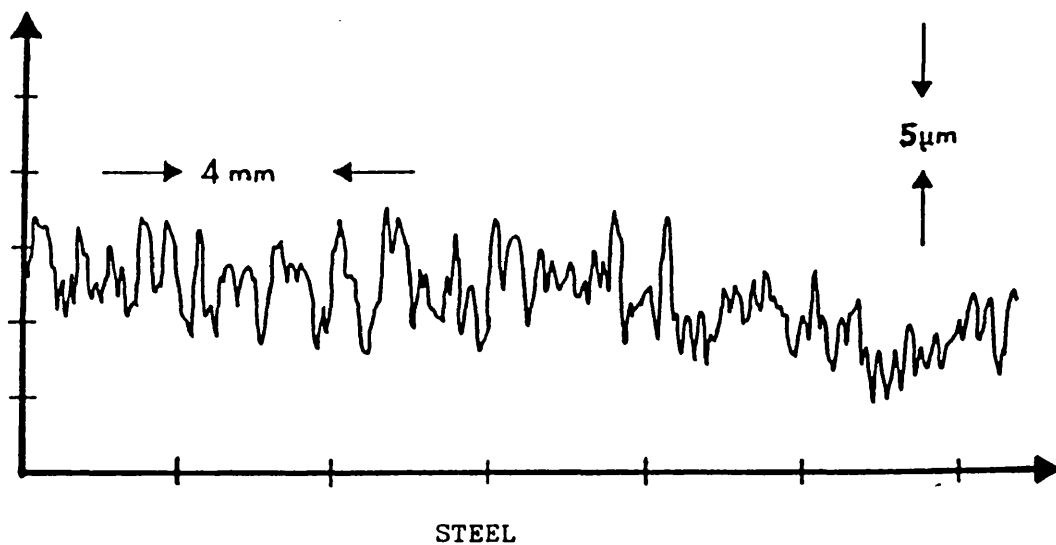
General purpose mild steel was used (B.S. 1149) supplied by Woodbery Chillcot, Bristol. Its thickness varied from 1,25 to 1,30 mm from sheet to sheet.

The copper was cut from a deoxidised sheet (B.S. 1172) which was 1,20 to 1,30 mm thick. It was supplied by H Righton, Bristol.

Many authors have reported on the importance of surface topography on adhesion. Although both metals were subsequently treated so that a reproducible metal topography could be achieved their "as received" surface roughness was measured using a Talysurf machine. For that measurement the metals were cut to small panels approximately 2 x 3 cm. The stylus of the machine was set to run at a direction parallel to the rolling lines on the metals and that was also the peeling direction during the peel tests. Two typical graphs for the two metals are shown at figure (3-6). The cut-off wave length was 25 mm in both cases. It is clear that steel in the "as received" state has a much rougher surface than copper.



Average roughness  $R_a = 0.38 \mu\text{m}$ .



Average roughness  $R_a = 1.77 \mu\text{m}$ .

FIGURE 3-6: Copy of a talysurf of steel and copper in the "as received" state.

### 3.3 PREPARATION OF TEST SAMPLES

#### 3.3.1 METAL PREPARATION

The metal preparation methods used were designed to produce three different surface topographies. The treatments follow those previously described by Packham and Evans (104) (12).

The steel panels were degreased in trichloroethane vapour for 10 minutes and then immersed in the boiling liquid for a further 10 minutes. That was followed by a 30 second room temperature etching in 5M hydrochloric acid, rinsing with distilled water and finally with Analar grade acetone. The steel surface produced was examined in a scanning electron microscope (Phot.3-1). The machining lines were visible as well as cavities along these lines approximately 60  $\mu\text{m}$  long.

The copper panels were initially washed with 5M hydrochloric acid to remove any oxide and then rinsed with distilled water and finally acetone. They were next degreased in trichloroethane vapour for 10 minutes and in the boiling liquid for a further 10 minutes. The copper panels were then immersed for 10 minutes in a polishing solution consisting of:

60 ml orthophosphoric acid (S.G. 1,75)

10 ml nitric acid (S.G. 1,42)

30 ml acetic anhydride and

8 ml distilled water

Finally, they were rinsed with plenty of water and acetone.

It was found that immediate rinse with water removes most of the viscous polishing solution and improves the polish.

Some of the copper panels were used for coating at that stage.

Their surface is relatively smooth and the grain structure can be seen under a S.E.M. (Phot 3-2).

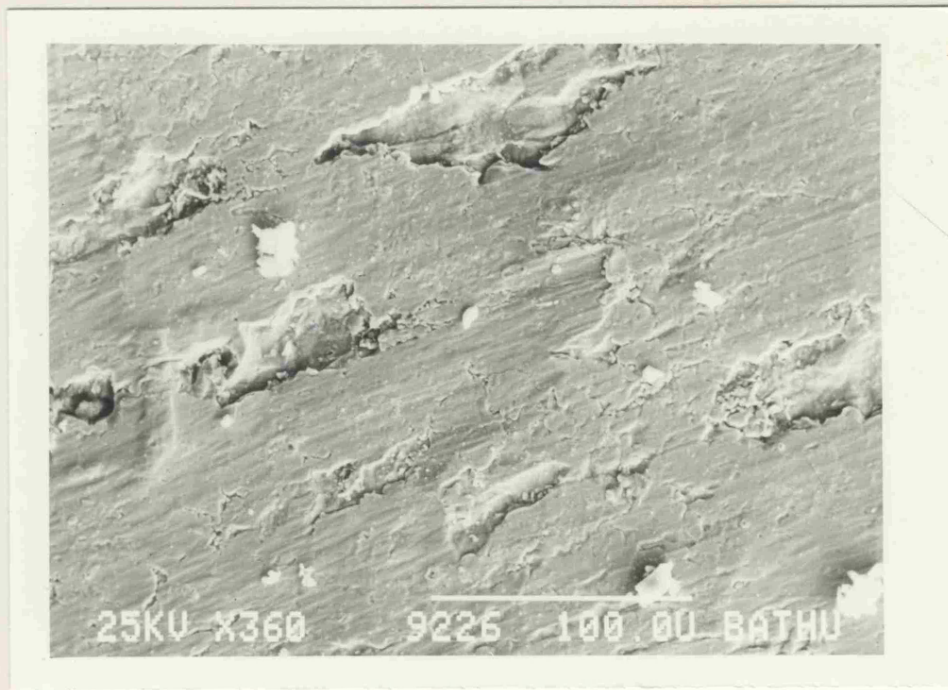
The remaining polished copper samples were given an additional chemical oxidation treatment by immersion for 20 minutes in a solution maintained at 90° C and consisting of:

3g/l sodium chlorite

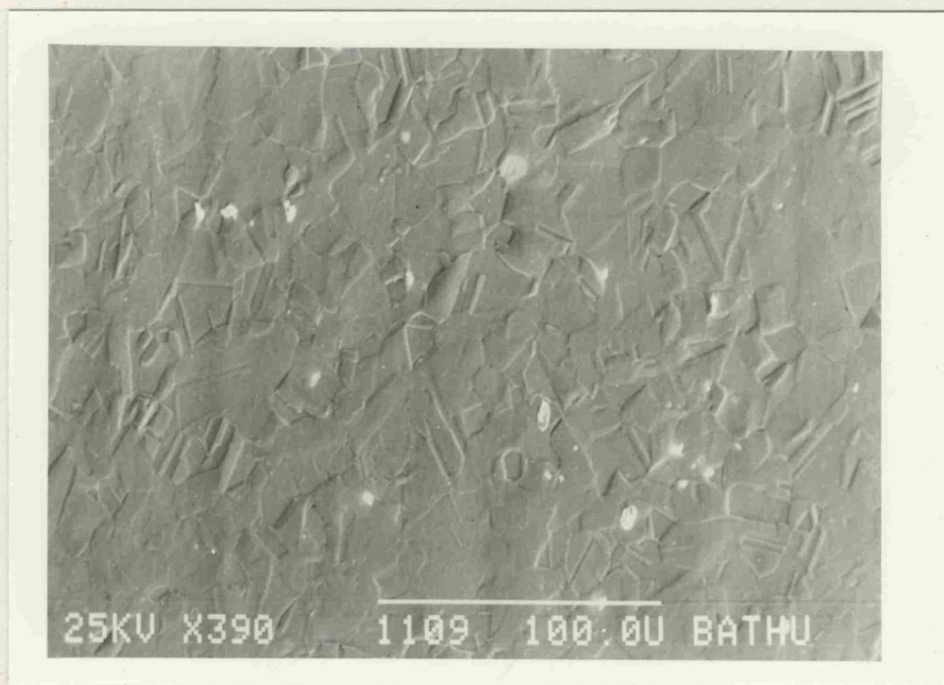
10g/l tri-sodium orthophosphate

5g/l sodium hydroxide

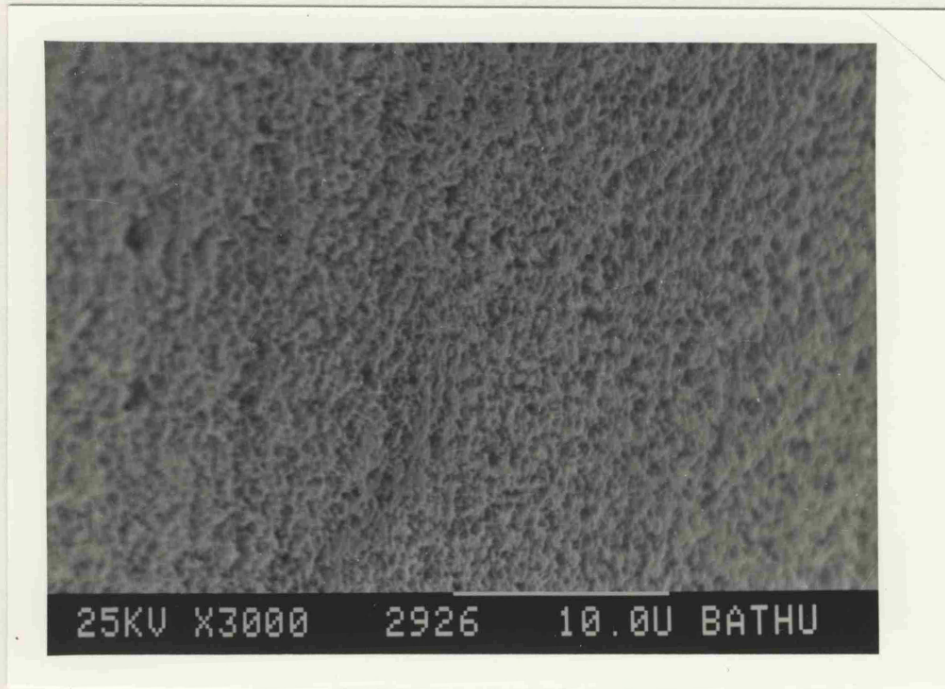
It has been found by Packham et al (12) that the copper oxide thickness increases with oxidation time. However the peel strength of polyethylene peeled from such a substrate remains practically constant after 20 minutes oxidation time. A typical topography of such an oxide is shown in photomicrograph (3-3). The grain structure of the polished copper is now covered by a uniform black fibrous copper oxide layer.



PHOTOMICROGRAPH 3-1:  
Surface of steel after etching in HCl.



PHOTOMICROGRAPH 3-2 :  
Surface of copper after chemical polishing.



PHOTOMICROGRAPH 3-3:  
Surface of chlorite oxidised copper  
prepared for coating.



### 3.3.2 PREPARATION OF COATINGS

The coating preparation was the same for all three different surface topographies. The panels were heated for 10 minutes in an oven at 200° C under a vacuum of approximately 150 torr in order to minimise the oxidation of the metal surface. They were then removed and one side was covered with ethylene vinyl acetate powder. The excess powder was then tipped off and the samples were returned to the oven for a total of 20 minutes coating period at 200° C. A vacuum was again applied for the first six minutes of the coating time to avoid air bubble entrapment at the polymer-metal interface and then the atmospheric pressure was restored. After a total of 20 minutes coating time the panels were left to cool at room temperature.

For some of the samples the coating time in the oven was 17 minutes. They were next removed from the oven and an inextensible non-dissipative fabric backing (loomstat cotton duck to B.S. 4F 55) was placed on top of the polymer. The samples were then pressed for 3 minutes at 200° C between the platters of a press using at the same time spacers to obtain the required polymer thickness.

### 3.3.3 ADHESION TEST

Strips 2 cm wide were scored on each sample and peeled at 180° on an Instron 1195 tensile test machine. The peel tests were carried out at room temperature and the cross head speed was 50 mm.min<sup>-1</sup>.

## CHAPTER 4

### RESULTS OF THE PEEL TEST

#### 4.1 PEEL LOAD OF UNBACKED SAMPLES

The force needed to peel a strip of unbacked E.V.A. polymer from a substrate increased sharply at the beginning of the peel test and then maintained a practically unchanged value. The unbacked strips showed considerable stretching during peeling, sometimes up to three times their initial length. A typical Instron trace is shown in fig (4-1). As "peel load" was taken the average recorded load during the test per unit strip width. The results for the unbacked samples are given in fig (4-2) and they refer to a standard polymer thickness. It is clear from fig (4-2) that both the type of polymer and substrate affect the measured peel load. The same results are presented in tabular form in table (4-1).

#### 4.2 PEEL LOAD OF BACKED SAMPLES

The procedure to obtain the peel loads of the backed samples was the same as for the unbacked. The backing prevented any stretching of the peeled strip. A typical Instron trace is shown in fig

(4-3) and the peel loads are given in fig (4-4). It is clear again that both the substrate and the polymer have an effect on the peel load. It is also obvious that the peel loads are generally higher than those for the unbacked samples, especially for the chlorite-formed oxide films on copper. That can be also seen in table (4-2) where the peel loads are presented in tabular form.

#### 4.3 EFFECT OF POLYMER THICKNESS

The effect that the polymer thickness has on the measured peel load has been investigated for the unbacked samples. The results are shown in fig (4-5) for oxidised copper, fig (4-6) for etched steel and fig (4-7) for chemically polished copper. There is a general increase in peel load with thickness for all the polymers and substrates. The same phenomenon has been also reported by other authors peeling polymers from rigid substrates. Gent et al (67), Igarashi (91) and Yamamoto et al (82) attribute the experimental increase in the peel force to additional energy dissipation within the bulk of the adhesive. Gardon (69) explains the observed dependence of the peel force on adhesive thickness in terms of the maximum stress developed in the adhesive layer at the failure point. Results by Aubrey et al (85) reported a similar trend which was more pronounced when slip-stick peel behaviour occurred at higher pulling rates.

Generally, one of the most extensively studied variables affecting the peel load is the thickness of the peeling member. The dependence of peel force upon the polymer thickness appears to be rather complex. Some authors have reported results indicating a maximum in the peel force with increasing coating thickness (105) (106). The stress analysis of the peel test carried out by Kaelble (65) predicts that the peel force is directly proportional to the thickness of the adhesive layer. The assumptions used by Kaelble were criticised by Gent and Hamed (84) who reported a different peel force/thickness relationship shown schematically in figure (4-8).

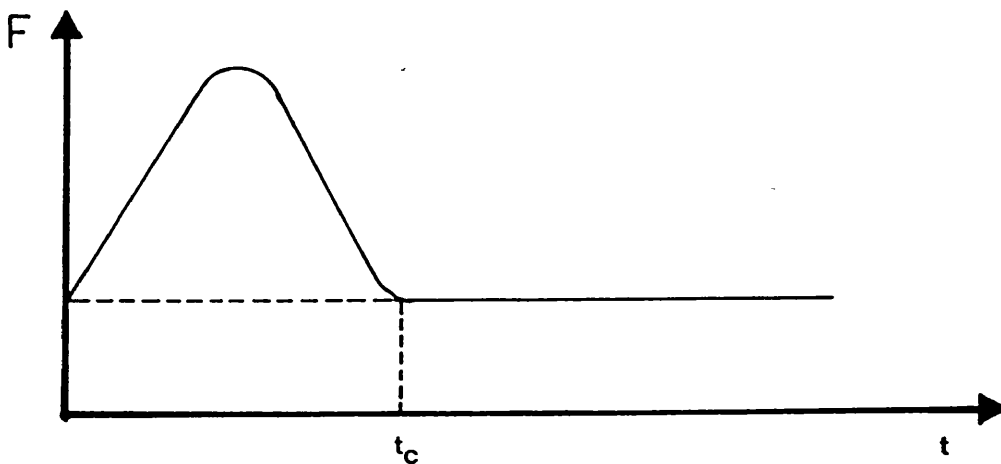


FIGURE 4-8: Variation of peel force with coating thickness (67).

For a Mylar strip bonded to styrene-butadiene-styrene triblock copolymer they found (67) that there is a critical adhesive thickness  $t_c$  above which no plastic yielding occurs and argued that energy considerations account for the dependence of fig (4-8).

In conclusion there is no universal expression describing the above relationship. It is suggested that the trends shown in figures (4-5), (4-6) and (4-7) are attributed to the increasing energy being dissipated in the polymer by the various mechanisms discussed in chapter 2.

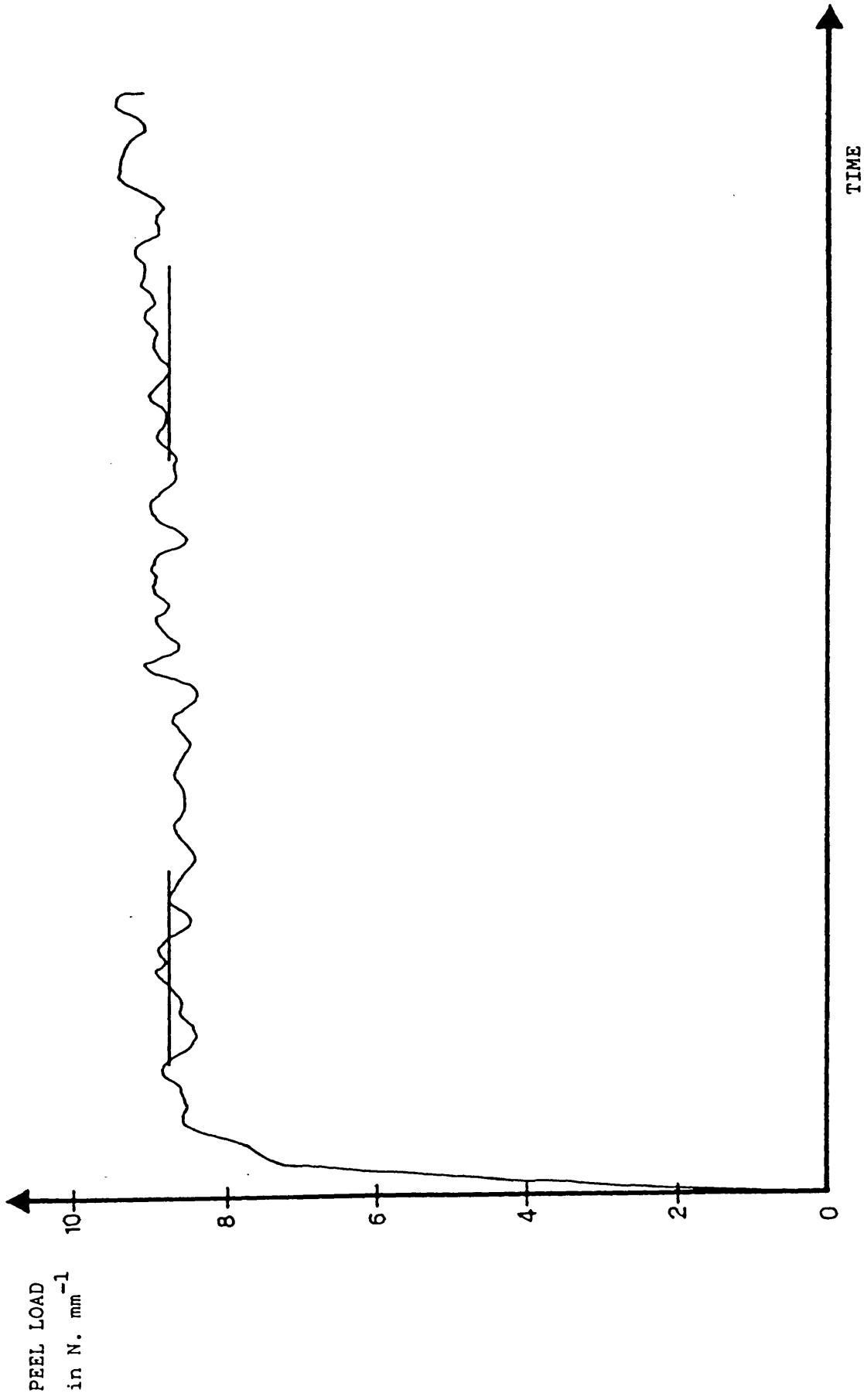


FIGURE 4-1: Copy of a typical Instron trace for unbacked samples.

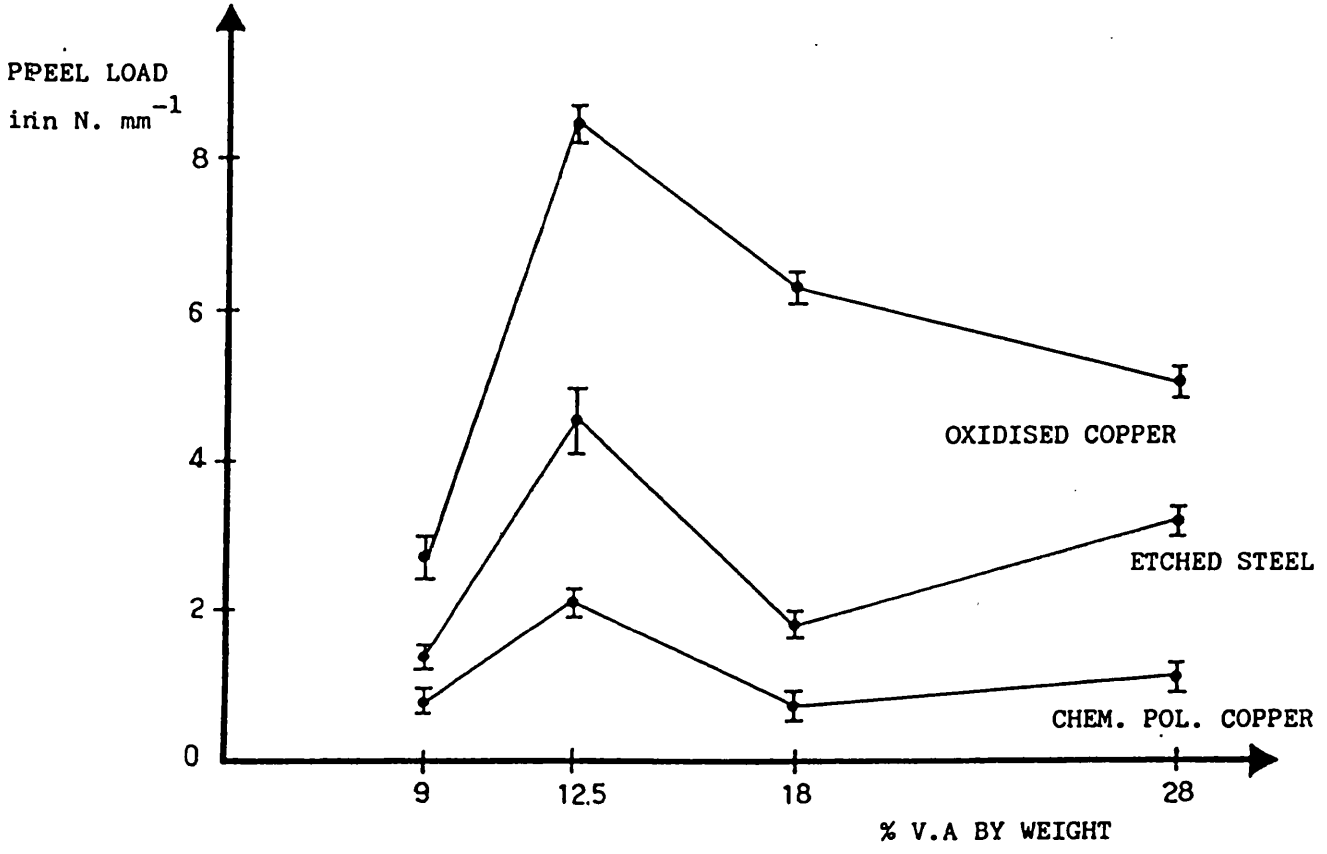


FIGURE 4-2: Peel load for unbacked strips of polymers A, B, C and D peeled from the substrates indicated. Polymer thickness 1.50 to 1.70 mm. (Bars indicate 95% confidence limits)

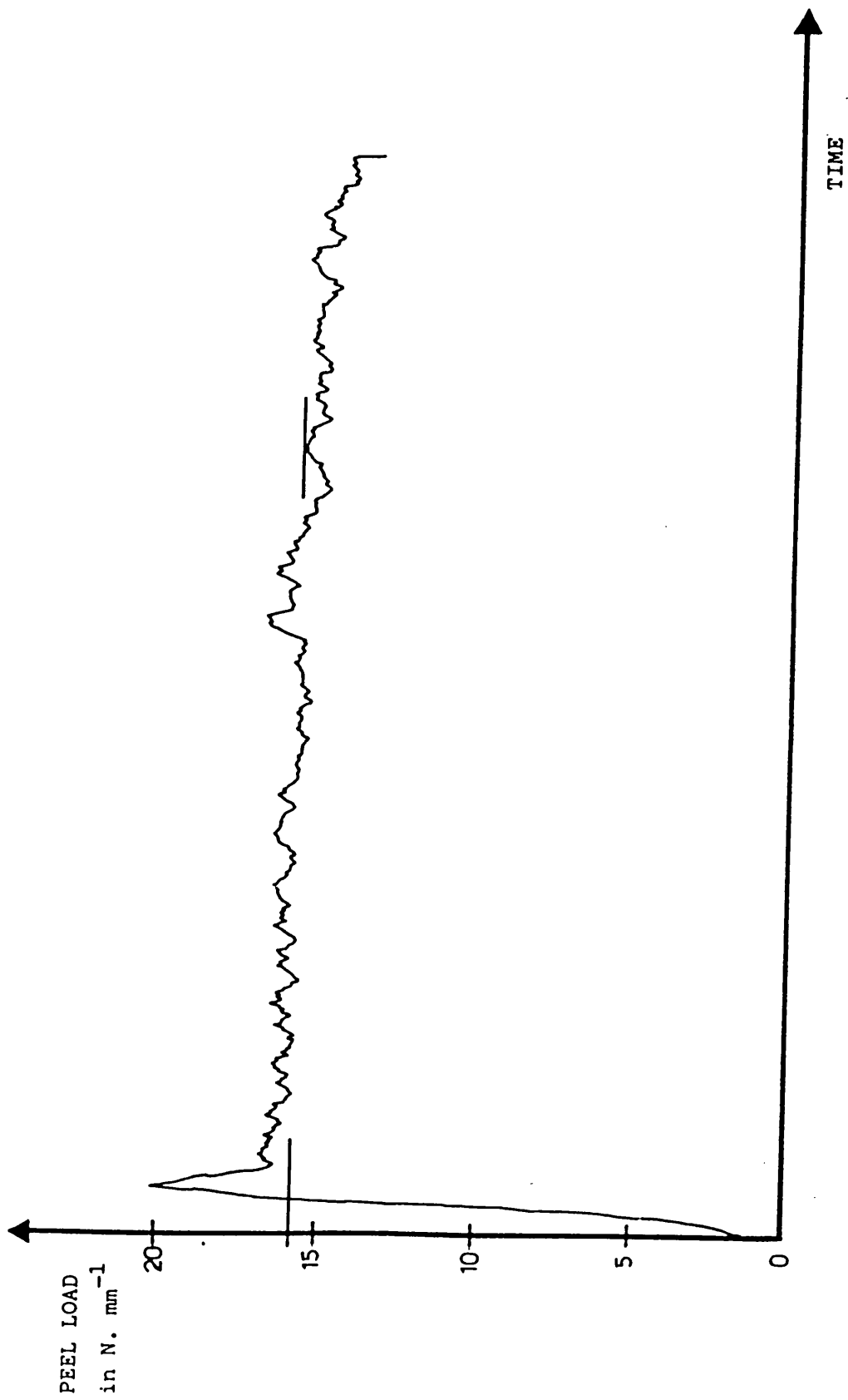


FIGURE 4-3: Copy of a typical Instron trace for backed samples.



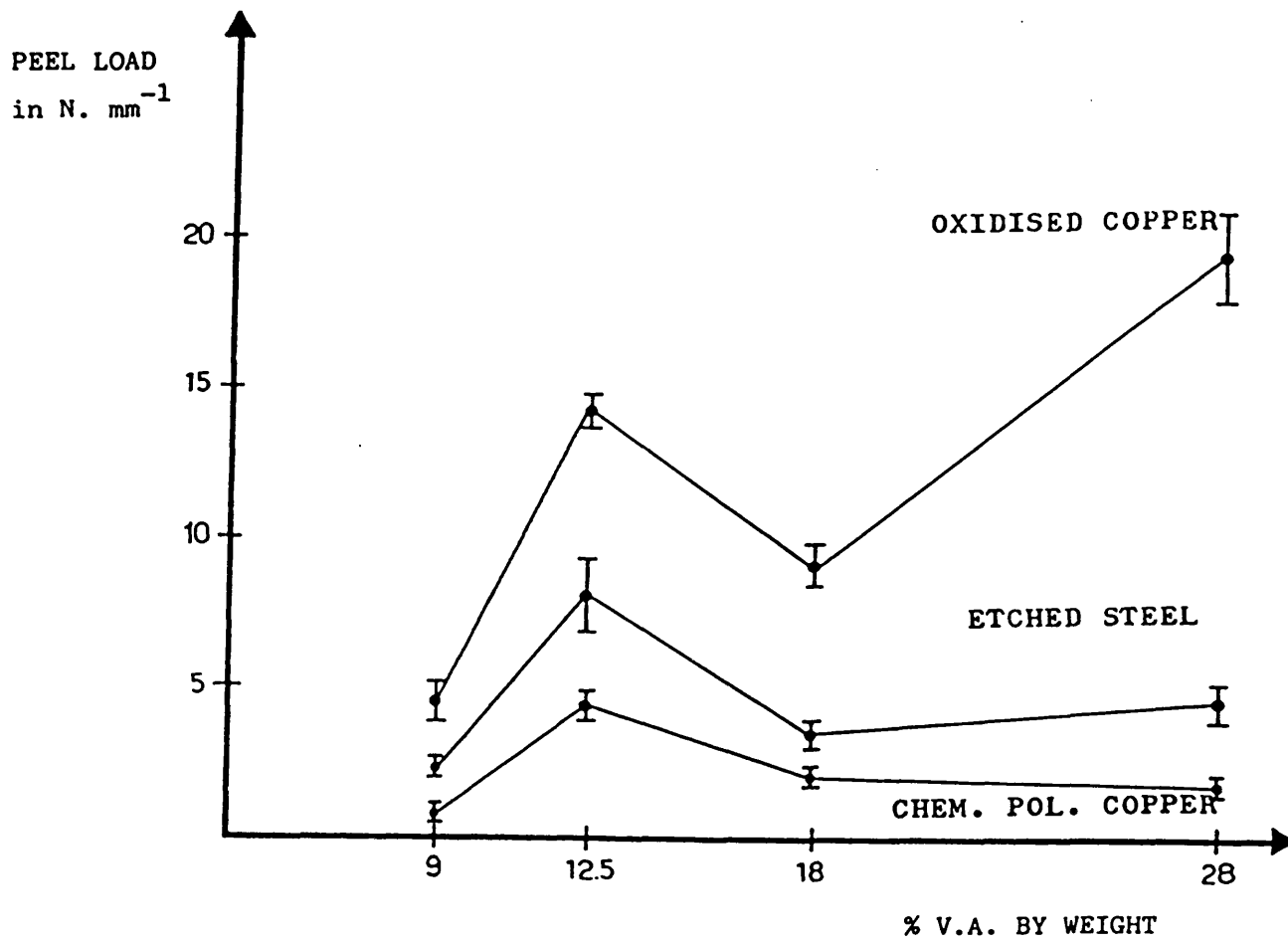


FIGURE 4-4: Peel load for backed strips of polymers A, B, C and D peeled from the substrates indicated. Polymer thickness 1.50 to 1.70 mm.  
 (Bars indicate 95% confidence limits)

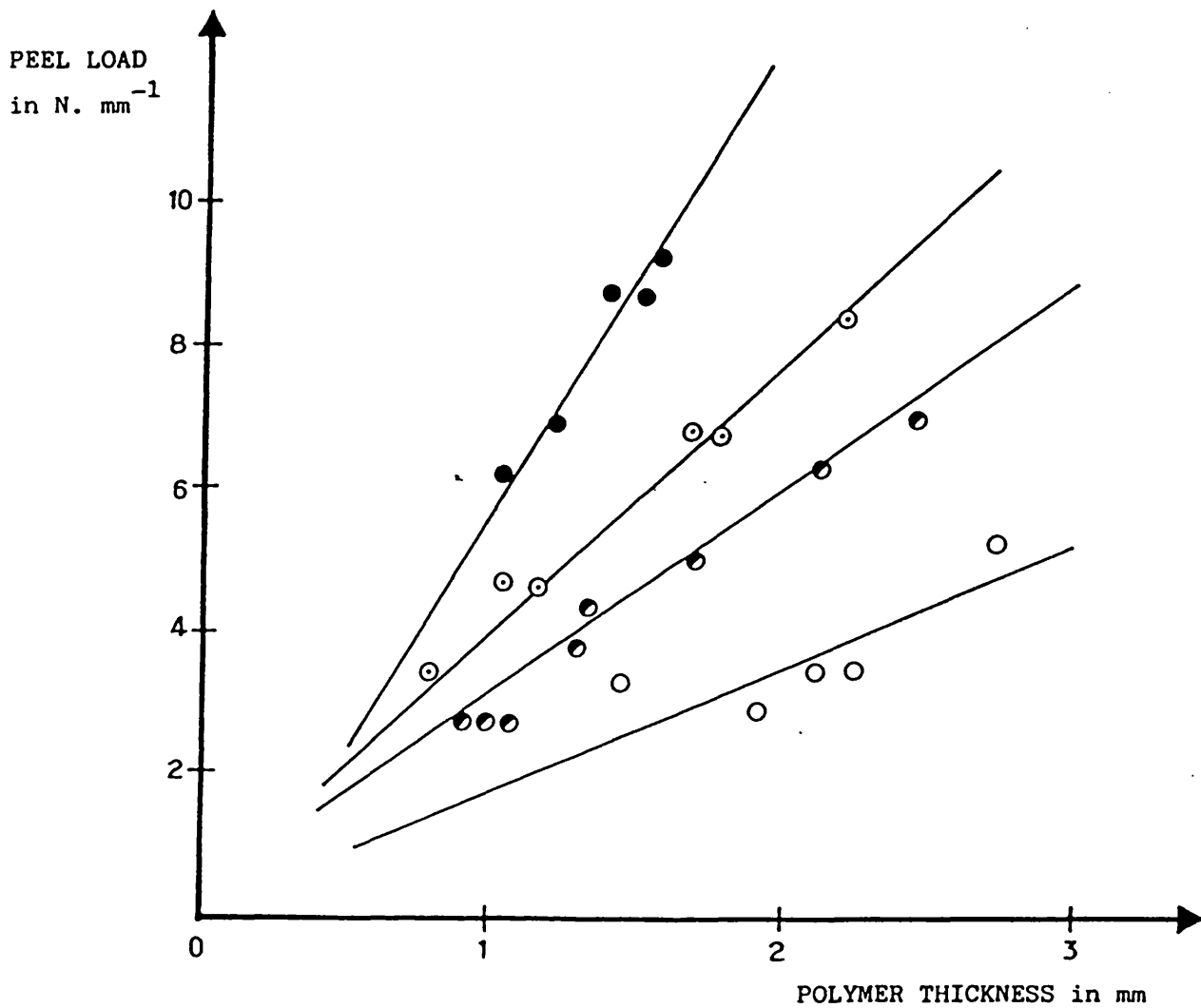


FIGURE 4-5: Peel load for unbacked samples copolymers peeled from oxidised copper.

● Polymer A, ○ Polymer B, ● Polymer C, ○ Polymer D.

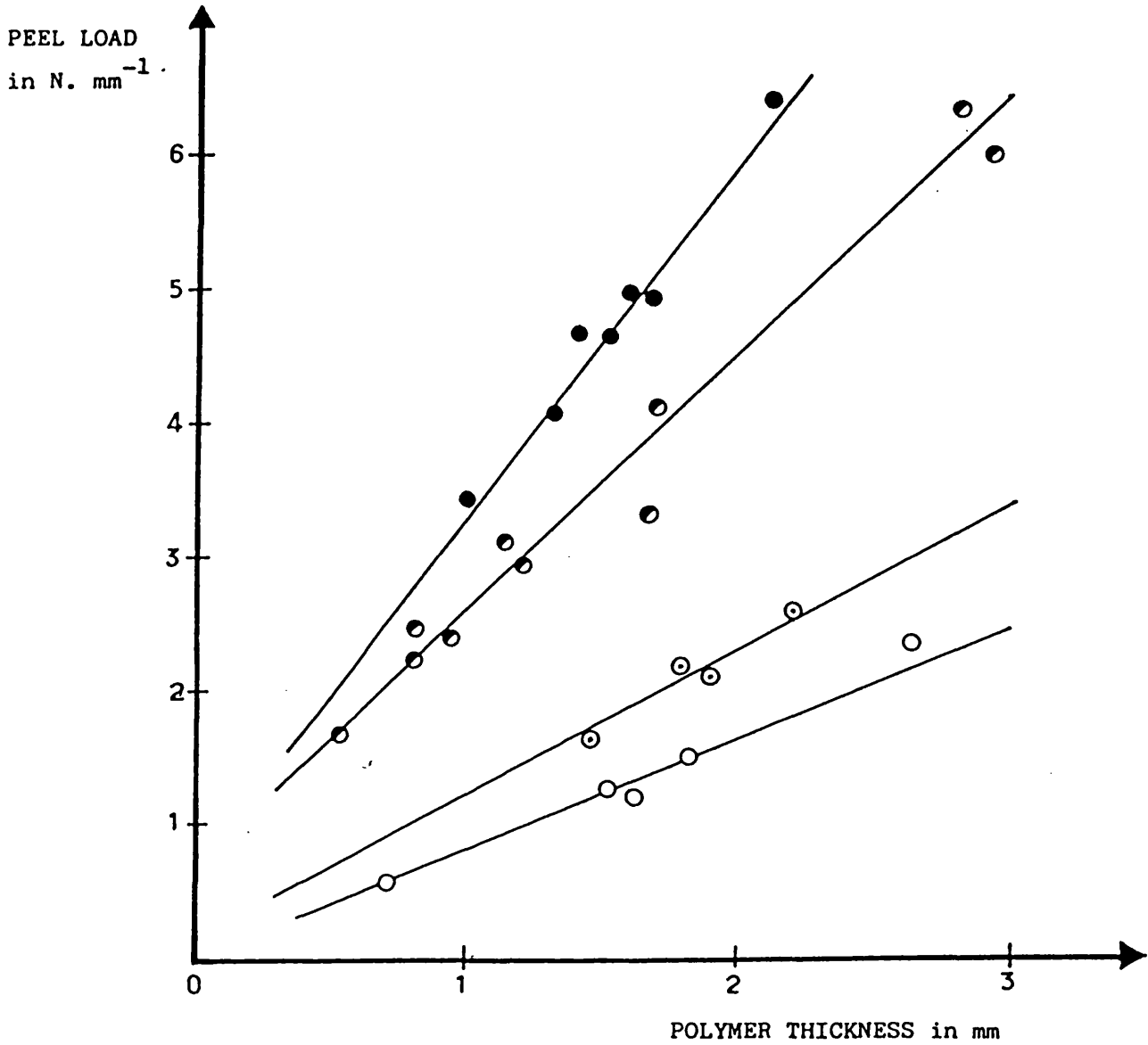


FIGURE 4-6: Peel load for unbacked E.V.A. copolymers peeled from etched steel.

● Polymer A, ○ Polymer B, ● Polymer C, ○ Polymer D.

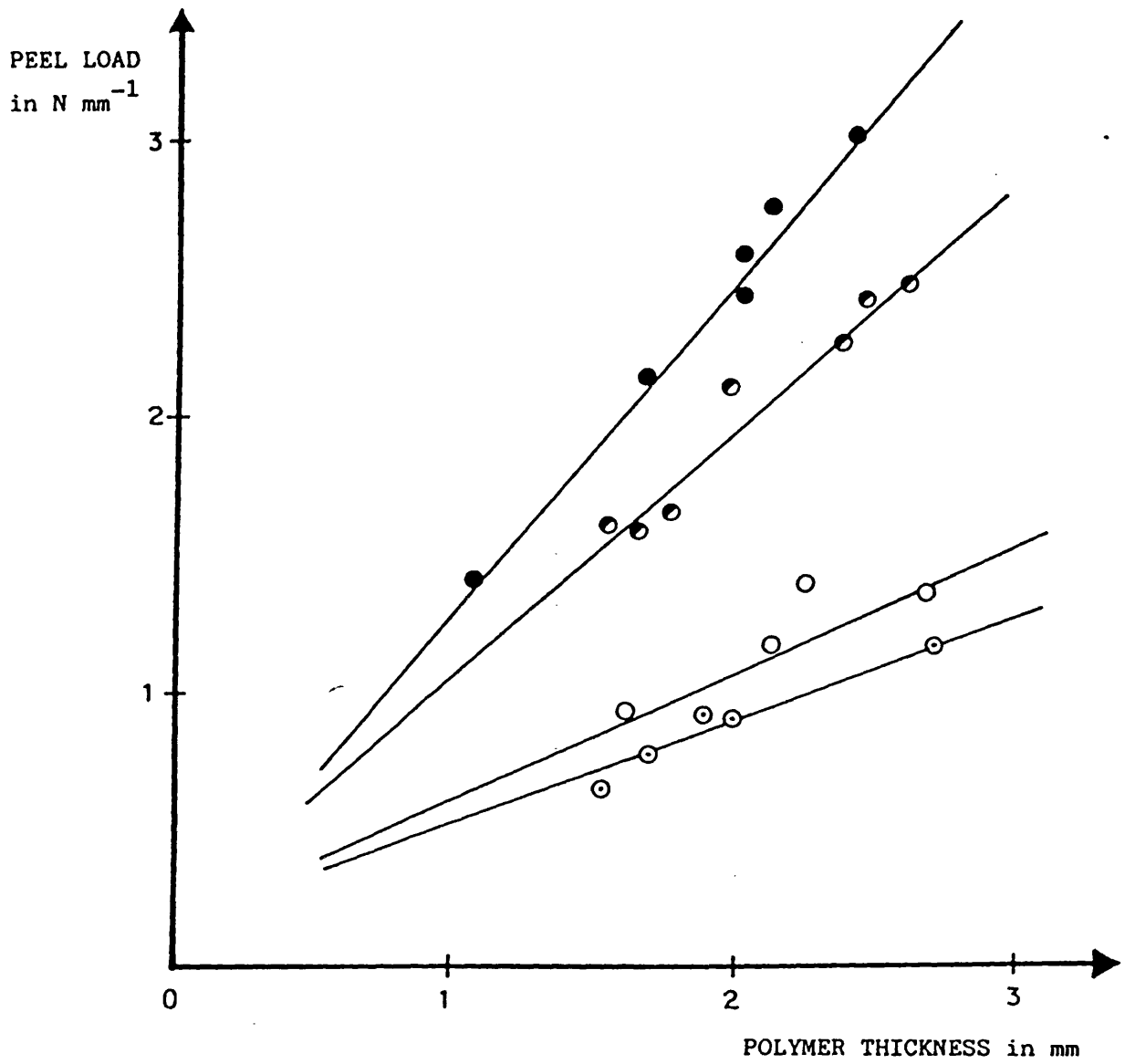


FIGURE 4-7: Peel load for unbacked E.V.A copolymers peeled from chemically polished copper.

● Polymer A, ○ Polymer B, ● Polymer C, ○ Polymer D.

TABLE 4-1

Peel load in  $N.mm^{-1}$  for unbacked strips of polymers A, B, C and D peeled from the substrates indicated. Polymer thickness 1.50 to 1.70 mm. In parenthesis are the number of strips peeled.

(95% confidence limits are indicated)

	Chem Pol Copper	Etched Steel	Oxidised Copper
Pol A	1.15 $\pm$ 0.11 (16)	3.36 $\pm$ 0.15 (16)	5.41 $\pm$ 0.30 (16)
Pol B	0.88 $\pm$ 0.06 (16)	1.89 $\pm$ 0.18 (16)	6.41 $\pm$ 0.15 (16)
Pol C	2.14 $\pm$ 0.28 (16)	4.69 $\pm$ 0.42 (16)	8.52 $\pm$ 0.18 (16)
Pol D	0.93 $\pm$ 0.15 (16)	1.39 $\pm$ 0.19 (16)	2.68 $\pm$ 0.25 (16)

TABLE 4-2

Peel load in  $N.mm^{-1}$  for backed strips of polymers A, B, C and D peeled from the substrates indicated. Polymer thickness 1.50 to 1.70 mm. In parenthesis are the number of strips peeled.

(95% confidence limits are indicated)

	Chem Pol Copper	Etched Steel	Oxidised Copper
Pol A	1.75 $\pm$ 0.15 (10)	4.85 $\pm$ 0.35 (24)	19.85 $\pm$ 1.35 (17)
Pol B	2.08 $\pm$ 0.07 (16)	2.77 $\pm$ 0.13 (20)	8.75 $\pm$ 0.87 (18)
Pol C	3.94 $\pm$ 0.19 (24)	7.71 $\pm$ 0.87 (21)	13.99 $\pm$ 0.43 (18)
Pol D	1.09 $\pm$ 0.16 (12)	2.28 $\pm$ 0.13 (12)	4.10 $\pm$ 0.33 (16)

## CHAPTER 5

### MECHANICAL TESTING OF E.V.A. COPOLYMERS

#### 5.1 INTRODUCTION

An increasing number of adhesives scientists have come to recognize the importance of the mechanical response of the adherends during a destructive test of an adhesive bond. Without overlooking the role of the interfacial forces in the measured bond strength, by using the energy balance approach adopted in this work it will be attempted to correlate the peel strengths (see chapter 4) with the mechanical properties of the coatings.

In some cases the adhesive's mechanical response during an adhesion test can be measured simultaneously (107) with specially designed devices. However, for large displacements or non-linearly elastic behaviour these measurements must be carried out separately.

Hamed (108) demonstrated that clearly when he compared the peel adhesion to a Mylar film of a styrene - butadiene-styrene triblock copolymer to that of a random styrene-butadiene copolymer. After tensile and hysteresis tests performed on the two polymers he showed that although their interfacial energies were approximately equal the difference in joint strengths were due to a great difference in the energy dissipative capacities of the materials.

In the following sections of this chapter the mechanical properties of ethylene vinyl acetate copolymers connected to the energy dissipation mechanisms discussed in chapter 2 will be determined. The results presented in the following sections will be used in a later chapter where a full analysis of the measured peel loads will be attempted.

## 5.2 TENSILE PROPERTIES

The first category of mechanical properties to be studied is tensile. Parameters obtained in a tensile test like the yield stress, the yield strain and strain energy to failure are introduced in expressions describing the various energy loss mechanisms (chapter 2) and therefore they were measured. The initial tensile tests were performed on rectangular strips cut from a polymer sheet. That sheet was prepared from the polymer powder using a procedure similar to that used in producing peel test specimens.

A metal plate 15 cm x 15 cm was the "substrate" and to avoid adhesion of the polymer it was sprayed in advance with a PTFE mold release agent. The sheet was left to cool on the bench, then removed from the metal and the rectangular strips were cut with the sharp knife to dimensions identical to those of strips of the peel test samples. The next step was to check whether the deformation on the testpiece would be spread uniformly along its length. That was achieved by drawing thin parallel lines with a marker on the polymer 5 mm apart and measuring the distance between them at various extensions. For the four polymers tested the uniformity of the deformation was found satisfactory up to near failure strains but the rectangular test pieces proved inaccurate to measure the ultimate tensile properties of the materials; at high elongations the polymer became thinner and was gradually slipping through the Instron grips, thus changing the volume of the material



being tested and introducing errors. That problem occurred at all the cross head speeds tried, and these were 10, 20, 50 and 100 mm min<sup>-1</sup>.

At that stage samples cut according to BS 2782 Method 320A to a dumb-bell shape were tried, the polymer sheet being prepared as described before. The uniformity of the extension was again checked by the same method over the "effective" length of the testpiece and found to be satisfactory.

Several methods were tried in order to measure the strain during the tensile test. The first method involved the use of an elastomeric extensometer which was connected to the polymer specimen. The two grips were clamped to the gauge length of the specimen and an electrical signal from each grip monitored the separation. However, this method was abandoned because the force needed to keep the extensometer attached to the specimen was too large creating thus three separate "regions" on the polymer. When this force was reduced, slipping of the specimen through the grips of the extensometer occurred. At very high elongations the weight of the attachment could also become important because it increases the load imposed on the specimen and introduces errors. Therefore that method was not accurate for testing the E.V.A. copolymers.

The second technique to measure the polymer extension was by holding alongside the specimen a set of spacers open at increasing lengths and mark on the chart the moment that the extension of

the testpiece equaled that of the hand-held scale. It was proved to be a very tedious method to obtain a full stress-strain curve requiring a lot of experiments for one curve. In addition, the accuracy of this method was very poor especially for high test speeds.

Finally, the stress-strain curve was obtained directly from the Instron chart (force/time) by measuring the initial distance between the grips and knowing the speed of grip separation and of chart movement. Both speeds were beforehand checked with a chronometer and found accurate within + 2% of the machine settings. Then at regular time intervals of 12 seconds on the time axis of the chart the stress and strain were calculated by referring to the time-load experimental line.

That was achieved by dividing each load by the original cross-section area of the testpiece (stress) and by converting time to cross-head movement and dividing this by the original undeformed testpiece length which was kept constant at 72 mm (strain). Four sets of experimental stress-strain results were carried out for each polymer and strain rate. The average values of the four stresses corresponding to a particular strain were initially plotted and connected with a line drawn by hand. The shape of the resulting stress-strain curve (figure 5-1) was such that an analytical expression for it, ie an equation, was extremely difficult to obtain. Instead, the experimental points were fed in a Commodore

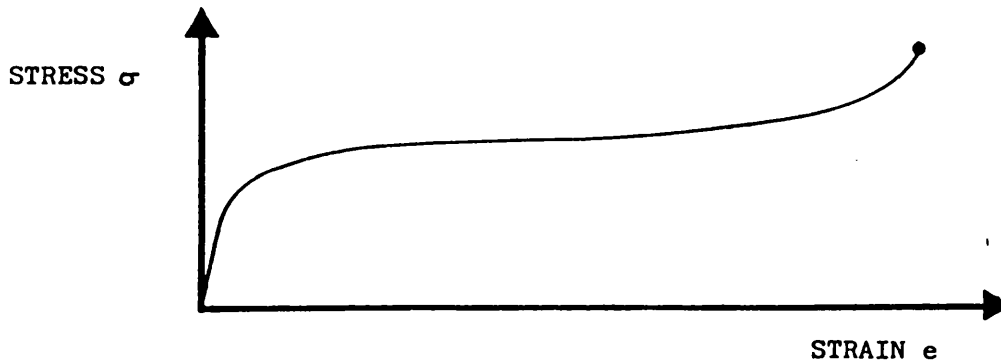


FIGURE 5-1: The shape of a typical stress-strain curve of an E.V.A. copolymer.

PET computer and a cubic function was fitted between every two successive points. The number of experimental points was large to ensure a satisfactory approximation of the resulting line to the shape of the stress-strain curve. The advantage of using the computer was that the program was capable of calculating fast and accurately the area under the stress-strain curve for any strain value required, an operation used extensively in the energy analysis that followed (chapter 7). Three different cross-head speeds were used which when divided by the original undeformed length of the testpiece of 72 mm correspond to the following strain rates: 0.27, 1.38 and  $6.94 \text{ min}^{-1}$ . A copy of such a stress-strain curve is

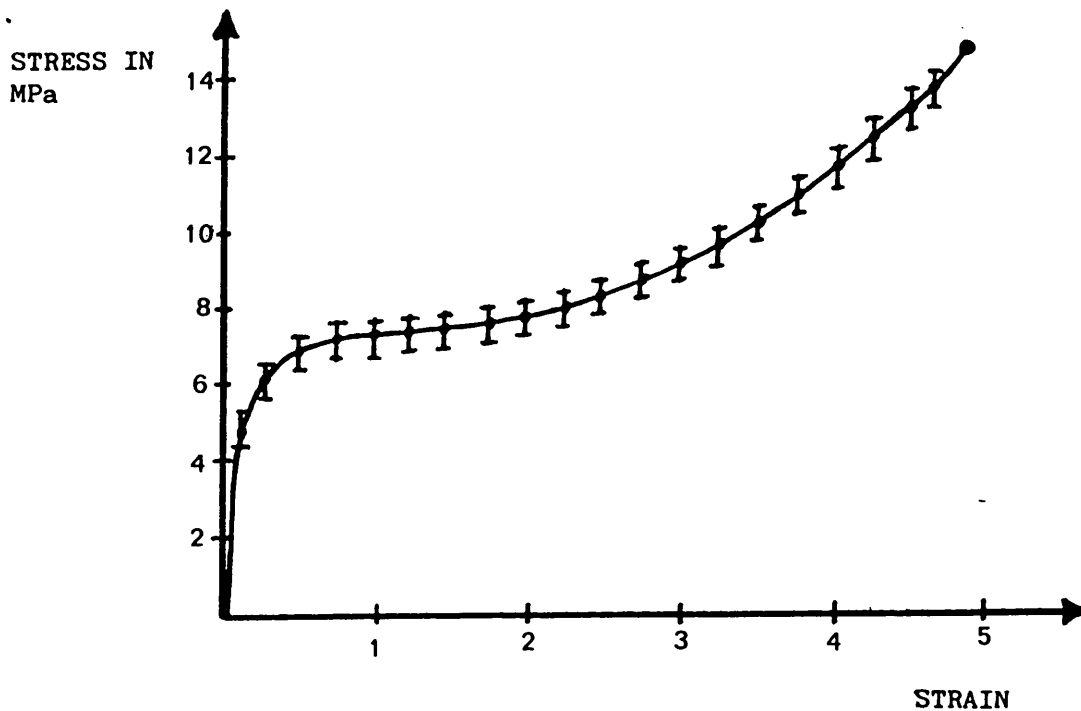


FIGURE 5-2: Stress-strain curve for a dumb-bell specimen of polymer D. Strain rate:  $1,38 \text{ mm}^{-1}$

shown in figure (5-2) for a strain rate of  $1.38 \text{ min}^{-1}$  and for polymer D. Generally, there was significant variation among the various stress-strain curves depending upon the polymer tested and the strain rate used. That was reflected in the total energy that a dumb-bell shaped specimen required to break in tension. This strain energy density to failure was calculated directly from the stress-strain results stored in the computer and the obtained values are shown in table (5-1). It is clear from table (5-1) that for a particular strain rate the strain energy density does not follow the decrease of vinyl acetate content from polymer A to polymer D. That is an indication that although the amount of vinyl acetate dominates the behaviour of these copolymers, other properties can also exert a certain influence on their mechanical

TABLE 5-1

Strain energy density (in  $\text{MJ.m}^{-3}$ ) for dumb-bell shaped specimens of E.V.A. copolymers tested in tension.

(95% confidence limits are indicated)

	$0.27 \text{ min}^{-1}$	$1.38 \text{ min}^{-1}$	$6.94 \text{ min}^{-1}$
Pol A	$55.3 \pm 6.7$	$153.3 \pm 30.9$	$186.6 \pm 44.3$
Pol B	$44.7 \pm 3.0$	$110.4 \pm 11.4$	$77.6 \pm 8.6$
Pol C	$49.2 \pm 5.7$	$114.8 \pm 4.3$	$98.0 \pm 6.6$
Pol D	$38.4 \pm 2.9$	$80.95 \pm 27.6$	$79.5 \pm 20.4$

resonse, eg their molecular weight and molecular weight distribution (49).

From the same stress-strain curves three more parameters were measured; the maximum tensile strength, the maximum elongation at break and the Young's Modulus.

The maximum tensile strength at break was calculated by dividing the maximum load at break by the original cross-section of the specimen. Results for three cross-head speeds are shown in table (5-2).

The maximum elongation at break was calculated from the time needed for failure as it was recorded in the Instron chart and from the known test rate. The results expressed as a percentage of the original specimen gauge length are given in table (5-3).

Finally, the Young's Modulus of the polymers was measured graphically from the  $\sigma/e$  curves; two points close to each other were selected on the initial linear portion of the  $\sigma/e$  curve and the difference  $\Delta\sigma$  in the stresses corresponding to these points was divided by the corresponding difference in strains  $\Delta e$  to give the elastic modulus. This linear part was relatively small so the use of a ruler ensured that the two points chosen were actually lying on that part. The moduli for three crosshead speeds are shown in table (5-4).

TABLE 5-2

Maximum tensile strength at break of EVA copolymers tested according to BS 2782, Method 320 (in MPa)

(95% Confidence Limits are Indicated)

	0.27 min <sup>-1</sup>	1.38 min <sup>-1</sup>	6.94 min <sup>-1</sup>
Pol A	19.14 + 1.31	18.95 + 1.16	17.66 + 0.95
Pol B	16.16 + 0.83	16.58 + 0.55	10.69 + 0.98
Pol C	17.94 + 0.42	17.10 + 0.27	13.52 + 0.56
Pol D	13.23 + 0.67	14.90 + 0.46	11.23 + 0.40

TABLE 5-3

Maximum elongation at break of EVA copolymers tested according to BS 2782, Method 320 (as % of init. length)

(95% Confidence Limits are Indicated)

	0.27 min <sup>-1</sup>	1.38 min <sup>-1</sup>	6.94 min <sup>-1</sup>
Pol A	899 + 28	842 + 37	708 + 41
Pol B	593 + 34	574 + 22	506 + 31
Pol C	563 + 24	538 + 14	534 + 16
Pol D	395 + 17	421 + 71	472 + 130

TABLE 5-4

Elastic Modulus of EVA copolymers tested according to BS 2872, Method 320 (in MPa)

(95% Confidence Limits are Indicated)

	0.27 min <sup>-1</sup>	1.38 min <sup>-1</sup>	6.94 min <sup>-1</sup>
Pol A	13.7 + 1.2	16.6 + 1.1	19.5 + 1.0
Pol B	41.3 + 4.4	57.3 + 5.5	75.2 + 2.6
Pol C	72.9 + 3.9	86.9 + 2.4	99.1 + 2.3
Pol D	98.5 + 9.7	110.6 + 2.0	109.3 + 28.9

The results given in tables (5-2) (5-3) and (5-4) are consistent with those quoted in the literature (49) as well as with data provided by the manufacturers (109) (110).

In order to calculate the energy associated with plastic bending of the polymer strip during peeling it was necessary to have values of the yield stress and yield strain for the four polymers (chapter 2). For coatings of varying thickness the yield stress and strain in the region of the strip undergoing plastic deformation also varies. Therefore for the same peeling rate each coating thickness corresponds to a different strain rate and hence the appropriate  $\sigma/\dot{\epsilon}$  curve should be used to obtain the yield values.

Thus, the change of yield stress  $\sigma_y$  and yield strain  $\epsilon_y$  with the applied strain rate was studied. The strain rates used for that experiment were 0.027, 0.069, 0.27, 1.38 and 6.94  $\text{min}^{-1}$ . The polymer was again cut to dumb-bell specimens and the yield point was determined with a graphical method.

By making use of the ruler the elastic (linear) part of the load-time curve was first drawn as described in the measurement of the elastic modulus. As the (plastic) second part of the same curve was conventionally taken the near-parallel to the strain axis section and also that up to approximately one third of the total elongation. The equations of these two straight lines were then derived from experimental points lying on them and the load and time values which satisfied both equations were used to



calculate  $e_y$  and  $\sigma_y$ . The extrapolation method to determine the yield point is often used for polymers with no distinct change from elastic to plastic behaviour as it was exhibited by the E.V.A. copolymers. The so determined  $e_y$  and  $\sigma_y$  values are shown in table (5-5).

To check the validity of the extrapolation method the yield stress and strain were measured experimentally. The procedure consisted in loading and unloading the sample continuously - starting from very small loads - and gradually increasing that load. The trace of the pen was observed when the load was taken off. When it did not follow the path of the loading line for the first time (indicating plastic deformation) the previously applied load and extension were recorded and considered as  $e_y$  and  $\sigma_y$ . This method obviously relies on using load steps as small as possible to make sure that the yield point is not surpassed. Additionally the faster the test rate the more difficult it becomes to control these load steps. Table (5-6) contains results obtained with this method. Values for strain rate of  $6.94 \text{ min}^{-1}$  are not included due to the large errors involved when they were measured.

By comparing tables (5-5) and (5-6) it is obvious that the experimental values are generally lower than those from the extrapolation method. That should be expected since the yield point determined graphically is always found to be above the  $\sigma/e$  curve resulting in higher values for  $e_y$  and  $\sigma_y$ . However, the results of table (5-5)

TABLE 5-5

Yield stress and yield strain of EVA copolymers measured by the extrapolation method

$\sigma_y$ (in MPa)					
	$0.027 \text{ min}^{-1}$	$0.069 \text{ min}^{-1}$	$0.27 \text{ min}^{-1}$	$1.38 \text{ min}^{-1}$	$6.94 \text{ min}^{-1}$
Pol A	1.989	2.045	2.110	2.231	2.330
Pol B	3.120	3.406	3.842	4.320	4.831
Pol C	4.070	4.387	4.951	5.291	5.962
Pol D	4.232	4.951	5.370	5.897	6.107
$e_y$					
Pol A	0.099	0.114	0.145	0.159	0.190
Pol B	0.028	0.048	0.079	0.114	0.148
Pol C	0.014	0.030	0.054	0.082	0.109
Pol D	0.005	0.007	0.038	0.071	0.106

TABLE 5-6

Experimental values of yield stress and yield strain for EVA copolymers

$\sigma_y$ (in MPa)				
	$0.027 \text{ min}^{-1}$	$0.069 \text{ min}^{-1}$	$0.27 \text{ min}^{-1}$	$1.38 \text{ min}^{-1}$
Pol A	1.88	2.03	2.00	2.15
Pol B	3.09	3.38	3.68	4.15
Pol C	4.05	4.32	4.71	5.22
Pol D	4.88	4.94	5.01	5.71
$e_y$				
Pol A	0.095	0.110	0.138	0.150
Pol B	0.022	0.040	0.067	0.106
Pol C	0.011	0.025	0.047	0.074
Pol D	0.005	0.006	0.032	0.064

will be later used in the calculation of bending energy instead of those in table (5-6); although they are slightly different from the direct experimental values they are subject to less errors by the operator.

It is also worth noting that although the ultimate tensile properties do not change progressively with the vinyl acetate content of the polymers the yield properties generally do. (Tables (5-5) and (5-6)).

Finally the effect that aging of the polymers has on their mechanical (and consequently adhesive) properties was studied. The maximum period that a peel test sample was left in a dessicator before testing was seven days. Therefore dumb-bell specimens were "aged" in the same dessicator for periods starting from one to seven days and their tensile properties were then measured. The experiment revealed no significant change in mechanical properties, when possible experimental errors were considered.

### 5.3 TEAR STRENGTH OF E.V.A. COPOLYMERS

The fundamentals of the tearing behaviour of elastomers were established by the work of Rivlin and Thomas (76). In a tearing process the energy criterion may include energy dissipated in a variety of irreversible processes. For this energy to be characteristic of the material undergoing tearing it must be confined to a region close to the tear tip. Then, the critical energy release rate  $G_c$  can be defined as the amount of the total strain energy  $E$  necessary to produce a unit of torn area:

$$G_c = -2 \frac{dE}{dA} \quad (5-1)$$

For elastic materials certain geometries may be used in order to measure  $G_c$  (111). The ones that have a wider experimental use are shown in figures (5-3) to (5-6) and for each geometry equation (5-1) takes a different form.

The geometry adopted for the present work is that of fig (5-3). For a distance  $\Delta l$  torn the applied force  $F$  produces work spent directly to tearing equal to  $F \cdot \Delta l$ . The corresponding fractured area is  $t \cdot \Delta l$  where  $t$  is the testpiece thickness, so from equation (5-1) we have:

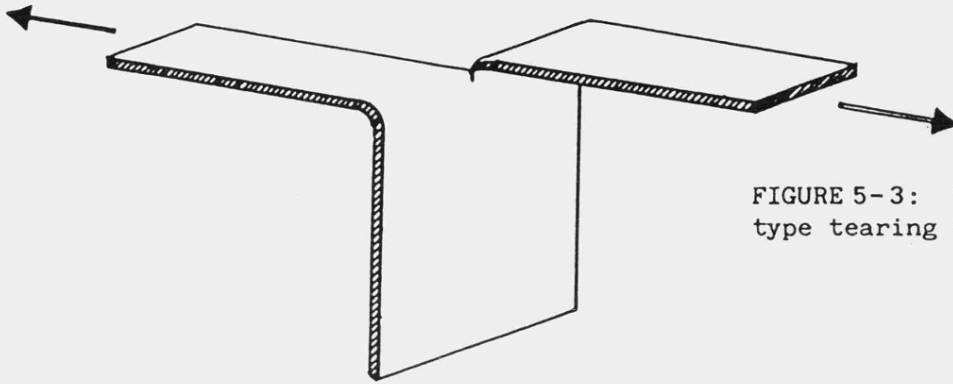


FIGURE 5-3: Trousers type tearing test.

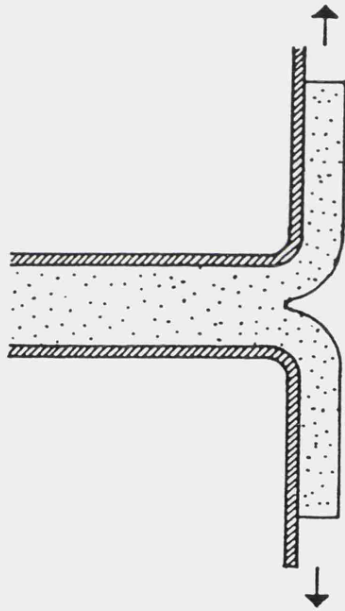


FIGURE 5-4: Cleavage test-piece.

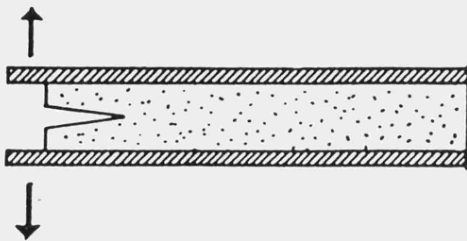


FIGURE 5-5: Pure shear test-piece.

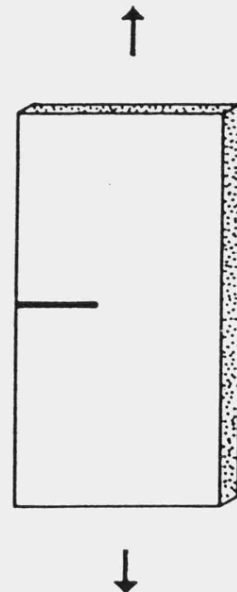


FIGURE 5-6: Tensile test-piece with edge cut.

$$G_c = \frac{2F}{t}$$

There are two ways of ensuring that no energy is dissipated within the torn legs; the sample is made much wider than thick or the legs are reinforced with a non-dissipative fabric backing. The first technique was initially tried with the ethylene vinyl acetate copolymers but it proved impossible to control the tear path. Therefore, the specimens were double-backed with the same cotton fabric used for the peel test samples.

The four polymers were subjected to the same treatment as that to produce a sample for peel testing and the backing was applied by the same process. The tear test specimens were cut to B.S. 2782 Method 360B specifications, ie 200 mm long by 50 mm wide with a 75 mm clean cut central to the width. Then they were tested in an Instron testing machine at a grip separation speed of 200 mm min<sup>-1</sup>, specified for rubbery materials. (The rate of tear

propagation is half the grip separation rate (112)). The macroscopic appearance of the various types of tear has been discussed by Greensmith et al (113). The tearing force-time curve obtained for the E.V.A. copolymers corresponds to that described as stick-slip behaviour. The testing rate remained constant but the tearing force fluctuated causing small variation in the rate of propagation (fig 5-7).

As the tearing force was taken the average of the maxima and



FIGURE 5-7 : Copy of a tearing force - time trace for E.V.A. copolymers.

minima (fig 5-7) and the results expressed as tearing energy are shown in fig (5-8).

Although tear tests are generally straightforward to carry out the reproducibility of the method is often poor (114). For elastomeric materials, the analysis in terms of stresses at the tear tip is extremely difficult. However, as Mullins (112) demonstrated for tearing tests of butadiene-styrene and butadiene-acrylonitrile copolymers, the tearing force determines the extent of internal energy dissipation upon deformation. A quantitative correlation between the tear force and specific dissipative parameters is difficult to achieve (111) but the results in fig (5-8) can be used qualitatively to reflect the capacity of the polymers for internal energy dissipation.

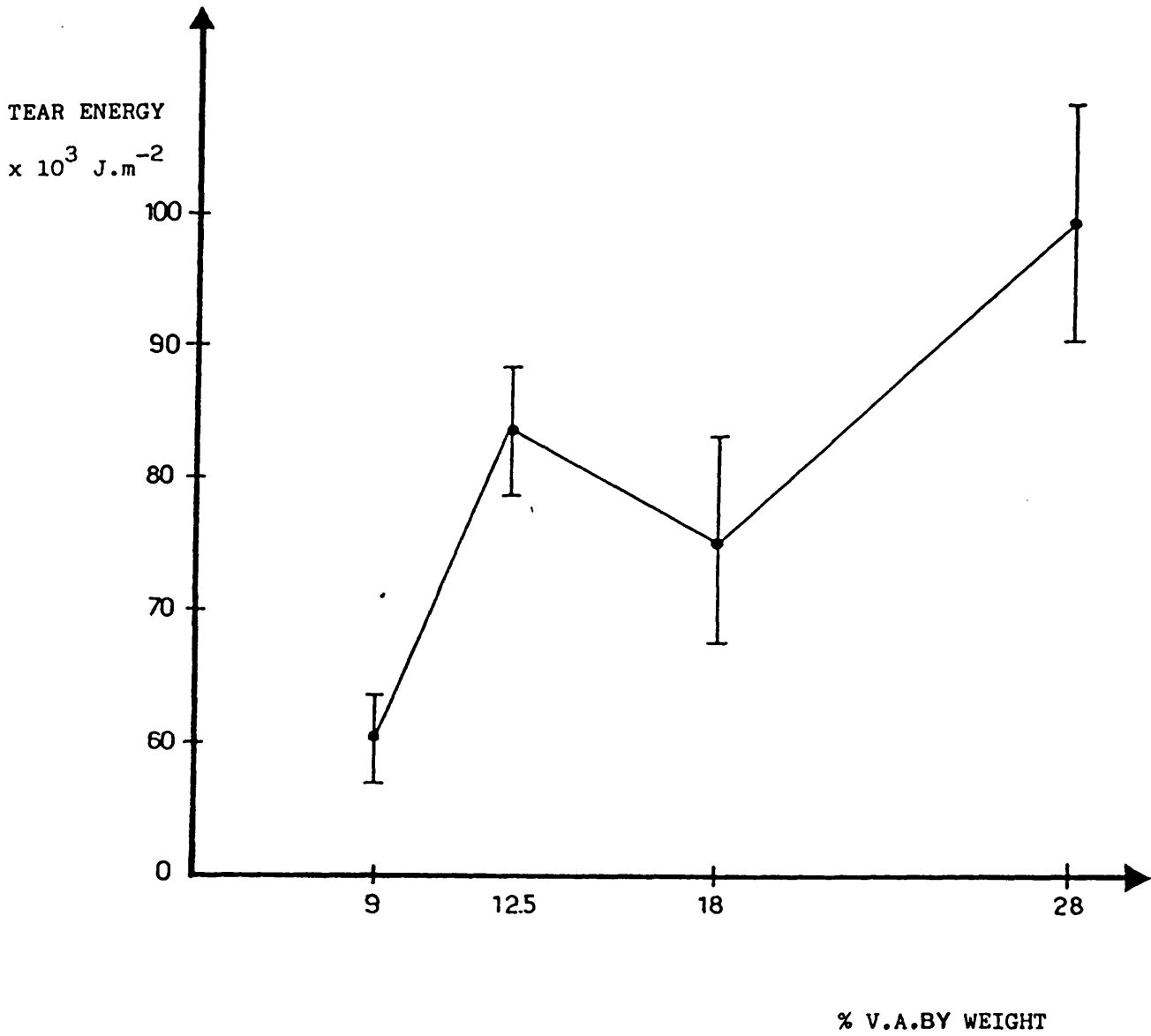


FIGURE 5-8: Tear strength of polymers A, B, C and D expressed as force per unit thickness to propagate a tear in a "trousers" type specimen.



In the context of adhesion tearing energy measurements have had limited use. Hamed (108) measured the tearing energy of S.B.S. and S.B.R. copolymers and correlated it to their work of detachment from Mylar. The ranking of the two materials was the same in the two experiments. That together with results from other mechanical tests, strongly suggested that the tearing energy reflected the dissipative capacity of the copolymers. Packham et al (115) treated the tearing energy of low density polyethylene as an alternative measure of fracture energy and studied its change with temperature. The fall in peel adhesion with temperature was attributed to a similar fall in fracture energy as measured by the tear test.

In the same manner, the trend shown between the tear energies of the four copolymers in the present project will be discussed in chapter 8 in correlation with the peeling energy of the same polymers and not as an absolute method to measure their fracture energy.

#### 5.4 ONE CYCLE LOADING

The polymer "legging" energy dissipation mechanism has been discussed before (Chapter 2). It was then suggested that a polymer segment at the line of detachment is subjected to a loading-unloading cycle.

Thus, a simple one cycle loading - unloading tensile test should be able to distinguish for different polymers the amount of input energy they dissipate upon deformation by that mechanism. That energy can be calculated from the area included in a hysteresis test performed in tension (fig 5-9).

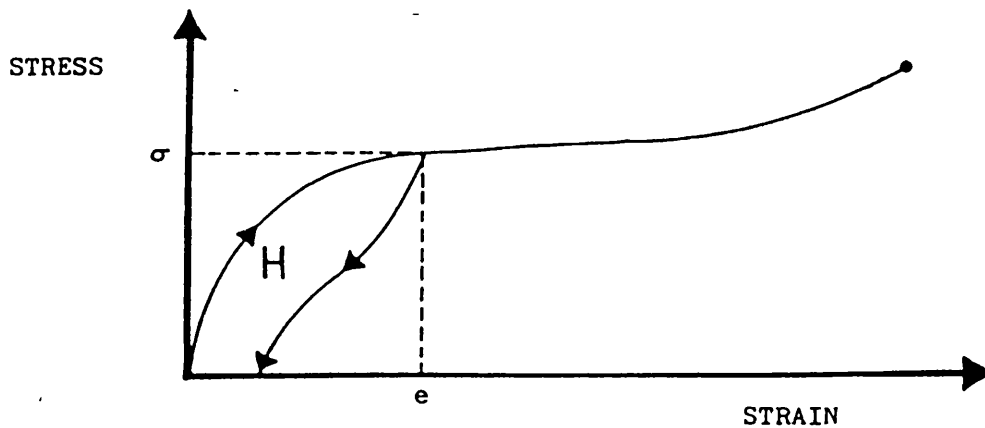


FIGURE 5-9 : One cycle loading curve up to a stress  $\sigma$ .

The tensile stresses set up inside the polymer lip at its maximum elongation vary from near zero at the top of the coating to near the failing stress at the line of detachment. Because the stress gradient between these two limits is not known the hysteresis tests were performed at four different stress limits: 10, 30, 50 and 80% of the failing stress of each polymer as it was measured in section 5.2. The aim therefore was to establish the relationship between the hysteresis energy  $H$  dissipated in one cycle and the corresponding stress limit in that cycle.

The specimens were dumb-bell shaped and they were prepared as those used in the tensile experiments. Four experiments were conducted for each polymer and each stress limit. Specimens subjected to one load cycle were not used again. The highest strain rate allowing an accurate control of the cycle was  $0.27 \text{ min}^{-1}$  and was used throughout the hysteresis tests.

(The corresponding strain rate in peeling is also very high.) The hysteresis energy was calculated from the area  $H$  in figure (5-9). That was measured with a planimeter and checked by cutting and weighing the chart paper to be measured. The results are shown in table (5-7) and it is clear at a glance that for the same fraction of the failing stress the energy dissipated varies from polymer to polymer. Also, it can be seen that for the same polymer the rate of increase of  $H$  is different. Generally, the shape of the hysteresis curves and the results of table (5-7) indicated that  $H$  increases fast as the applied stress limit approaches the failing

TABLE 5-7

Energy dissipated during one cycle loading of dumb bell EVA specimens in tension (in MJ.m<sup>-3</sup>)

(95% Confidence Limits are Indicated)

	10%	30%	50%	80%
Pol A	3.03 + 0.17	12.89 + 0.41	22.12 + 0.65	48.93 + 6.24
Pol B	0.28 + 0.04	0.78 + 0.07	14.86 + 0.38	36.00 + 1.08
Pol C	0.40 + 0.03	1.63 + 0.11	16.68 + 0.11	43.04 + 1.22
Pol D	0.15 + 0.06	0.63 + 0.06	5.77 + 0.16	23.57 + 1.22

stress. In other words, there is only a small difference between the total energy density to failure in a tensile test and the hysteresis energy dissipated in a load cycle up to a stress slightly lower than failing stress.

## CHAPTER 6

### INTERFACIAL INVESTIGATIONS

#### 6.1 SURFACE ANALYTICAL TECHNIQUES IN ADHESION

##### 6.1.1 INTRODUCTION

The strength of an adhesive joint can be measured by means of many physical tests. The load is increased, shear and tensile forces are developed and failure occurs. To improve the performance of an adhesive, the exact mechanism of fracture must be established and the first step towards that is the identification of the true locus of failure. That may be within one of the adherents, purely interfacial or of a mixed mode. To carry out this analysis, the adhesive scientist has a variety of tools, each of which provides him with different information. Baun (116) published a review of surface analysis techniques and identifies six aspects of adhesive bonding where various surface characterisation methods may be applicable:

- (1) adherent chemistry;
- (2) adherent structure and morphology;
- (3) adhesive chemistry;
- (4) adhesive structure and morphology;
- (5) interaction of polymers with metals; and
- (6) failure surfaces.

The number of available characterisation techniques listed by Baun (116) is 66 and they can be broadly divided into microscopic and spectroscopic methods (Figure 6-1).

Some of these techniques became, over the years, more popular than others in the study of fractured surfaces. Very often, a combination of instruments is necessary to take advantage of the strong points of each. This discussion will be confined to methods used in the present project, without suggesting that other methods are less useful in the study of fractured adherents. These methods were chosen because of the information that they provide as well as the availability of equipment for this work.

#### 6.1.2 MICROSCOPIC METHODS IN FRACTOGRAPHY

Very often, the most effective tool in a failure analysis is the naked eye. Visual examination may provide useful information about the fracture process and, in some cases, identify cohesive or adhesive separation. However, it is obvious that this examination has its limitations and a more sophisticated tool must be used. To obtain greater magnification, use can be made of an optical microscope.

In the context of fractography of adhesive bonds, the optical microscope has also certain limitations. For example, thin layers

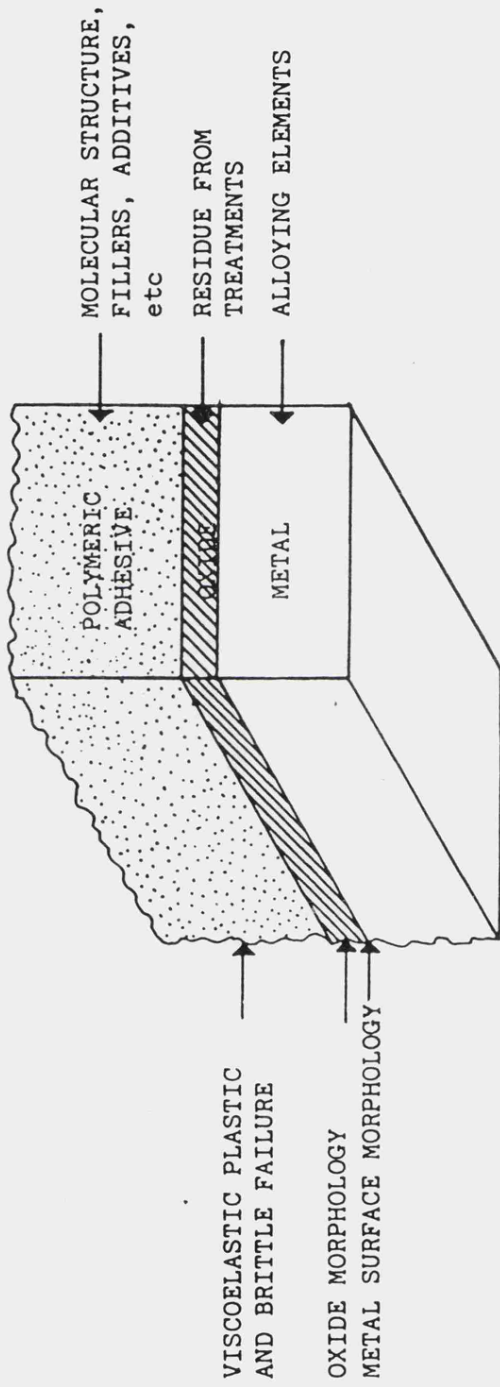


FIGURE 6-1: The role of microscopy and spectroscopy in the study of an adhesive/metal bond (116).



of adhesive are often nearly transparent and may appear as bare metal, (117) ie, adhesive failure, when the failure is, in fact, cohesive within the polymer and very close to the oxide. Further limitations of an optical microscope are its lack of great depth of focus and its resolution limit, which is about 2000 Å for an ordinary instrument (118). To avoid these limitations, a cross-section of the surface to be examined can be cut vertically or at an angle and looked at in the optical microscope. This technique magnifies the surface topography significantly. Cutting, however, may damage important morphological features, especially when soft polymeric materials are involved.

The scanning electron microscope has made it possible to examine in much greater detail surface phenomena and effects. In a S.E.M., the sample is bombarded with electrons which are finely focused to produce an electron spot. The electron lenses of the instrument deflect this spot continuously, so that the surface under study is scanned. Suitable detectors are placed near the sample, which collect secondary or back-scattered electrons emitted from the surface, the signal is amplified and the image of the object is produced and shown on a television screen (119).

Polymers are generally non-conductive materials, so the observation of their surface topography is enhanced by the addition of a conductive layer of gold. This layer "drains" most of the incident electrons and therefore reduces charging effects and so improves

the image of the surface significantly. This layer is normally less than 200 Å thick, which is below the resolving power of the S.E.M.

A typical commercial S.E.M. can magnify the surface up to 40,000 times, although at these magnifications there is a greater possibility of "charging" by the electron beam or, indeed, damage to the polymeric surface due to increased energy of the electrons. Modern instruments provide techniques to reduce the charging effect and with a straightforward sample preparation, S.E.M. allows an evaluation of the surface within minutes after the destruction of the bond.

The study of fractured polymer surfaces by microscopic methods provides the adhesives scientist with useful information and so it has been used extensively. Andrews (120) notes that since deviations from planar fracture as predicted by Griffith theory, occur in practical adhesive tests, a study of the surface provides information about the structure of the material itself. The fracture path is "attracted" by weakness points in the polymer, or it passes around hard particles like fillers. Also, the microstructure of the polymer can be revealed, ie, filler structure, and crystalline morphology. Bascom et al (121) bonded rods

of aluminium with a DGEBA-epoxy resin, in order to study their behaviour under static loading in moist air and water. They studied the fractured surfaces using light microscopy, S.E.M. and energy dispersive analysis of x-rays. They concluded that the failure process was associated with characteristic fracture markings observed on the failed surfaces. During their study with identical adhesives and adherents, Kinlock and Smart (122) used S.E.M. in conjunction with other techniques to investigate the morphology of fractured butt joints. The use of scanning electron microscopy in studies about the adhesion of similar brittle adhesives has also been reported by Smith, (123) Mulville et al., (124) Patrick et al., (125) Baker (126) and others. The nature of information that can be obtained by microscopic examination of fractured adhesive bonds was discussed by Patrick et al (127). In their work, they concluded that provided many samples are photographed, the S.E.M. technique can give valuable insight into the mechanism of joint failures, serve as a "fingerprint" analytical tool and even suggest further fracture mechanics experiments.

Microscopic techniques have also been used to characterise failure of ductile adhesives. Bair et al. (90) observed that a rise in the peel strength of branched polyethylene bonded to copper oxide leaves the residual polymer on the metal with an increasingly rougher surface. Their sequence of scanning electron micrographs illustrated this clearly. Evans et al. (128) made similar observations in the S.E.M. They demonstrated that highly

drawn polyethylene filaments seen on a fractured surface imply an increase in the peel strength; where the visual examination of the metal surface suggested no polymer remains, the peel strength was much lower.

In addition to fractography, electron microscopy can provide information about the adherents prior to bonding and a lot of microscopy work has been done to establish the structure of metal oxides (129) (12) or polymer surfaces (130) prior to adhesive bonding.

Although the references to the literature given so far are only a fraction of reported microscopy work on polymer fracture, they illustrate that to-day microscopy has become a very useful tool for the adhesives scientist.

### 6.1.3 SPECTROSCOPIC METHODS IN FRACTOGRAPHY

In addition to valuable information about the topography of fractured polymers, one may analyse them chemically. The information that is provided from a chemical analysis can be very important to adhesion research. Extremely thin layers of material can be detected and the chemical composition of the fractured adherents can be investigated at various depths.

Of the techniques described in reference (116), two have made a significant impact on polymer surface analysis (131): X-ray photoelectron spectroscopy (XPS or ESCA) and reflection infra-red spectroscopy; the use of many other techniques of surface analysis is restricted when organic materials are examined, because of charging effects or possible damage by electron beams.

Analysing a surface using the x-ray photoelectron spectroscopy technique involves irradiating the sample with low energy x-rays - commonly AlK $\alpha$  or MgK $\alpha$  - under high vacuum. The inner core electrons are then ionised and produce photo-electrons which are ejected from the atom. They carry a kinetic energy  $E_K$  given by:

$$E_K = h\nu - E_B$$

where  $h\nu$  is the energy of the incident x-rays and  $E_B$  is the binding energy for the core electron.  $E_K$  is measured and since  $h\nu$  is known, we deduce  $E_B$ , which is characteristic of the element.

An X.P.S. spectrum consists of a series of sharp bands corresponding exactly to the binding energies of the electron shells. As the chemical environment of an atom changes, the binding energy of core level changes accordingly. These variations are of the order of 10 eV at the maximum and are "chemical shifts". Thus, X.P.S. can provide not only elemental analysis of the fractured surface,

but also information on how the elements are combined, so that the possibility of chemical reactions taking place in an adhesive joint can be investigated. In addition to the qualitative analysis, X.P.S. allows a reasonable quantitative analysis of the surface (132); the intensity of the peak is proportional to the concentration of that element in the surface. In practice, a series of chemical standards can be used to obtain a set of sensitivity factors for the particular instruments.

The sampling depth for polymers usually varies between 15-100 Å for electrons of kinetic energy from 100-1500 eV (131). The elements which are commonly analysed are carbon, oxygen and nitrogen. The C1s spectrum may contain overlapping peaks due to secondary effects induced by neighbouring groups. The analysis of these broad peaks involves the use of deconvolution methods to identify the components. A unique solution to this procedure is not always possible, so the outcome should be treated with caution.

There are a lot of examples where X.P.S. was employed in adhesion research, analysing surfaces chemically both before bonding and after failure. Gettings et al. (26) used X.P.S. to elucidate the role of silane based primers in the bonding mechanism between primer and metal. Their work revealed differences between the various primers, yielded semi-quantitative information about their relative concentration and the results were directly related to the environmental resistance of the epoxy adhesive. The true

locus of failure was also established (36) by using Auger Electron Spectroscopy (A.E.S.) and X.P.S.; a metal oxide-epoxy failure appeared visually, which proved to be a complex pattern where the crack propagated close to, but not exactly at, the interface.

The locus of failure of some ductile adhesives has also been investigated. Yamamoto et al. (133) prepared metal joints bonded with ethylene-acrylic acid (EAA) co-polymer. The metal surfaces (chromated lead, tin and lead/tin alloy) were characterised before bonding and the fractured surfaces analysed by using S.E.M., X.P.S. and ion micro-analysis. For all the metals and environmental conditions investigated, the exact locus of failure was clearly identified. Briggs et al. (35) used X.P.S. extensively to detect chemical groups on the surface of chromic acid etched polyethylene and polypropylene and related the degree of polarity of the polymer surfaces to their adhesive properties. Later, (134) again using X.P.S., they detected substantial oxidation and unsaturation when polyethylene was melted at 150 or 175° C respectively, against aluminium, which also resulted in increased adhesion.

A substantial amount of X.P.S. work on polymers has concentrated on fluorinated materials (especially PTFE), because of the large shifts to C1s signals induced by the highly electronegative fluorine atoms. A typical study is by Dwight et al. (135) The wettability and surface characteristics of PTFE films were investigated with X.P.S., S.E.M. and contact angle measurements

after treatments such as reaction with sodium complex solutions or melting and recrystallising against a gold substrate.

In conclusion, the areas that x-ray photoelectron spectroscopy can contribute to in the science of adhesion can be identified (136)

as:

(a) the surface chemical analysis of metals after pre-treatments and prior to bonding;

(b) the type of bonding between adhesive and metal;

and

(c) the establishment of the exact locus of failure in joints.

A second spectroscopic method which is important in the field of adhesion science is multiple internal reflection infra-red spectroscopy (M.I.R.). The principle of this method requires that infra-red radiation is internally reflected at the interface between a reflection element (usually a TlBr-TlI crystal) and the sample under investigation (fig 6-2).

During the multiple reflection, penetration of the infra-red beam into the sample occurs and at selective energies,



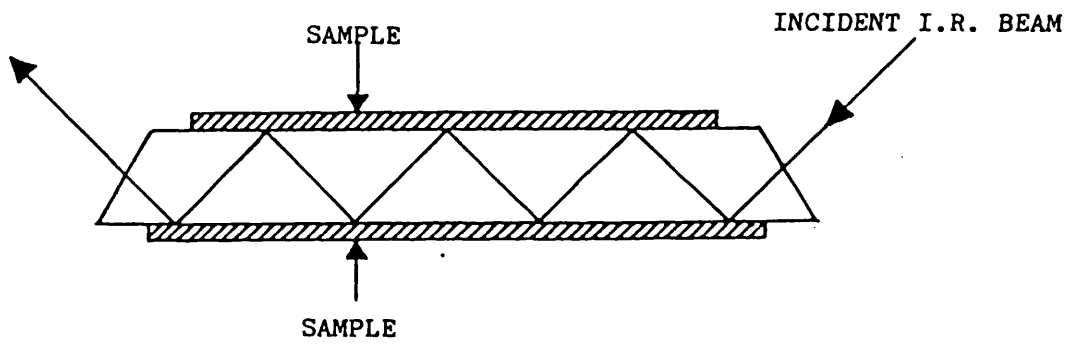


FIGURE 6-2: Reflections of an I.R. beam in Multiple Internal Reflection spectroscopy.

adsorption takes place. The spectrum is then obtained and normally gives information about the polymer's surface composition, orientation of chemical groups, degree of crystallinity, etc. Good contact between the sample and the crystal is obviously required, so very rough or inflexible films may be a source of difficulty. The M.I.R. method normally samples  $1\ \mu\text{m}$  (137) inside the polymer's surface, which is relatively thick compared with, say, X.P.S.

There are plenty of examples where M.I.R. was used to analyse a polymer surface. Luongo et al. (138) studied the surface of thin polyethylene films nucleated on high and low energy substrates. They concluded that films formed in contact with gold are more crystalline than those formed in contact with PTFE. Also, information about the spherulite size in the film were obtained from the penetrating I.R. beam. Willis et al. (139) examined the surface of polyethylene and polypropylene after corona-discharge treatment by using M.I.R. spectroscopy. Their work revealed oxygen and nitrogen containing groups which led them to suggest reactions on the polymer surface during that treatment. In the same report, the behaviour of M.I.R. bands was related to surface orientation in a one-way drawn polypropylene film due to the production process. The carbonyl content of P.E. extruded on aluminium foil was directly proportional to the measured peel strength of that bond. Chemical reactions during the curing phase

of an adhesive can be monitored by M.I.R. spectroscopy, as well as the detection of additives (138) (130).

Although M.I.R. spectroscopy should be used quantitatively with caution, it provides the adhesives scientist with useful information about the chemical composition of fractured surfaces.

#### 6.1.4 CONCLUSIONS

It has long been recognised that a detailed examination of fractured surfaces can improve our understanding of bond formation and bond failure mechanisms.

The principles of some microscopic and spectroscopic methods have been described and their use in the field of adhesion has been demonstrated by reference to particular cases in the literature.

The methods discussed previously were those employed for the present project. The required information from the examination of the surfaces after peeling concerned:

- (a) The fracture path (cohesive or adhesive failure).
- (b) The topography of the fractured surfaces (mechanism of fracture) and;

(c) Possible chemical modification of the E.V.A. copolymers when they are applied as hot-melts on the metals used in this work. The results of these investigations are presented in the following section.

## 6.2 EXAMINATION OF FRACTURED SURFACES

### 6.2.1 RESIDUAL POLYMER AFTER PEELING

The examination of the fractured surfaces is normally the stage after the peel test in a complete analysis. The initial visual observation of the metal side of the bond showed in the case of oxidised copper that there was a thin layer of residual polymer. That was later verified with the scanning electron microscope where polymer remains could also be clearly seen on etched steel. (See section 6.2.2). Working with polyethylene and copper prepared under similar conditions, Evans et al (128) showed the residual polymer thickness to rise monotonically with peel strength. A similar influence on the peel strength by the amount of polyethylene left on copper after peeling was reported by Bair et al (90). It would be useful therefore to investigate any correlation of the peel load with the residual thickness for the E.V.A. copolymers of this project.

Although there was microscopic evidence for cohesive failure in the cases of etched steel and oxidised copper, the mode of fracture was not so obvious when chemically polished copper was the substrate. That meant that either the failure was adhesive or a thin polymer film existed on the substrate but with a relatively smooth appearance when looked at under the scanning electron microscope.

The technique employed to resolve this ambiguity was the measurement

of the contact angle between three liquids and the fractured surface. When a drop of a liquid is placed on the surface of a solid it takes a particular configuration characteristic of the interaction between the liquid and the solid. The angle  $\theta$  that the drop forms with the solid can be measured and is also affected by the roughness of the surface. This factor is not taken into account for the purpose of this experiment; the effect on the contact angle of a metallic (adhesive failure) or a polymeric surface (cohesive failure) is expected to be stronger than that of its roughness (140).

The values of the contact angle for the pure polymers will be later used for the calculation of their surface energy. (Chapter 7). Therefore, three liquids with well characterised in the literature polar and dispersion contributions to their surface tension were chosen (water, glycerol and formamide). So, to investigate the mode of failure in peeling E.V.A. copolymers from chemically polished copper, the contact angle of:

(a) distilled water; (b) glycerol and (c) formamide was measured on: (a) polished copper after peeling; (b) on the peeled polymer strip from polished copper (backed and unbacked) and; (c) on freshly prepared chemically polished copper.

To measure the contact angle the sample under examination was

stuck with a double sided tape on a glass slide capable of horizontal and vertical movement inside a perspex chamber. The volume of the liquid drop was controlled by a syringe attached to a micrometer and its profile was suitably illuminated in front of an optical microscope equipped with a goniometer. The contact angles on the left and right hand sides of the drop were measured at room temperature. A time of two minutes was allowed for the initial spreading of the liquids to be completed before the contact angle was measured. The results in table (6-1) are the average angles of three drops for each category. They clearly suggest the existence of a residual polymer film on chemically polished copper for all the polymers, ie a cohesive failure.

The first method attempted to measure the residual polymer was the pyrolysis of the polymer combined with gas chromatography. The technique involves the pyrolysis of the residual polymer in a ceramic tube furnace similar to that shown in figure (3-1). The gaseous products of the pyrolysis are then carried by an inert gas and burned in the flame detector of a gas chromatograph. The electrical signal produced is proportional to the burned polymer weight. To use this method, rectangular samples of 2 to 4 cm<sup>2</sup> were cut from the peel test specimens after peeling. Their area was accurately measured. The samples were placed on a porcelain boat and pushed inside a ceramic tube heated at 650° C. The constantly flowing gas was nitrogen. The ions produced by burning these products were collected by the cathode and the

TABLE 6-1

Contact angles (degrees) of three liquids on the surface of:

- (a) polymer sheet; \*
- (b) chemically polished copper substrate after peeling unbacked and backed polymer strips and;
- (c) freshly prepared polished copper.

	WATER	GLYCEROL	FORMAMIDE
Pol A only:	51.6 $\pm$ 1.2	70.5 $\pm$ 1.9	56.4 $\pm$ 1.4
Pol B only:	59.3 $\pm$ 0.9	84.4 $\pm$ 2.0	59.6 $\pm$ 1.4
Pol C only:	62.9 $\pm$ 0.5	85.8 $\pm$ 0.5	61.8 $\pm$ 2.0
Pol D only:	74.5 $\pm$ 0.5	90.4 $\pm$ 0.6	64.2 $\pm$ 0.4
<b>Copper substrate after peeling:</b>			
Pol A - unbacked	52.4 $\pm$ 1.4	69.4 $\pm$ 2.4	57.0 $\pm$ 0.6
Pol B - unbacked	58.2 $\pm$ 1.6	84.2 $\pm$ 1.2	60.2 $\pm$ 1.2
Pol C - unbacked	63.4 $\pm$ 0.8	86.6 $\pm$ 0.6	62.4 $\pm$ 2.4
Pol D - unbacked	73.0 $\pm$ 0.6	91.0 $\pm$ 1.2	65.8 $\pm$ 1.0
Pol A - backed:	52.4 $\pm$ 1.6	71.2 $\pm$ 1.0	55.4 $\pm$ 0.6
Pol B - backed:	59.4 $\pm$ 1.6	84.4 $\pm$ 1.8	61.0 $\pm$ 0.8
Pol C - backed:	62.4 $\pm$ 1.4	85.8 $\pm$ 1.1	62.0 $\pm$ 1.2
Pol D - backed:	75.0 $\pm$ 1.3	91.6 $\pm$ 0.6	64.2 $\pm$ 0.9
<u>Polished Copper only:</u>	32.1 $\pm$ 1.4	73.1 $\pm$ 1.0	48.1 $\pm$ 1.8

\* The polymer sheet was prepared from polymer powder by a similar procedure to the peel test specimens. The surface used for the contact angle measurements was cut through the polymer with a microtome.



resulting electrical signal was amplified and recorded in a recorder. Obviously a calibration was necessary in order to calculate polymer weights from the recorded electric potentials. To achieve that a series of increasing polymer weights were pyrolysed and the corresponding signals were recorded. The weights were cut from a polymer sheet prepared under similar conditions to the peel specimens. The weights varied from 1,4 mg - the smallest weight which could be handled conveniently - to 15,2 mg. Increasing weights of each polymer were used to produce the calibration curves which were straight lines to a good approximation (fig 6-3). A series of six samples for each polymer was then prepared and placed into the boat for residual polymer determination. The results are in table (6-2) and it is clear that the majority of the samples had not produced any electrical signal.

It can be seen that the chemically polished copper samples did not produce any electrical signal at all even when the sensitivity of the recorder was at a maximum and the chart speed at a minimum. When a peak was actually recorded the weight of the residual polymer was calculated from the equation of the corresponding calibration curve. But that weight was between approximately 2 and 100 times smaller than the lower calibration limit and consequently outside the calibration line. For practical reasons the use of smaller calibration weights was restricted (this would also involve larger errors) as well as a massive increase in the sample area (the diameter of the tube was only 5 cm). In addition to the above experimental problems there were indications of

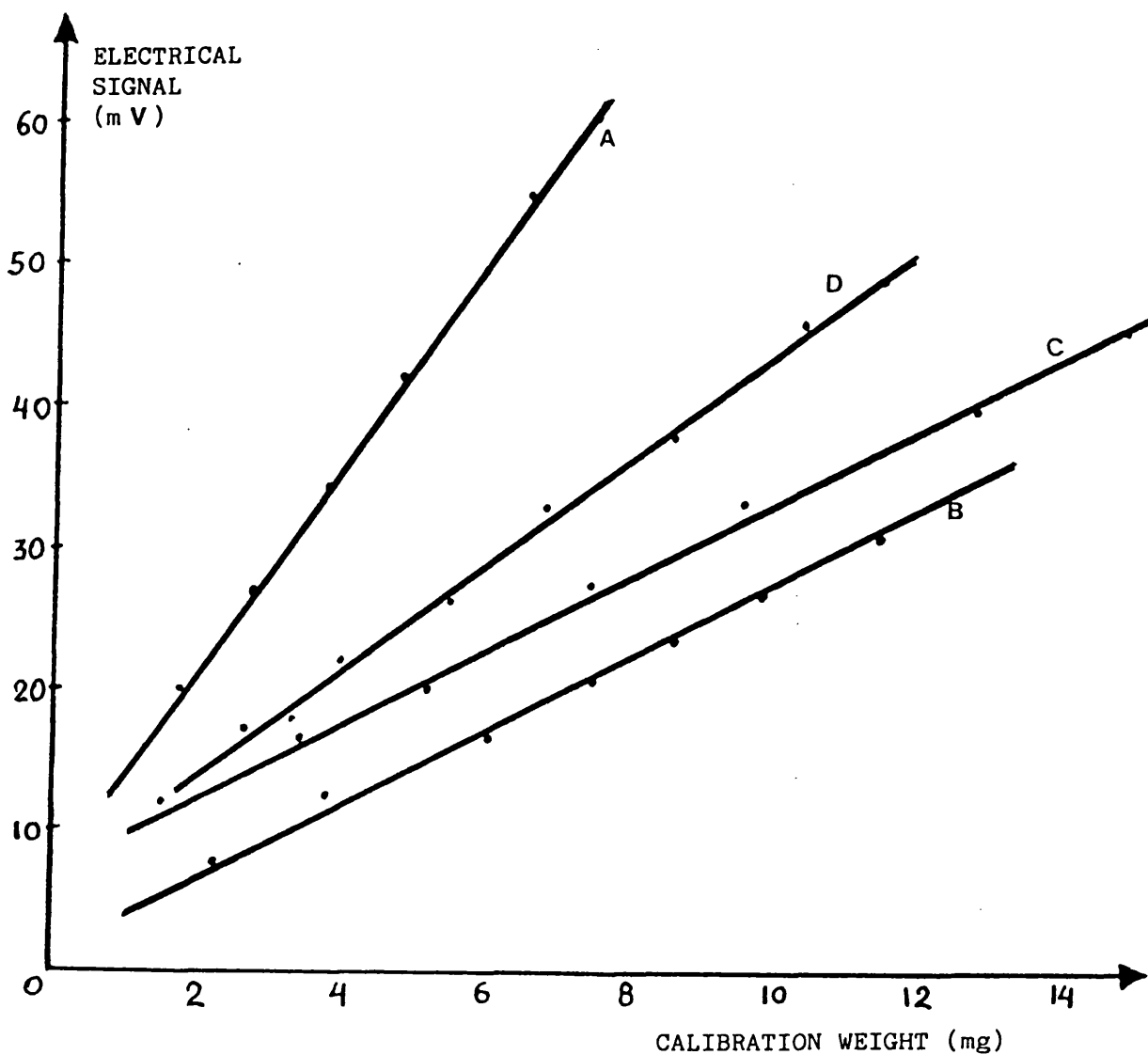


FIGURE (6-3): Calibration lines for polymers A, B, C and D for the pyrolysis - gas chromatography method of measuring the residual polymer after peeling.

TABLE 6-2

Residual polymer determination by pyrolysis-gas chromatography.

SUBSTRATE	POLYMER	PEEL LOAD (N mm <sup>-1</sup> )	WEIGHT OF RES POL (mgr/cm <sup>2</sup> )
Chem Pol Copper	A	3.61	No signal
" " "	A	3.91*	" "
" " "	B	2.03*	" "
" " "	B	2.66*	" "
" " "	C	4.20*	" "
" " "	C	4.82	" "
" " "	D	1.23	" "
" " "	D	0.26*	" "
Oxidised Copper	A	21.34*	No signal
" "	A	20.66	" "
" "	A	16.84	" "
" "	B	10.70	" "
" "	B	9.81	0.760
" "	C	12.39	0.054
" "	C	7.25*	No signal
" "	C	13.20	" "
" "	D	3.42	" "
" "	D	2.27	0.240
Etched Steel	A	2.31	No signal
" "	A	6.54	0.014
" "	B	1.43	No signal
" "	B	2.32	0.231
" "	C	4.58	0.057
" "	C	4.37	No signal
" "	D	1.92	" "
" "	D	0.90	" "
* Indicates 2 experiments for the same sample.			

chemical changes in the oxides of the substrates which could interfere with the pyrolysis products, ie the colour of the black copper oxide change to brown, the etched steel changed from silver to brown and the polished copper from bronze to yellow-red. Therefore the reasons mentioned above made the pyrolysis method to determine the amount of residual polymer inadequate for the particular analysis.

The second method attempted employed a Hilger and Watt surface finish microscope.

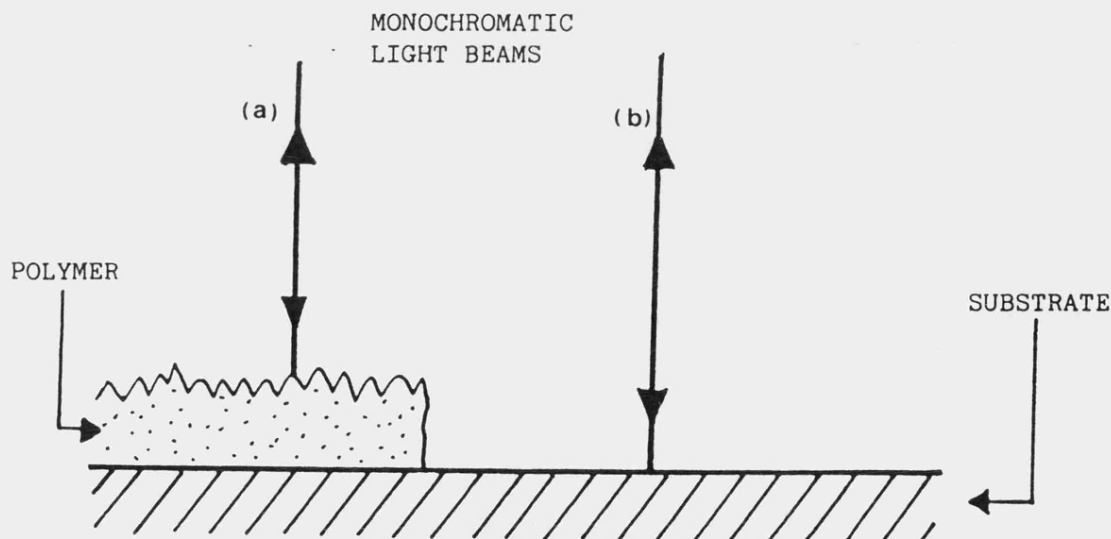


FIGURE 6-4: The principle of the Hilger and Watt surface finish microscope.

In that method two monochromatic beams of light (a) and (b) in figure (6-4) are directed towards the object which must have a surface capable of reflecting the beams back. A surface irregularity on the object produces interference fringes and compensating for

them with a micrometer allows an accurate measurement of the height of the irregularity. However, to use this technique for the purpose of the present project it is essential that the polymer film must be the "irregularity" on a smooth metal surface. It was proved difficult in practice to create such a well defined polymer "step" without damaging the metal or the polymer film. In addition, metals that are normally evaporated on surfaces in this technique like silver or aluminium, failed to produce a good reflecting surface on the polymer part of the specimen. That is attributed to the surface topography of that film, ie drawn out polymer fibres, clearly seen on a S.E. micrograph.

The thickness of the residual polymer on black oxidised copper only was determined directly by scanning electron microscopy. Dilute hydrochloric acid was used to destroy the copper oxide underneath the film and release it. The floating film was carefully collected onto a piece of cellophane and dried thoroughly.

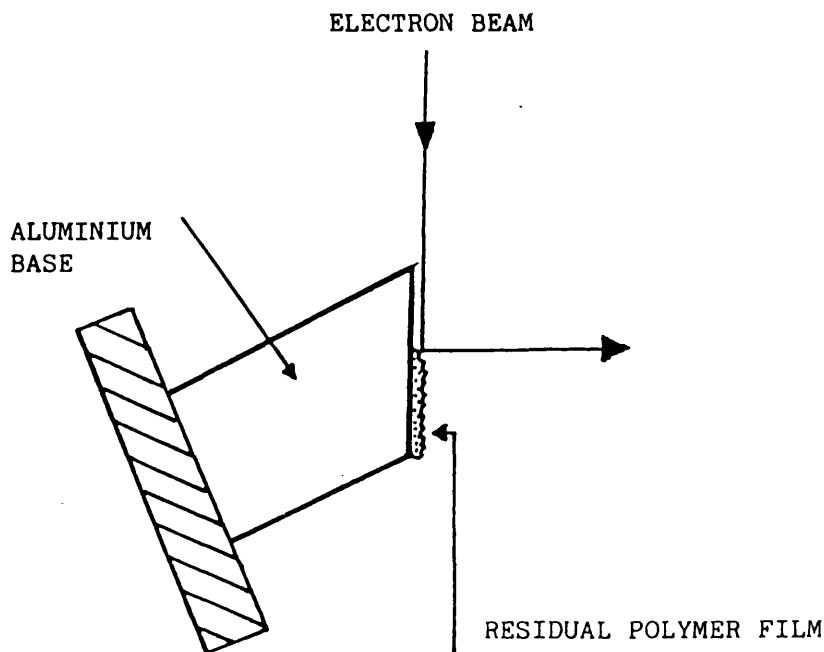


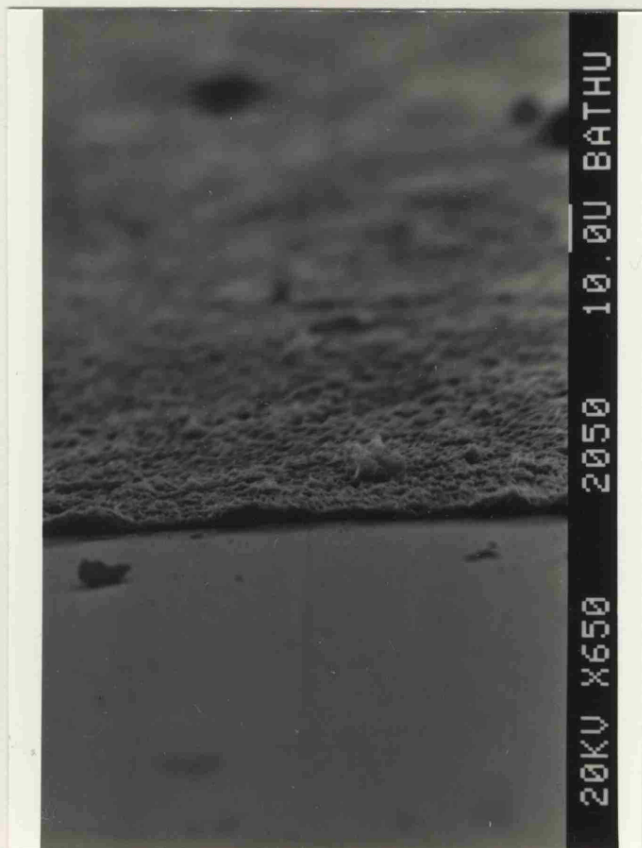
FIGURE 6-5: Experimental set up for measuring the thickness of residual polymer by SEM.

The cellophane was then glued on an aluminium cylinder appropriately cut so that the microscope's 60° tilt could allow an almost vertical viewing of the film. The thickness was measured directly on the microscope's screen from the known magnification and by using a vernier. Four different readings for each sample were taken by rotating the cylinder and viewing the film from different sides (fig 6-5). Pictures of the polymer film taken at a larger angle in order to demonstrate the technique can be seen in photomicrographs (6-1) and (6-2). The thickness results for oxidised copper are given in table (6-3).

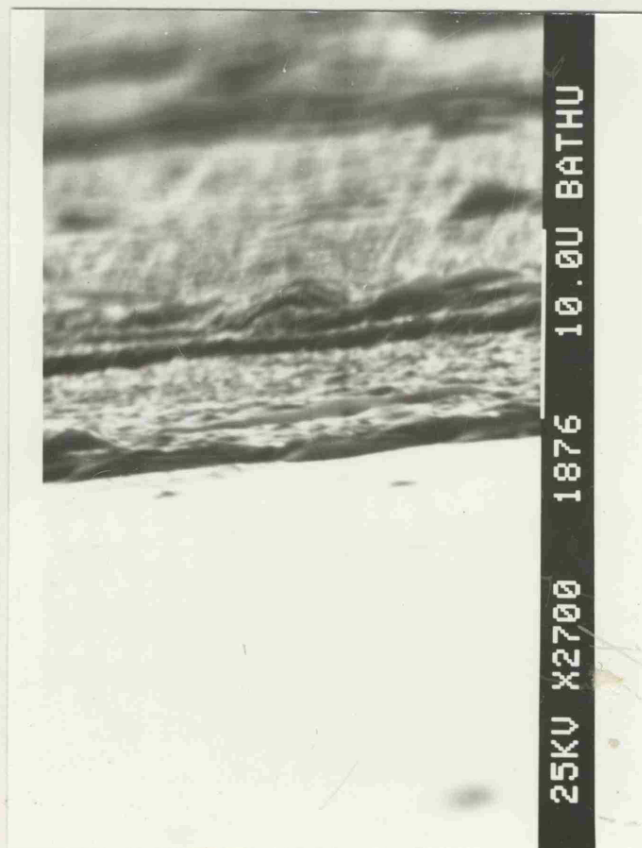
The thicknesses shown in table (6-3) are not absolute because of the polymer being heavily drawn. Where these fibres appeared in the profile of the polymer film the average value is taken as the thickness.

The results in table (6-3) indicate that the use of backing does not generally affect the thickness. It is also clear that the peel load for a particular polymer does not influence the residual thickness significantly although for the coating thickness range examined the load does not vary enough for a positive correlation to be established. Compared with residual polymer thickness results for polyethylene peeled from oxidised copper (128), ethylene vinyl acetate copolymers appear to leave behind thinner films after peeling.

6-1



6-2



PHOTOMICROGRAPHS (6-1) and (6-2): Measurement of residual polymer film released from oxidised copper by SEM.

TABLE 6-3

Residual polymer thickness (in  $\mu\text{m}$ ) for oxidised copper samples. Numbers in parenthesis indicate the corresponding peel load in N.mm. Four measurements were made for each sample and the 95% confidence limits are indicated.

UNBACKED SAMPLES			
Pol A:	$1.28 \pm 0.31$ (5.0)	$1.38 \pm 0.07$ (5.3)	
	$1.15 \pm 0.15$ (4.9)	$1.22 \pm 0.19$ (5.1)	
Pol B:	$2.63 \pm 0.36$ (6.4)	$2.39 \pm 0.14$ (6.5)	
	$2.42 \pm 0.17$ (6.3)	$2.47 \pm 0.23$ (6.5)	
Pol C:	$1.82 \pm 0.17$ (8.4)	$1.70 \pm 0.13$ (8.5)	
	$1.89 \pm 0.28$ (8.4)	$1.66 \pm 0.32$ (8.7)	
Pol D:	$1.99 \pm 0.22$ (2.5)	$2.15 \pm 2.08$ (2.9)	
	$2.07 \pm 0.13$ (2.5)	$2.17 \pm 0.31$ (2.6)	
BACKED SAMPLES			
Pol A:	$1.35 \pm 0.22$ (20.6)	$1.13 \pm 0.13$ (15.4)	
		$1.41 \pm 0.18$ (23.0)	
	$1.28 \pm 0.24$ (20.6)	$1.16 \pm 0.09$ (15.4)	
Pol B:	$2.27 \pm 0.31$ (8.4)	$2.72 \pm 0.46$ (10.2)	
	$2.51 \pm 0.52$ (7.8)	$2.21 \pm 0.15$ (8.4)	
Pol C:	$1.10 \pm 0.14$ (13.2)	$1.25 \pm 0.17$ (14.4)	
	$2.07 \pm 0.16$ (14.0)		
Pol D:	$2.64 \pm 0.30$ (3.8)	$2.79 \pm 0.09$ (4.3)	
	$2.64 \pm 0.38$ (5.2)	$2.50 \pm 0.19$ (4.9)	
	$2.26 \pm 0.23$ (5.0)		



### 6.2.2 SCANNING ELECTRON MICROSCOPY

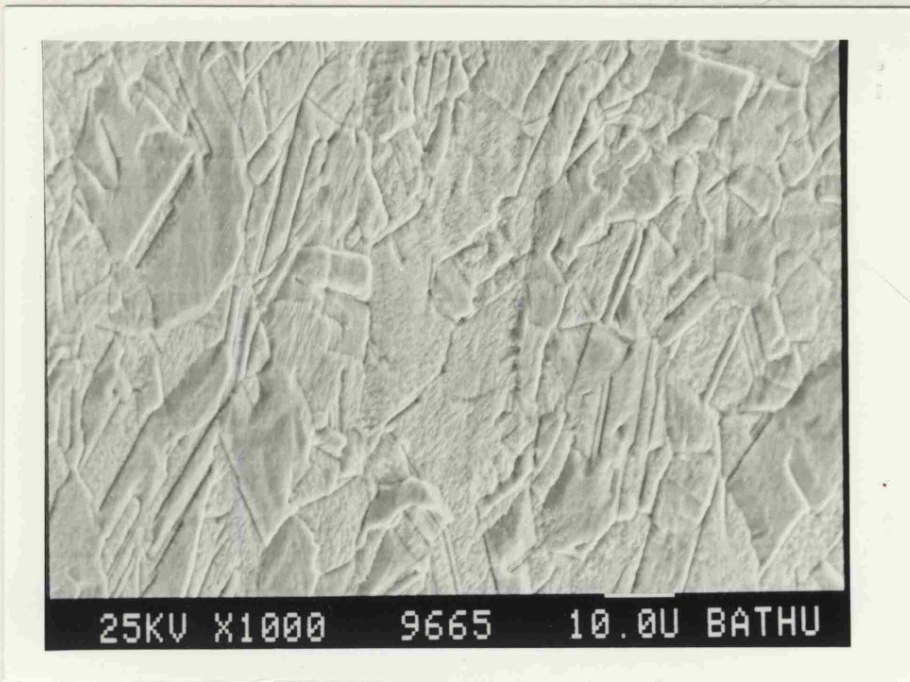
After the peeling test both parts of the fractured bond were examined in the electron microscope. There were 48 categories of fractured surfaces for investigation; four polymers, three substrates, backed and unbacked specimens and polymer and metal side of fracture. The electron microscope was used to provide information about the topography of the fractured sides, establish a possible connection between the degree of surface deformation and the corresponding peel loads and possibly identify different patterns of fracture.

To prepare a sample for the S.E.M. pieces of about 1 cm<sup>2</sup> were cut carefully from the peel test specimens with an electric saw. Care was taken to avoid contact with the fracture surface. That surface was then coated with gold under vacuum for 10 minutes. The electric current used never exceeded 8 mAmpères so that the soft polymeric surfaces would not be damaged. The instrument used was a JEOL-35C scanning electron microscope. Photographs were taken for all 48 categories of samples and at various magnifications. For similar categories eg same polymer or same substrate, photographs at the same magnification were taken so that a comparison would be possible. The discussion and comments to follow are based on a comparative examination of all the photomicrographs the most representative of which are shown in the following pages.

Starting with the chemically polished copper a typical photograph of the substrate is picture 1. Although the metal surface is covered by a thin film of residual polymer as the contact angle measurement indicated, the structure of the copper can be clearly seen ie the grains, and grain boundaries. The corresponding polymer part (polymer B in this case) is a replica of the copper substrate (as it can be seen in picture 2 at the same magnification). The rest of the polymers gave similar pictures showing the polymer side to follow the irregularities of the substrate. However there were signs of small differences between the polymers as the ductility increased with vinyl acetate content; polymer C in picture 3 for example shows a lot of "spikes" drawn out of the polymer mass in contrast to polymer A in picture 4 which at a comparable magnification looks much smoother. That difference can be related to a more than threefold increase of the peel load from polymer A to polymer C for the same polished copper substrate.

Looking at higher magnification at the sample of picture 3 one can observe the topography of the polymer film remaining on polished copper (picture 5). Finally, for the case of that substrate and for both sides of the fracture there was not any clear or distinct difference between backed and unbacked samples.

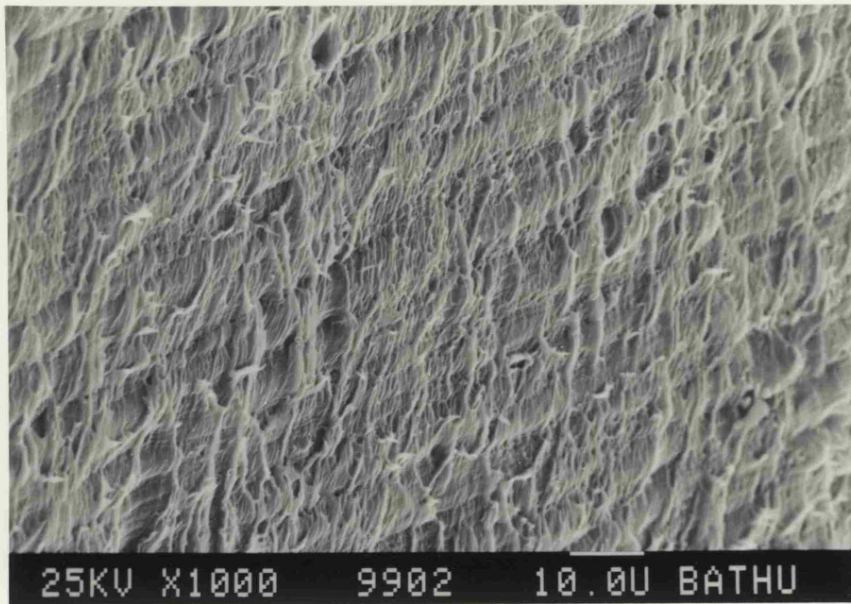
The second substrate to be discussed is etched steel. The peel loads that etched steel gave for each particular polymer were higher than those for polished copper. The general features of



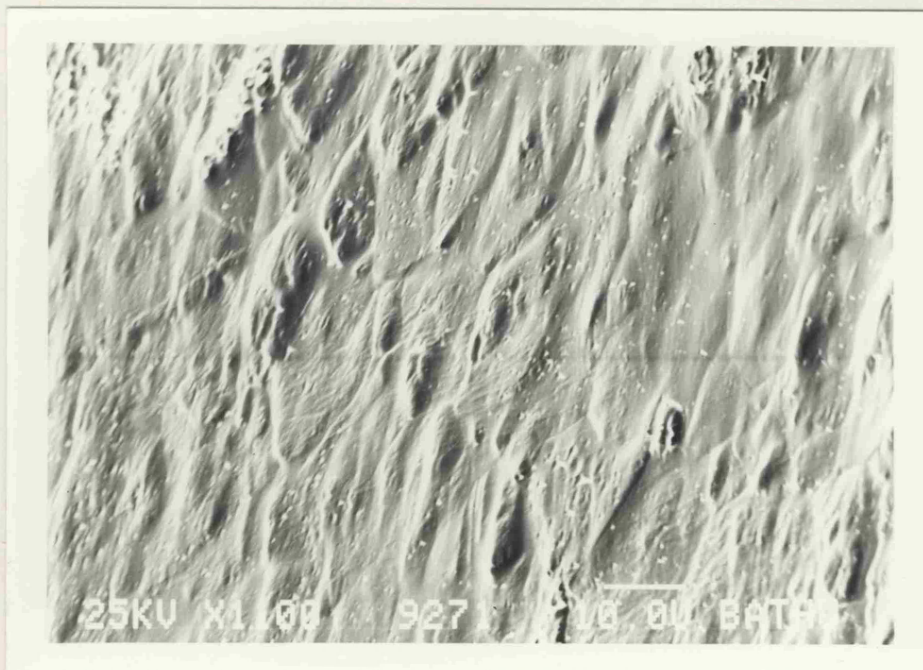
PICTURE 1: Backed polymer B peeled from chemically polished copper (metal side). Peel load  $2.09 \text{ N.mm}^{-1}$



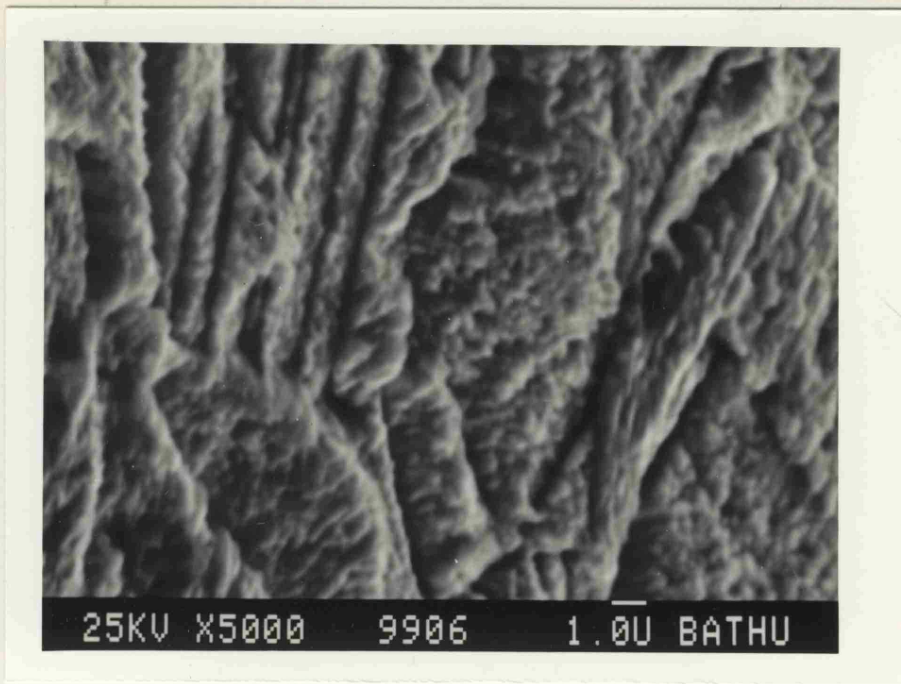
PICTURE 2: Backed polymer B peeled from chemically polished copper (polymer side). Peel load  $2.09 \text{ N.mm}^{-1}$



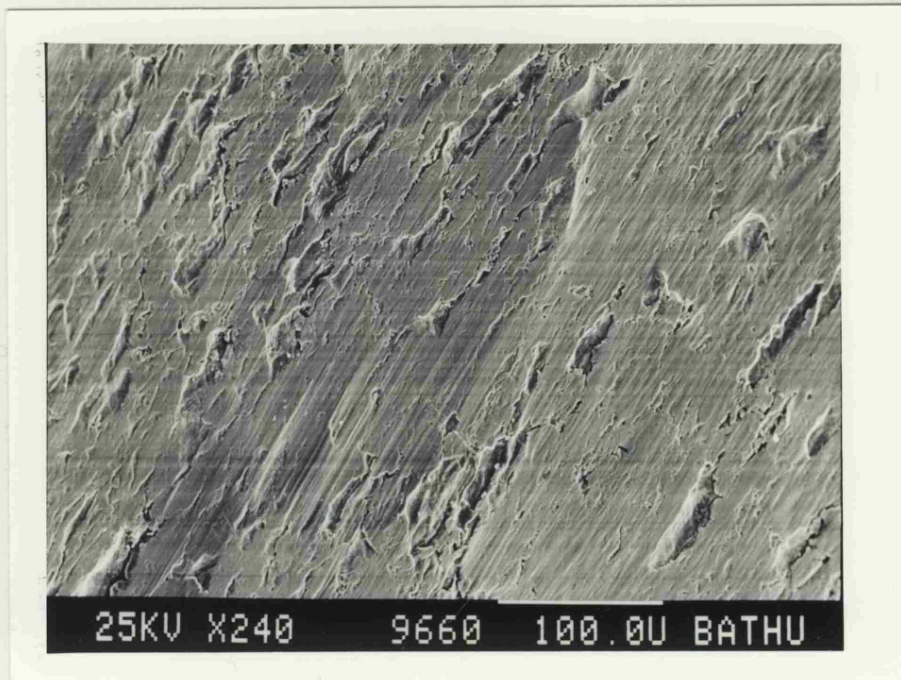
PICTURE 3: Backed polymer C peeled from chemically polished copper (polymer side). Peel load  $4.33 \text{ N.mm}^{-1}$



PICTURE 4: Backed polymer A peeled from chemically polished copper (polymer side). Peel load  $1.32 \text{ N.mm}^{-1}$



PICTURE 5: Backed polymer C peeled from chemically polished copper (metal side). Peel load  $4.33 \text{ N.mm}^{-1}$



PICTURE 6: Backed polymer B peeled from etched steel (metal side). Peel load  $2.76 \text{ N.mm}^{-1}$

this substrate after peeling were the parallel rolling lines from the manufacturing process of the sheet and grooves of around 70  $\mu\text{m}$  length and 20  $\mu\text{m}$  width. All these features can be seen at low magnification in picture 6. Pictures 7 and 8 show polymer remains on the substrate which have the appearance of scattered lumps of polymer. The polymer side of the fracture provides more evidence about its path. In picture 9 the parallel rolling lines of the steel can be seen imprinted on the polymer. Picture 10 is a typical photomicrograph of the polymer side. The size of the drawn polymer lumps as well as their alignment imply that they correspond to the previously described grooves on the steel surface. The failure is for all polymers cohesive within the polymer as a typical photomicrograph of the polymer side at high magnification also suggests (picture 11). There was not any clear distinction between backed and unbacked samples as regards the appearance of both sides of fracture.

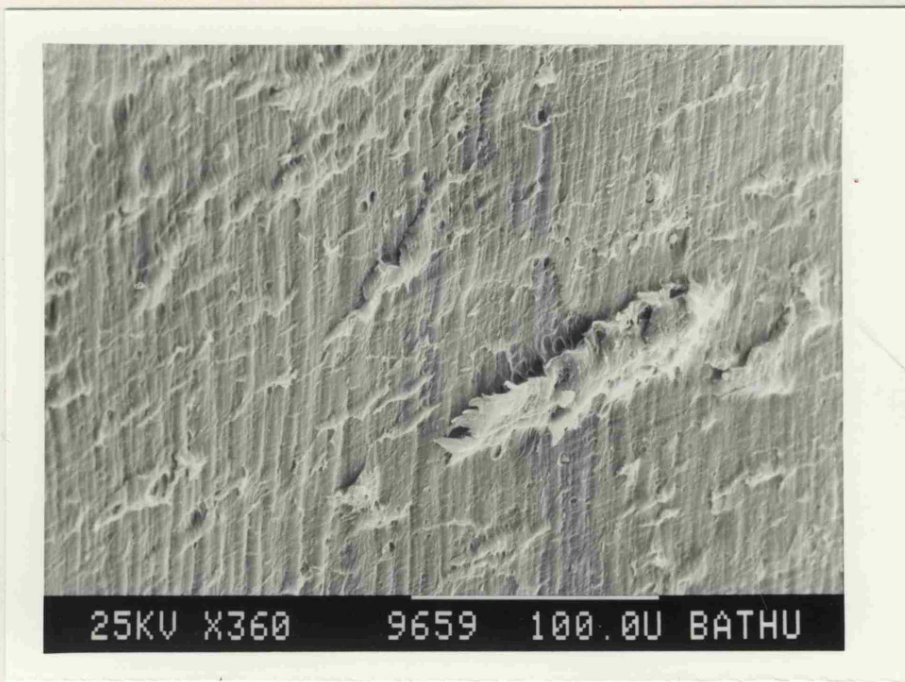
The third and final substrate to be examined was oxidised copper. A typical substrate with the polymer film on it is shown in picture 12. The micrographs in section 6.2.1 were identical to those of the polymer film in situ ie a surface packed with spheroidal polymer formations of approximately 1  $\mu\text{m}$  diameter. More interesting are the micrographs of the polymer side. There is extensive drawing of the polymer with closely packed fibres pointing outwards. The ductility of each polymer is visible in the shape, sharpness and length of these fibres; polymer A in



PICTURE 7: Backed polymer D peeled from etched steel (metal side). Peel load  $2.35 \text{ N.mm}^{-1}$



PICTURE 8: Backed polymer B peeled from etched steel (metal side). Peel load  $2.76 \text{ N.mm}^{-1}$

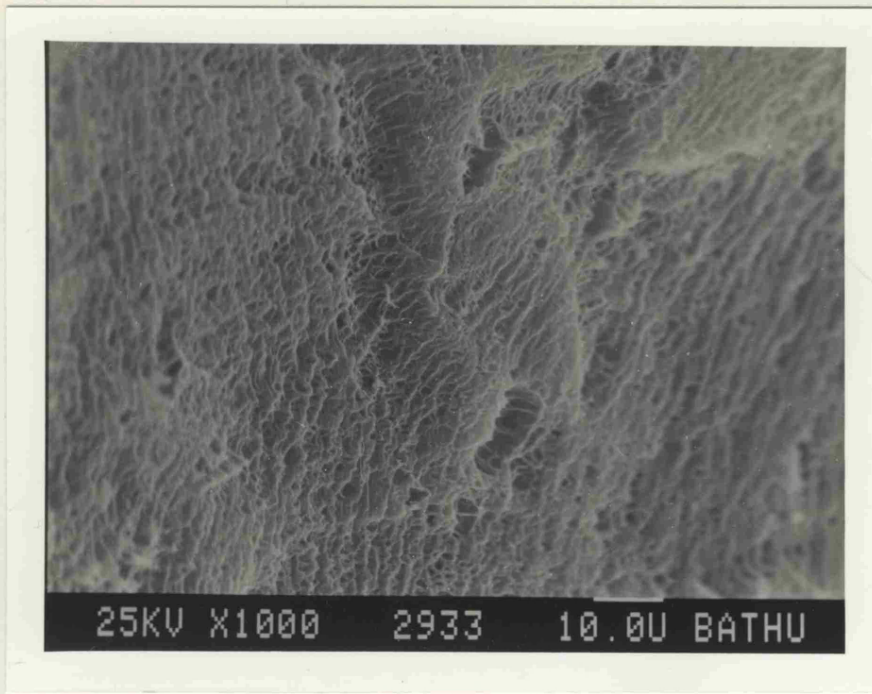


PICTURE 9: Backed polymer B peeled from etched steel (polymer side). Peel load  $2.76 \text{ N.mm}^{-1}$

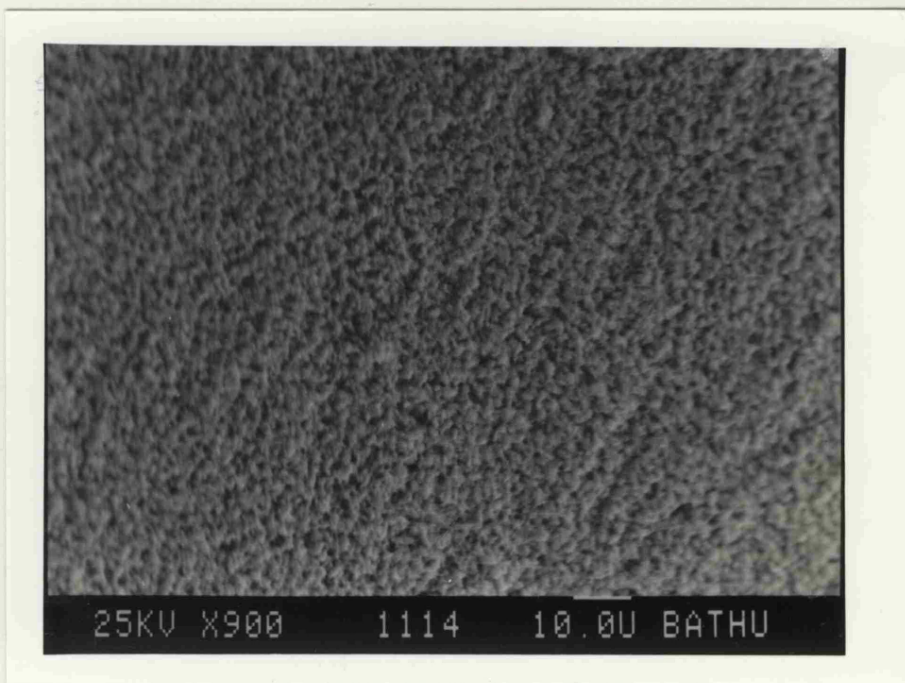


PICTURE 10: Unbacked polymer A peeled from etched steel (polymer side). Peel load  $3.03 \text{ N.mm}^{-1}$





PICTURE 11: Unbacked polymer D peeled from etched steel (polymer side). Peel load  $1.30 \text{ N.mm}^{-1}$



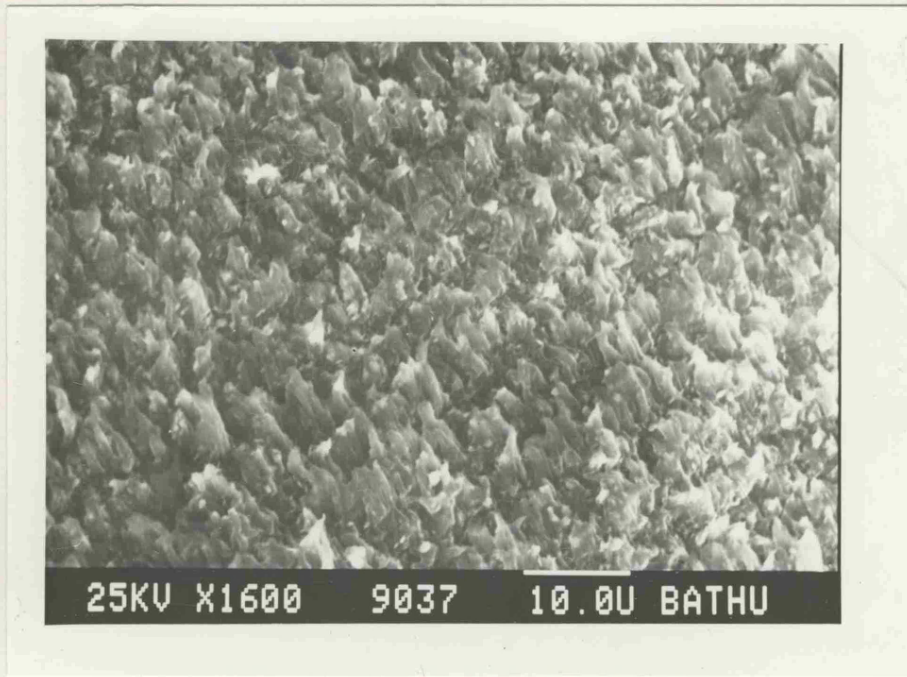
PICTURE 12: Backed polymer D peeled from oxidised copper (metal side). Peel load  $3.60 \text{ N.mm}^{-1}$

picture 13 may for that purpose be compared to polymer D in picture 14. Fabric backed polymers C and B also showed a similar pattern of fracture ie ductile tearing of polymer filaments (see picture 15). A somewhat different pattern is produced by the same substrate when the polymer strips are not supported by the fabric backing: The polymer fibres form regular wrinkles normal to the direction of peeling and at a distance of approximately 1 to 1,5  $\mu\text{m}$  between their peaks. Pictures 16 and 17 are typical of this pattern. There appears to be no obvious reason for their formation but they are associated with a marked decrease in peel load compared to the backed samples.

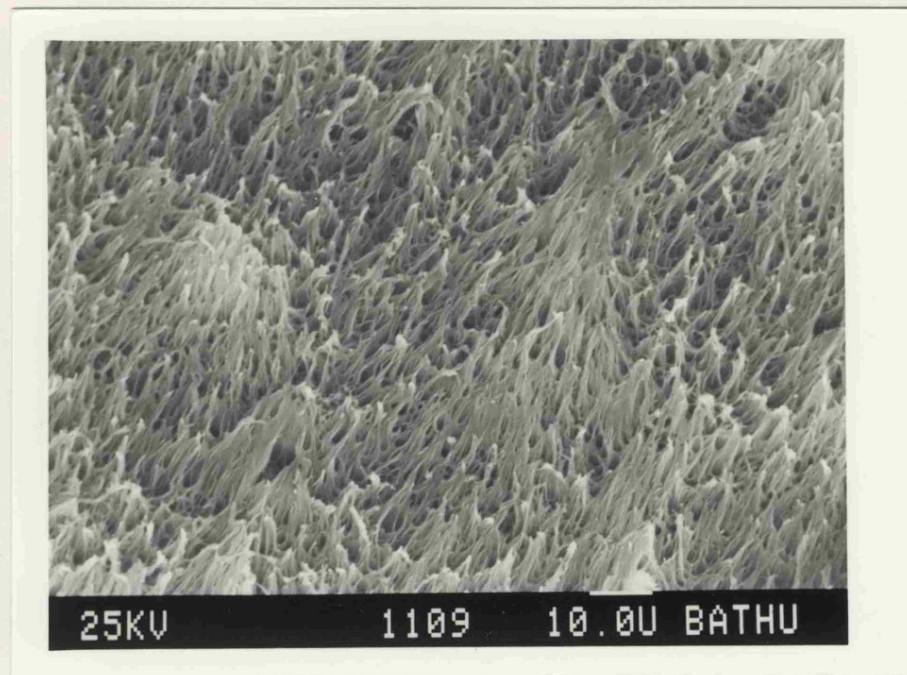
Summarising the electron microscope observations for all the 48 different categories it is concluded that:

(a) When the substrate is chemically polished copper the metal side of the fracture still shows some of the topographical features of the bare metal (eg grain structure) as shown in photom. (3-2). That suggests that the existing residual polymer film (see contact angle results) is very thin which is also consistent with the absence of an electrical signal in the pyrolysis technique.

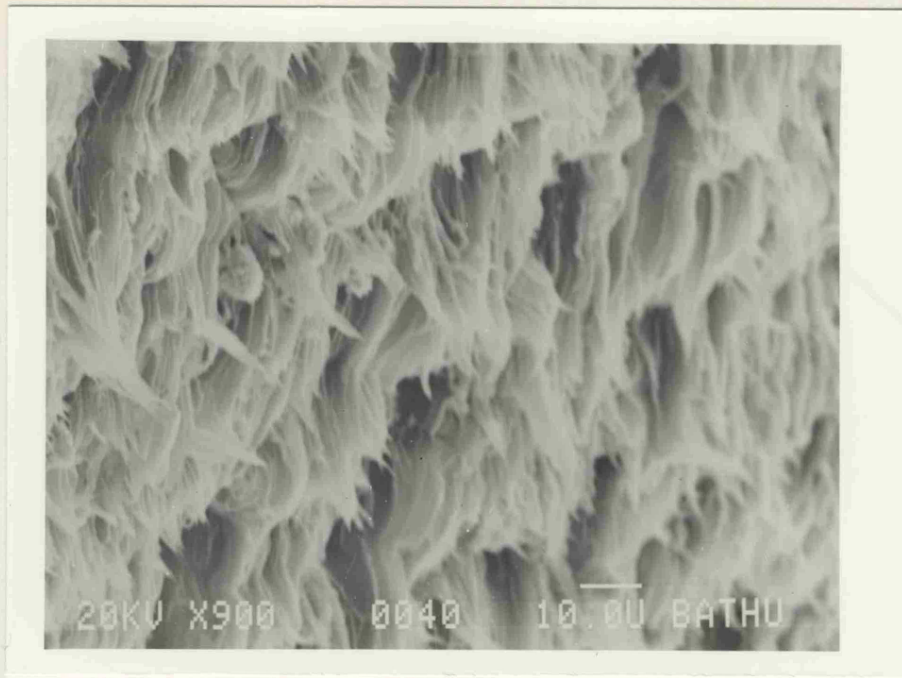
(b) When the substrate is etched steel the polymer side of fracture is an inprint of the metals cavities (see photomicrograph 3-1) and machining lines.



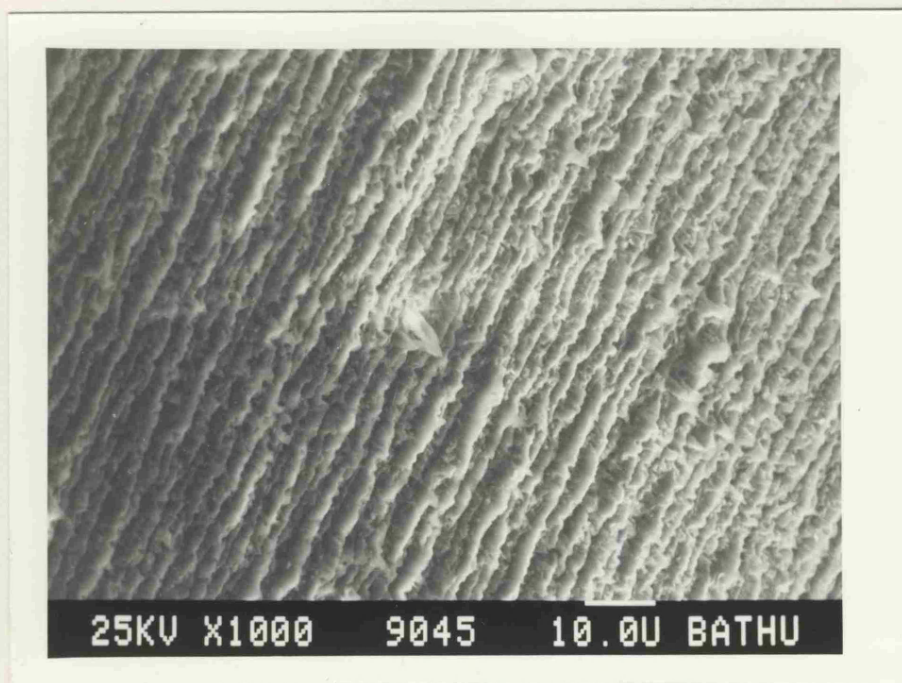
PICTURE 13: Backed polymer A peeled from oxidised copper (polymer side). Peel load  $18.20 \text{ N.mm}^{-1}$



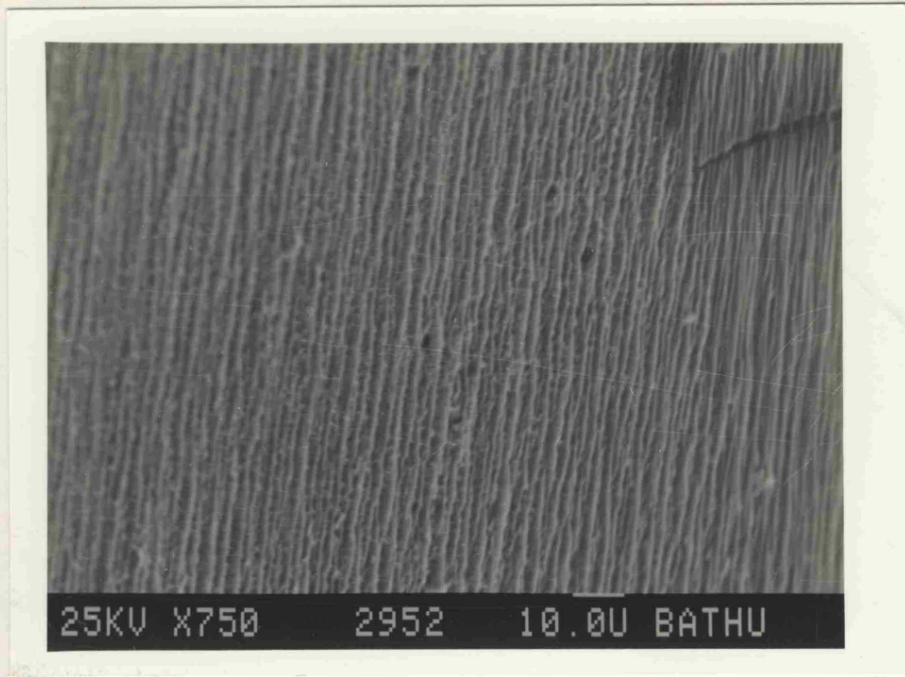
PICTURE 14: Backed polymer D peeled from oxidised copper (polymer side). Peel load  $3.60 \text{ N.mm}^{-1}$  (X900)



PICTURE 15: Backed polymer C peeled from oxidised copper (polymer side). Peel load  $13.29 \text{ N.mm}^{-1}$



PICTURE 16: Unbacked polymer A peeled from oxidised copper (polymer side). Peel load  $4.43 \text{ N.mm}^{-1}$



PICTURE 17: Unbacked polymer C peeled from oxidised copper (polymer side). Peel load  $8.35 \text{ N.mm}^{-1}$

(c) When the substrate is oxidised copper the metal side of the fracture has the appearance of closely packed small spheroidal polymer formations. The polymer side of the bond shows heavily drawn polymer filaments when a backing is used whereas the unbacked samples show in addition to that a larger pattern of waves parallel to the line of detachment. That extra pattern can be due to the stretching that the peeled strip is subjected <sup>to</sup> during the peel test. Generally, the use of the fabric backing affects the fracture pattern significantly only in the case of oxidised copper.

(d) The decreasing ductility of the coatings from polymer A to D is reflected in the appearance and the extent of deformation of the polymer fibres seen on the fractured surfaces. Both of them are reflected in the corresponding peel energies; when there are such signs of extensive viscoelastic losses on both sides of the fracture plane the peel energy is generally large.

### 6.2.3 CHEMICAL CHANGES AT THE INTERFACE

The suggestion that adhesion of polyolefines to metals is connected to polymer oxidation has been made before. Many authors have investigated that correlation especially for polyethylene. They observed improved adhesion of polyolefines to metals when they were modified by incorporating acid groups, chlorinated polyethylene

or ethylene vinyl acetate copolymer itself (50). Smarook and Bonotto (53) reported an increase in adhesion of ethylene acrylic acid copolymers with acrylic acid content and attributed that to the increased strength of interfacial bonds due to the presence of polar carboxyl groups.

In that context, ethylene vinyl acetate copolymers can be treated as modified polyethylenes. The content of carboxyl groups increases from polymer D to polymer A and it is important to examine whether the same oxygen content is maintained when the polymers are applied on the substrates as hot melts. The suggestion that steel has a catalytic effect on polyethylene oxidation (141) provides another reason to examine the side of the polymer in contact with the metal for possible chemical changes in comparison to the bulk of the polymer.

To start this investigation multiple internal reflection infra-red spectroscopy was employed to search for possible changes in the state of oxidation of the polymer. The easiest substrate to remove the coating from without peeling was oxidised copper. That was achieved by immersing the laminate in dilute hydrochloric acid - normally for less than an hour - and then rinsing the polymer with plenty of distilled water and drying in cold air. The sample was then placed in the M.I.R attachment of a Perkin-Elmer 1430 Ratio Recording Infra-red Spectrophotometer in close contact to a KRS-5 crystal. The incident beam entered the crystal at 45°. The spectra obtained with this technique were similar to many respects

to the transmission spectra. Two bands were used to measure the degree of oxidation:  $1730\text{ cm}^{-1}$  for the carbonyl absorption and  $1470\text{ cm}^{-1}$  for the asymmetric methylene absorption. The baseline was drawn as shown in a typical spectrum in figure (6-6) and the ratio of the peak heights of carbonyl over methylene absorption was recorded. A second series of M.I.R infra-red spectra was obtained for the bulk of the coatings so that a comparison would be possible. The results are shown in table (6-4). It is clear that there is not a marked increase in the  $\frac{\text{C} = \text{O}}{\text{CH}_2}$  ratio to indicate extensive oxidation. The sampling depth of the M.I.R. technique is approximately  $10.000\text{ \AA}$  and it is difficult to detect any chemical changes likely to occur within the first hundredths of angstrom of the sample.

The coatings released from steel and chemically polished copper were also examined by M.I.R infra-red spectroscopy. However, the polymer was released from the substrates only after immersion in diluted hydrochloric acid for significantly longer times than those necessary for oxidised copper. The peaks in the corresponding spectra were not sharp enough to allow an accurate quantitative determination and therefore table (6-4) contains results only for oxidised copper. These results are consistent with those of Evans et al (104) and Bright et al (141) (142) for polyethylene coatings on copper prepared under similar conditions. Bright and co-workers also suggested that copper generally retards polyethylene oxidation



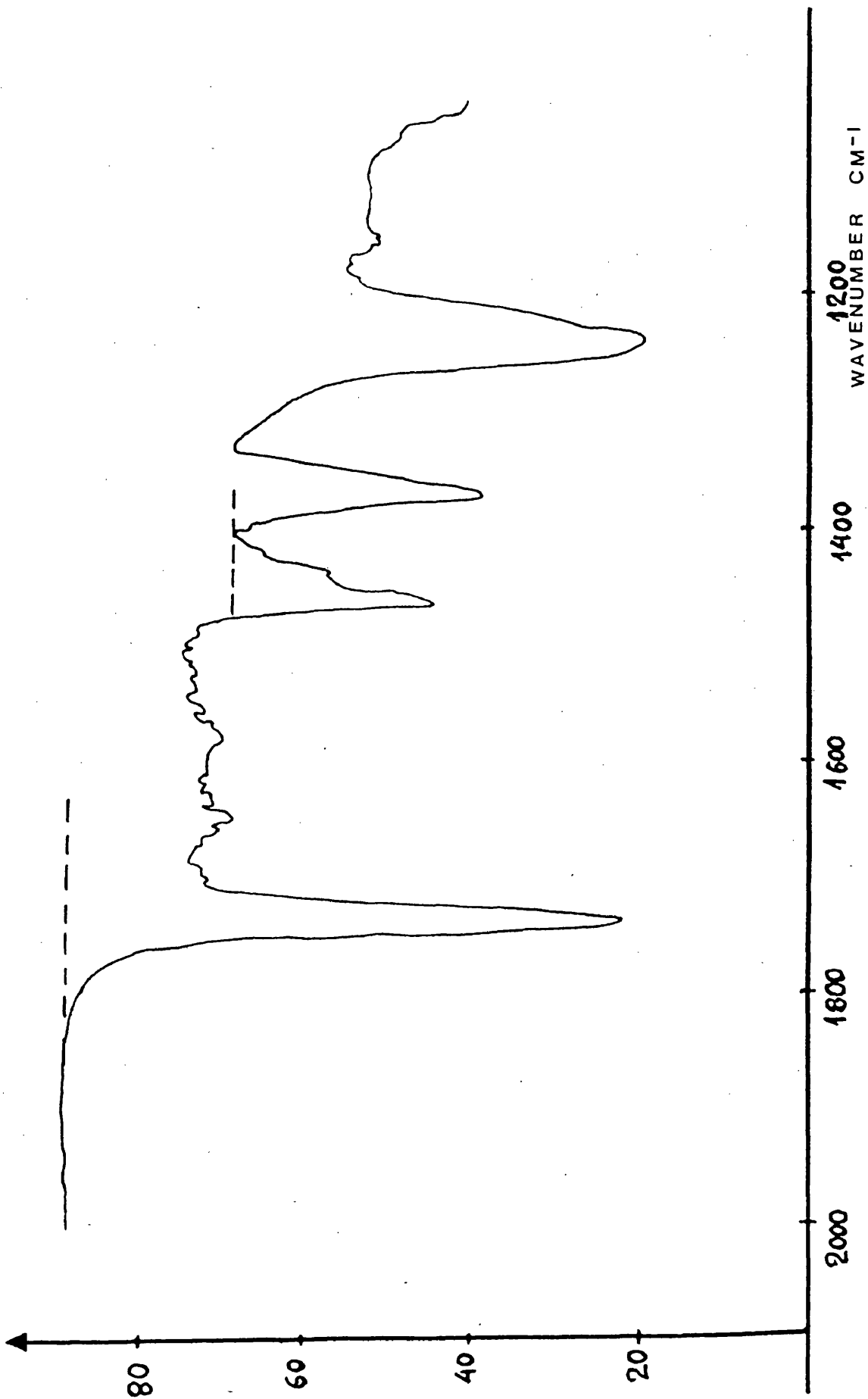


FIGURE 6-6: Copy of a M.I.R infrared spectrum of polymer A soaked off chlorite oxidised copper. The baselines for the 1730 cm<sup>-1</sup> and 1470 cm<sup>-1</sup> peaks are indicated.

TABLE 6-4

Carbonyl/methylene M.I.R infra-red peak ratios for:

- (a) the bulk of E.V.A. copolymers and;
- (b) coatings soaked off black oxidised copper.

	BULK OF POLYMER	SOAKED OFF OXIDISED COPPER
Polymer A	2.56	2.72 - 2.74
Polymer B	1.94	1.86
Polymer C	1.72	1.75
Polymer D	1.52 - 1.47	1.54 - 1.63

and a similar effect could be expected for the E.V.A. copolymers of the present project.

To investigate that, a more sensitive surface analytical technique was employed, X-ray photoelectron spectroscopy, the principle of which is outlined in section 6.1.

The preparation of the samples was similar to that for M.I.R spectroscopy ie releasing the polymer from the substrate with mild hydrochloric acid. To compensate for any affect by the acid the spectra of the so released polymer samples were compared with those of a corresponding set of bulk polymer samples immersed in hydrochloric acid of identical strength for the same period of time. A third set of samples consisting of bulk polymer only was also examined by X.P.S. as a reference. The last two sets of samples (bulk of polymer) were prepared like those for the contact angle.

To avoid any contamination the samples were handled with clean tweezers. The spectra were obtained with a V.G. Scientific instrument equipped with a MgK $\alpha$  source producing an exciting energy of 1253,6 eV. The samples were introduced in the instruments chamber and were outgassed by the normal procedure. The X.P.S. spectrum was then obtained and the various peaks on the wide scan (0 to 1000 eV binding energy) were identified from the corresponding binding energies in standard tables (143). Narrow scans for the

C1s and O1s peaks were also obtained for each case. The areas of these peaks were measured by the computer attached to the X.P.S. instrument. The sensitivity factors for the particular experimental conditions were 0,2 for C1s and 0,61 for O1s. The above areas divided by the corresponding sensitivity factors yielded the results of C/O ratio shown in table (6-5). The samples were not subjected to cleaning by ion bombardment after degassing, a method that usually removes monolayers contributing to the analysis. A further correction of the above ratios was therefore necessary to take into account a layer of sorbed hydrocarbon contamination (144).

That was achieved by reducing the peak areas by the factor exp.

$\left[ -t/\lambda_c(E_A) \cdot \cos \theta \right]$  where  $t$  is a typical carbon thickness of 0.75 nm (144) and  $\lambda_c(E_A) \cos \theta$  the escape depth of the electrons.

The carbon/oxygen ratios for the bulk of the E.V.A. copolymers measured by X.P.S (first column in table (6-5)) is consistent with the theoretical obtained by a simple stoichiometric calculation: 9.90 for polymer A, 15.69 for polymer B, 20.6 for polymer C and 22.75 for polymer D. By comparing the corrected carbon/oxygen ratios in the second, third and fourth columns of table (6-5) it can be seen that steel gives smaller ratios than copper. That is due to an increase in the oxygen content since a change in the carbon content is unlikely. This observation is consistent with the work of Bright and co-workers for polyethylene (141) (142). Further evidence comes from the binding energies for the C1s peaks of the third column which are higher by approximately 0.25 to 0.95

TABLE 6-5

C1s/01s ratios for EVA copolymers soaked off metal substrates and determined by XPS.

	Bulk of polymer		Dipped in HCl	Soaked off Etc St	Soaked off Oxid Copp
Polymer A	a*	3.296	2.585	1.399	1.923
	b**	10.054	7.886	4.268	5.866
	c***	10.047	7.880	4.265	5.862
Polymer B	a	5.039	3.299	1.605	2.190
	b	15.369	10.063	4.896	6.682
	c	15.358	10.056	4.892	6.677
Polymer C	a	6.299	4.135	1.982	3.411
	b	19.212	12.613	6.048	10.405
	c	19.199	12.604	6.044	10.398
Polymer D	a	7.018	4.635	2.312	4.10
	b	21.408	14.138	7.052	12.530
	c	21.393	14.128	7.047	12.521

\* (a) Peak area ratios.

\*\* (b) Peak area ratios corrected for the instrument's sensitivity factors.

\*\*\* (c) Peak area ratios corrected for a 0.75 nm carbon layer contamination (144).

eV than those in the second column in table (6-5); that indicates the introduction of an electronegative atom in the molecule and the wide scan suggests that this atom is oxygen. The oxygen peaks also become slightly broader suggesting oxygen species other than those expected in the acetic acid group - COOCH<sub>3</sub>. Finally, the effects of polymer oxidation for both steel and copper become more significant as the vinyl acetate content decreases from polymer A to polymer D suggesting that oxidation affects mainly the hydrocarbon segments of the molecule.

## CHAPTER 7

### ENERGY DISSIPATION

#### 7.1 THE ENERGY OF SEPARATION

In trying to determine quantitatively the contribution of the various energy loss terms described in chapter 2 it is essential to know the exact amount of input energy which is being dissipated. The equation that gives the input energy available for peeling per unit area  $P$  from the recorded peel load  $F$  is, as mentioned in chapter 2:

$$P = \frac{F}{b} (1 + \lambda) \quad (7-1)$$

where  $\lambda$  is the extension ratio of the peeled strip and  $b$  its width. When a backing is used the extension ratio  $\lambda$  is 1 and so for the backed samples the above expression becomes:

$$P = \frac{2F}{b} \quad (7-2)$$

For the unbacked samples the extension ratios were measured by drawing parallel lines 1 cm apart across the width of the strip with a fine marker before peeling. When the crosshead had stopped and before the strip was released from the test machine the

distance between the lines was measured and the average value of  $\lambda$  was calculated. The results for strips of thickness between 1.50 and 1.70 mm are shown in table (7-1). The input energy per unit area for the unbacked samples can be now calculated by using equation (7-1) and the peel loads of table (4-1). Similarly, equation (7-2) allows the calculation of the input energy per unit area for the backed samples from the peel loads of table (4-2). The results of both calculations are given in tables (7-2) and (7-3).

The P values in tables (7-2) and (7-3) are significantly higher than those calculated from peel loads of various polyethylenes peeled from similar substrates. There are no published results to the author's knowledge for a 180° peeling test of unmodified E.V.A. resins from metals with similar surface topography. Therefore a direct comparison of the P values of tables (7-2) and (7-3) is not possible.



TABLE 7-1

Average extension ratios  $\lambda$  measured in peeling unbacked samples of 1.50 to 1.70 mm polymer thickness.

(95% confidence limits are indicated)

	Chem Polished Copper	Etched Steel	Oxidised Copper
Pol A	2.18 $\pm$ 0.15	2.40 $\pm$ 0.21	3.98 $\pm$ 0.34
Pol B	1.95 $\pm$ 0.10	2.16 $\pm$ 0.17	3.84 $\pm$ 0.30
Pol C	1.15 $\pm$ 0.09	1.30 $\pm$ 0.13	3.01 $\pm$ 0.22
Pol D	1.22 $\pm$ 0.19	1.20 $\pm$ 0.17	2.95 $\pm$ 0.20

TABLE 7-2

Input energy per debonded area ( $\times 10^3 \text{ J. m}^{-2}$ ) for unbacked samples calculated from the peel loads of table (4-1) and the extension ratios of table (7-1)

(95% Confidence Limits are Indicated)

	Chem Polished Copper	Etched Steel	Oxidised Copper
Pol A	3.65 $\pm$ 0.35	11.42 $\pm$ 0.51	25.59 $\pm$ 1.50
Pol B	2.59 $\pm$ 0.17	5.97 $\pm$ 0.38	31.07 $\pm$ 0.72
Pol C	4.60 $\pm$ 0.60	10.78 $\pm$ 0.54	34.16 $\pm$ 0.74
Pol D	2.06 $\pm$ 0.33	3.12 $\pm$ 0.42	10.58 $\pm$ 0.98

TABLE 7-3

Input energy per debonded area P ( $\times 10^3 \text{ J.m}^{-2}$ ) for backed samples calculated from the peel loads of table (4-2)

(95% Confidence Limits are Indicated)

	Chem Polished Copper	Etched Steel	Oxidised Copper
Pol A	(3.5 $\pm$ 0.30)	(9.70 $\pm$ 0.70)	(39.70 $\pm$ 2.70)
Pol B	(4.16 $\pm$ 0.14)	(5.54 $\pm$ 0.28)	(17.50 $\pm$ 1.76)
Pol C	(7.88 $\pm$ 0.38)	(15.42 $\pm$ 1.74)	(27.98 $\pm$ 0.86)
Pol D	(2.18 $\pm$ 0.32)	(4.56 $\pm$ 0.26)	(8.20 $\pm$ 0.66)

## 7.2 THERMODYNAMIC WORK OF COHESION $W_c$

The significance of the term  $W_a$  (or  $W_c$  for cohesive failure) has been previously mentioned. In the present work the fracture for the three metal substrates was cohesive within the polymer, therefore the analysis will be concerned only with  $W_c$ .

There are no data in the literature for the exact value of  $W_c$  for ethylene vinyl acetate copolymers. However, it was possible to calculate an approximate value for  $W_c$  from the contact angle results in section 6.2. If the value for the surface energy of the copolymers is  $\gamma_s$  then the work of cohesion  $W_c$  is twice the work necessary to create the new polymer surfaces:

$$W_c = 2\gamma_s$$

Fowkes (145) suggested that the total free surface energy of a solid is the sum of contributions associated with different intermolecular forces, for example dispersion, polar and hydrogen bonding:

$$\gamma_s = \gamma_s^d + \gamma_s^p + \gamma_s^h + \dots$$

For cases where both the solid (ethylene vinyl acetate) and the liquid (water, glycerol and formamide) are polar Owens and Wendt (23) suggested that all polar interactions can be combined in one term, so the surface energy of the solid becomes the sum of two

terms,  $\gamma_s^d$  and  $\gamma_s^p$ . By assuming that polar forces can be approximated by a geometric mean (as Fowkes suggested for the dispersion forces) they obtained an expression for the interfacial tension between a liquid and a solid:

$$\gamma_{s1} = \gamma_{sv} + \gamma_{1v} - 2\left(\gamma_s^d \gamma_1^d\right)^{1/2} - 2\left(\gamma_s^p \gamma_1^p\right)^{1/2}$$

This equation combined with the well known Young-Dupre equation and neglecting the surface pressure of the liquid's vapour gives:

$$\gamma_1(1 + \cos\theta) = 2\left(\gamma_s^d \gamma_1^d\right)^{1/2} + 2\left(\gamma_s^p \gamma_1^p\right)^{1/2} \quad (7-3)$$

The contact angle between the above mentioned liquids and the four ethylene vinyl acetate copolymers measured in section 6.2, can be now used in equation (7-3) to obtain the dispersion  $\gamma_s^d$  and polar  $\gamma_s^p$  contributions to the surface energy  $\gamma_s$ . Values for the terms  $\gamma_1^d$ ,  $\gamma_1^p$  and  $\gamma_1$  for the three liquids were taken from the literature (146) (147). The calculated values for  $\gamma_s^d$ ,  $\gamma_s^p$  and  $\gamma_s$  are the average of three sets of  $\gamma_s^d$  and  $\gamma_s^p$  data for each polymer obtained by combining the three liquids by two each time. These values are shown in table (7-4). Obviously more liquids are needed for a better approximation but for the purpose of defining the order of magnitude of  $W_c$  it is clear from table (7-4) that it is many orders smaller than the input energy  $P$  measured in section 7.1. Thus the contribution of  $W_c$  in equation (2-8) as an additive is minimal compared to other energy terms determined in the following sections of this chapter.

TABLE 7-4

Average values of  $\gamma_s^d$  and  $\gamma_s^p$  for the ethylene vinyl acetate copolymers calculated by combining the contact angles of three liquids\* in pairs.

(in  $\text{mJ. m}^{-2}$ )

	Dispersion Contribution $\gamma_s^d$	Polar Contribution $\gamma_s^p$	Total Surface Energy $\gamma_s$
Pol A	7.55	41.73	49.28
Pol B	9.23	32.60	41.83
Pol C	9.79	28.86	38.65
Pol D	12.12	21.65	33.77

\* Liquid 1: Water

Liquid 2: Glycerol

Liquid 3: Formamide

### 7.3 ENERGY LOSSES IN STRETCHING THE PEELING STRIP

During the peel testing of the unbacked samples it was clearly noticed that the part of the polymer strip already peeled was stretching considerably. Part of the input energy  $P$  shown in table (7-2) was spent to extend the freed strip. As described by equation (2-5) of chapter 2 the energy per unit area  $W_s$  dissipated by the above mechanism will be given by the area of a stress-strain curve up to the same strain experienced in the peel test (energy per unit volume  $E_{\frac{e}{p}}$ ) multiplied by the thickness of the strip (energy per unit area). The stress-strain curve used for that calculation was that obtained at a deformation rate of  $0.27 \text{ min}^{-1}$  (see chapter 5) because it was the closest to the deformation rate during the peel test. For the standard polymer thickness of 1.50 to 1.70 mm and for the extension ratios  $\lambda$  of table (7-1) the values of strain energy were calculated directly from the computer stored stress-strain data for the particular polymer. By multiplying by the corresponding thickness the values of the energy per unit area lost in stretching  $W_s$  were deduced and are given in table (7-5). Obviously,  $W_s$  is part of the input energy  $P$  (table 7-2) and it can be expressed as a percentage of  $P$ ,

$$\text{i.e. } \frac{W_s \cdot 100}{P}$$

The values from that simple calculation are shown in table (7-6).

Two effects can be noted in the values of table (7-6).

TABLE 7-5

$W_s$  of unbacked samples ( $\times 10^3 \text{ J. m}^{-2}$ ) (stretching energy per unit area)

(95% Confidence Limits are Indicated)

	Chem Polished Copper	Etched Steel	Oxidised Copper
Pol A	3.30 $\pm$ 0.35	10.57 $\pm$ 0.20	23.07 $\pm$ 1.23
Pol B	2.03 $\pm$ 0.24	4.35 $\pm$ 0.17	24.70 $\pm$ 1.41
Pol C	3.02 $\pm$ 0.28	6.96 $\pm$ 0.32	22.72 $\pm$ 0.89
Pol D	1.24 $\pm$ 0.12	1.88 $\pm$ 0.11	6.36 $\pm$ 0.44

TABLE 7-6

$W_s$  of unbacked samples as a percent of the total input energy per debonded area. Coating thickness between 1.5 and 1.7mm.

	Chem Polished Copper	Etched Steel	Oxidised Copper
Pol A	90.41	92.55	90.15
Pol B	78.37	75.25	79.49
Pol C	65.65	64.56	66.51
Pol D	60.19	60.25	60.11

The first is that more energy is absorbed in stretching as the vinyl acetate content is increased. Considering the plasticizing effect that an increase of the vinyl acetate content has in these copolymers this trend is not surprising. The second and more important observation is that the proportion of energy dissipated in stretching remains relatively constant for each polymer regardless of the substrate. This correlation between the experimental data shows the importance of the mechanical properties of the polymers, in this case the energy absorbing capacity of the four polymers which of course is expected to remain constant in stretching without being affected by the substrate. In other words although the substrate determines the force required for steady peeling - and hence the total energy needed for fracture - it is shown that the fraction of that energy lost in stretching remains constant for a particular polymer.

It is useful to examine the effect that stretching has over a wider range of thickness. It has been shown in chapter 4 that the peel load increases sharply with the polymer thickness (figures 4-5, 4-6 and 4-7). If the input energy per unit area (table 7-2) is considered instead of the peel load and the stretching energy per unit area  $W_s$  is subtracted, then the remaining energy  $W_r$  available for peeling can be calculated. For the same thickness range examined in figures (4-5), (4-6) and (4-7) the terms  $W_r$  were calculated and plotted against the thickness.



There is still a dependence upon the polymer thickness as it is shown in the resulting figures (7-1), (7-2) and (7-3). This dependence is now reduced but the slope of the lines indicates that the remaining energy absorbing mechanisms incorporated in the term  $W_r$  are still affected by the volume of the polymer being peeled.

The energy dissipation mechanism examined above affected only the unbacked samples. The practically inextensible fabric support was used in the backed samples exactly to prevent that elongation. However, the possibility that the fabric backed strip extends during the peel test - and especially when the peel load is large - has been investigated. The same method of measuring the extension ratio as in the unbacked samples was used, but the distance between the two lines was now 5 cm.

The highest  $\lambda$  value recorded for the backed samples was 1.03 and that corresponded to the highest peel load, ie approximately  $20 \text{ N mm}^{-1}$ . This extension represents, at least for these peel loads, an energy loss. But a simple tensile test of a fabric backed strip up to the same extension followed by unloading showed clearly that:

- a. The energy involved was small compared to say the corresponding input peel energy, and

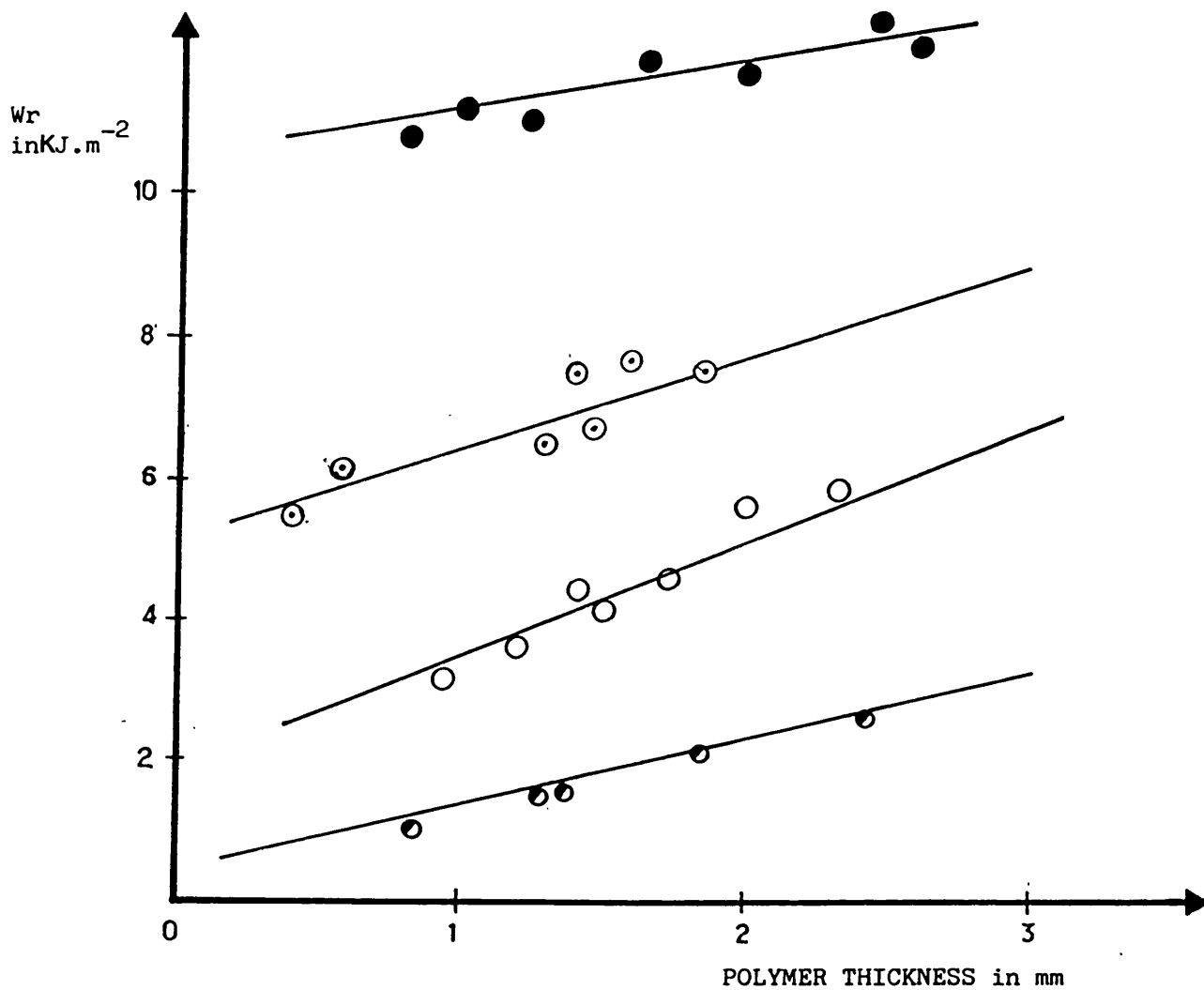


FIGURE 7-1: Dependence of  $W_r$  upon the thickness of unbacked samples peeled from oxidised copper ( $W_r$  is the remaining energy per unit area after the stretching term  $W_s$  subtracted from the input energy).

◌/ Polymer A, ◌• Polymer B, ● Polymer C, ◌ Polymer D.

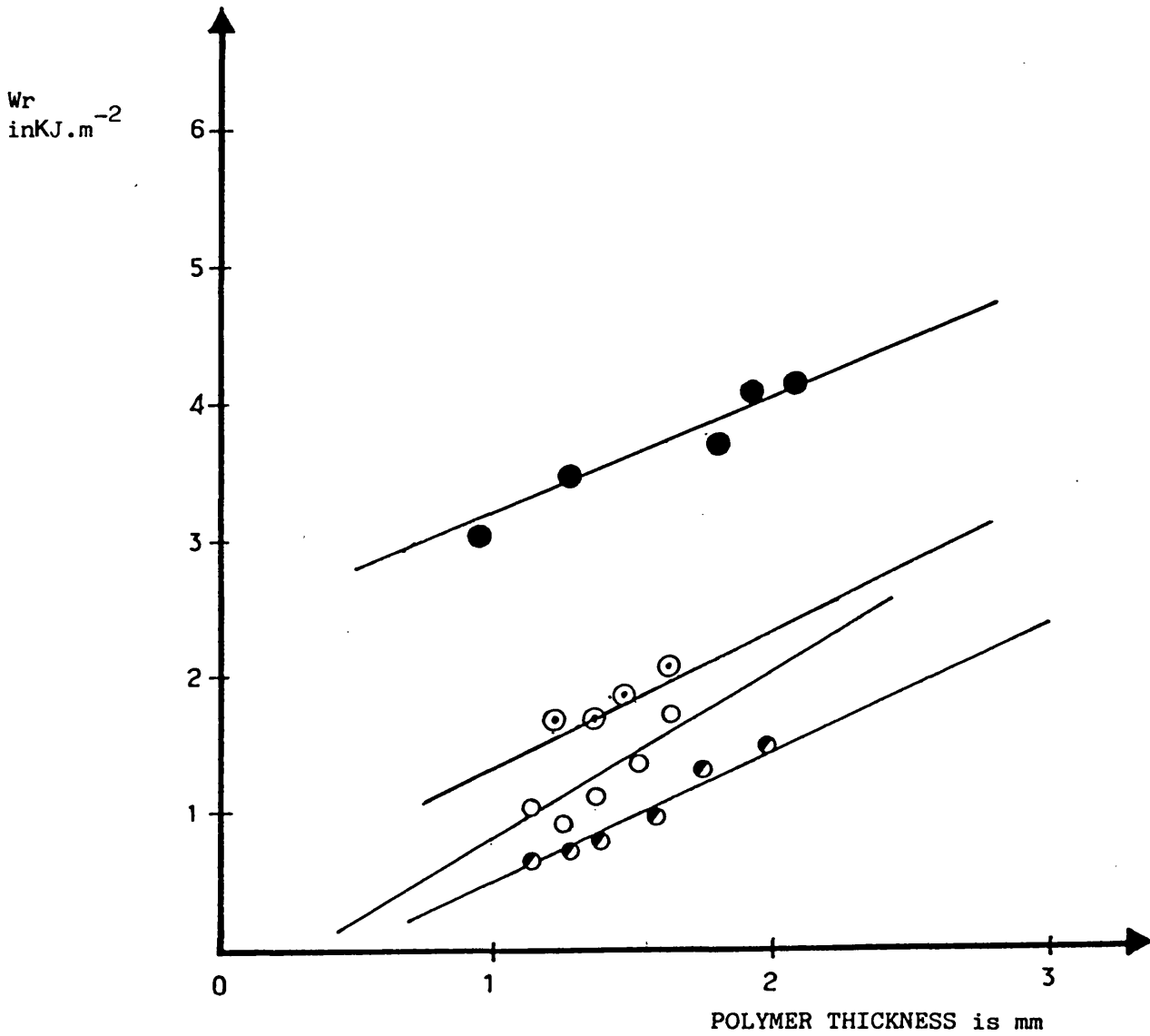


FIGURE 7-2: Dependence of  $W_r$  upon the thickness of unbacked samples peeled from etched steel.

( $W_r$  is the remaining energy per unit area after the stretching term  $W_s$  is subtracted from the input energy).

● Polymer A, ○ Polymer B, ● Polymer C, ○ Polymer D

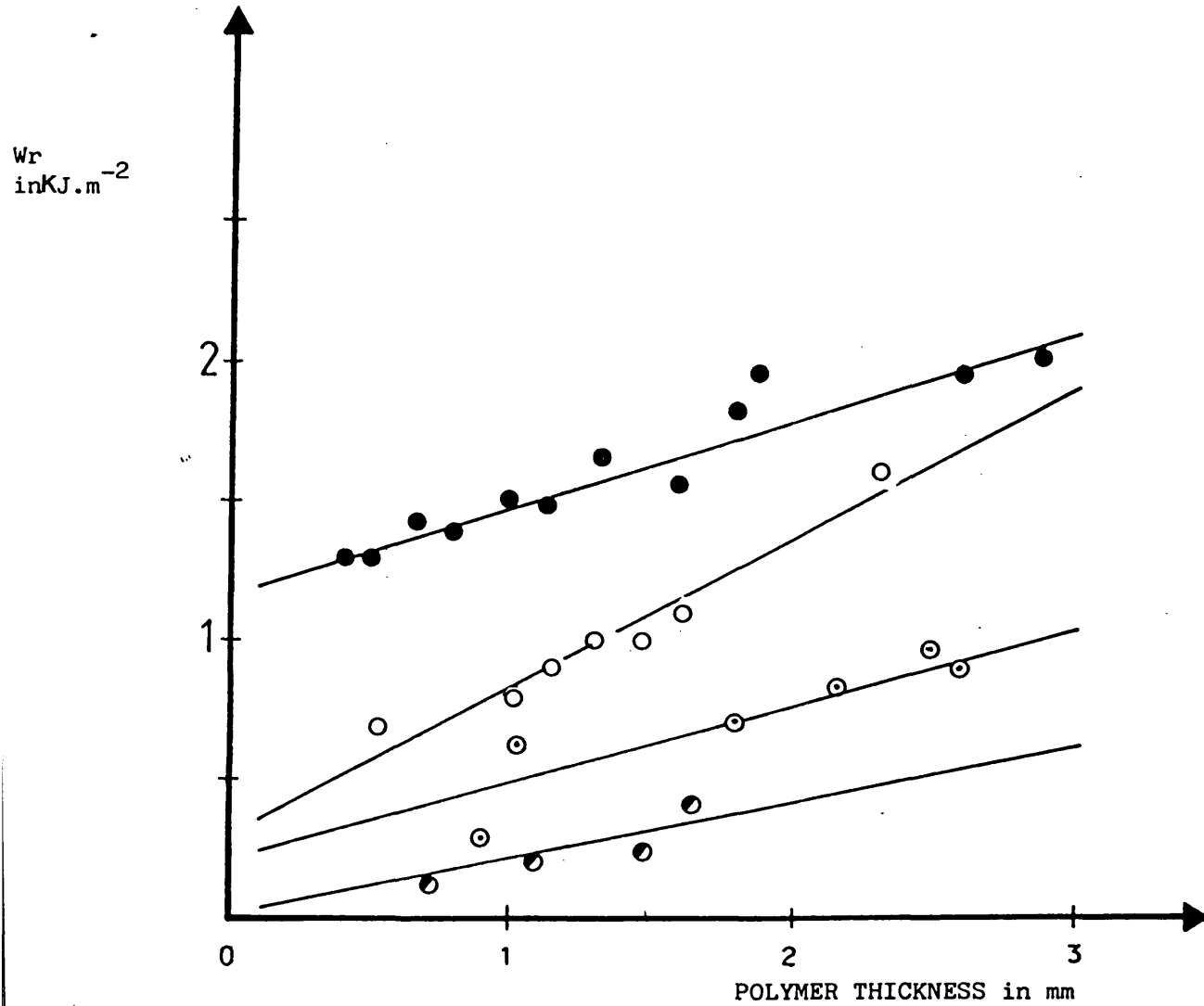


FIGURE 7-3: Dependence of  $W_r$  upon the thickness of unbacked samples peeled from polished copper.

( $W_r$  is the remaining energy per unit area after the stretching term  $W_s$  is subtracted from the input energy).

● Polymer A, ○ Polymer B, ● Polymer C, ○ Polymer D.

b. A significant part of the extension was elastic and so recoverable.

So, in this analysis the extension of the freed strip as a mechanism of energy absorption for the backed samples will be ignored.

#### 7.4 ENERGY LOSSES DUE TO PLASTIC BENDING

The theory developed by Gent et al (84) to measure experimentally the energy lost due to plastic bending and described in detail in chapter 2 will be followed in this work. To use equation (2-7) values of the radius of curvature  $R$  (fig 2-3) were necessary. The radius  $R$  was measured while the polymer strip was peeling by taking photographs of the peel profile. An initial enlargement of four times was directly achieved by the special lens of a NIKON F1 camera. The negatives were again enlarged about  $3 \frac{1}{2}$  times by projecting them on a separate sheet of paper. The outer and inner regions of the bent strip in the projected profile were carefully traced on the paper. That trace is part of a circle the centre of which was graphically established from the verticals on three tangents at different points on that section. The position of the centre was checked by following the circular section with a pair of compasses. The minimum radius of curvature  $R$  of the neutral line  $OO'$  in figure (2-3) was the opening of the compasses minus half the strip thickness. With the procedure described above forty three measurements of  $R$  were made for various thicknesses of the four E.V.A copolymers peeled from the three substrates. Twenty one of these were for unbacked samples and twenty two for backed.

In chapter 5 the yield stress and yield strain of the four E.V.A. copolymers were determined in tension for strain rates of 0.027,

0.069, 0.27, 1.38 and 6.94 min<sup>-1</sup>. The relationships between the yield stress and yield strain in table (5-5) and the logarithm of the imposed strain rates are described by the equations shown in table (7-7).

For a particular strip thickness Gent et al (84) have suggested a simple relationship for the maximum strain rate ( $\dot{\epsilon}$ ) in bending:

$$\dot{\epsilon} = \frac{\dot{c}}{t} \quad (7-4)$$

where  $\dot{c}$  is the peeling rate and  $t$  the thickness of the strip. For all the samples used in the measurement of the radius of curvature  $R$  the different strain rates  $\dot{\epsilon}$  in bending were calculated from equation (7-4). These strain rates were now used to obtain a pair of yield strain and yield stress values for each particular case by referring to the relationships of table (7-7). So, for the forty three samples mentioned above, values were available for the radius of curvature  $R$ , polymer thickness  $t$ , and yield stress  $e_y$  and yield strain for the particular strain rate. That allowed the calculation of the energy per unit area  $W_b$  which is expended in plastic bending from equation (2-7). The calculation of four  $W_b$  terms for unbacked samples and four  $W_b$  terms for backed samples is demonstrated in table (7-8). All the  $W_b$  terms determined by this method are shown in table (7-9) for the unbacked and backed samples as well as the corresponding input energy per unit area  $P$

TABLE 7-7

Equations describing the relationship the yield stress  $\sigma_y$  and yield strain  $e_y$  of E.V.A. copolymers with the strain rate ( $\dot{\epsilon}$ ) in a tensile test of dumb bell specimens.

Polymer A	$e_y = 0.158 + 0.038 \log (\dot{\epsilon})$	$\sigma_y = 2.210 + 0.142 \log (\dot{\epsilon})$
Polymer B	$e_y = 0.106 + 0.050 \log (\dot{\epsilon})$	$\sigma_y = 4.236 + 0.717 \log (\dot{\epsilon})$
Polymer C	$e_y = 0.076 + 0.076 \log (\dot{\epsilon})$	$\sigma_y = 5.300 + 0.788 \log (\dot{\epsilon})$
Polymer D	$e_y = 0.064 + 0.049 \log (\dot{\epsilon})$	$\sigma_y = 6.485 + 2.960 \log (\dot{\epsilon})$



TABLE 7-8

Examples of calculating the energy lost in plastic bending  $w_b$  per unit area for backed and unbacked samples.

Unbacked samples

	t (mm)	R (mm)	$e_y$	$\sigma_y$ (MPa)	$w_b$ (KJ.m <sup>-2</sup> )
Pol A	1.83	0.95	0.202	2.372	0.691
Pol B	1.40	1.96	0.169	5.133	0.178
Pol C	1.50	1.62	0.125	7.120	0.675
Pol D	1.07	1.35	0.132	10.53	0.496
	Backed samples				
Pol A	1.13	1.08	0.210	2.402	0.127
Pol B	1.42	0.75	0.169	5.129	1.257
Pol C	1.54	1.49	0.124	6.255	0.718
Pol D	1.51	3.21	0.122	10.09	0.207

TABLE 7-9

Energy dissipated in plastic bending  $W_b$  ( $K.J.m^{-2}$ ) with the corresponding input energy in parenthesis from all three substrates and for a variety of thicknesses.

Unbacked samples			
Pol A:	0.691 (15.99),	0.269 (6.50),	0.089 (2.16)
	0.441 (10.50),	0.426 (9.90),	0.096 (2.30)
Pol B:	0.178 (1.36),	0.381 (3.44),	1.528 (12.64)
	1.513 (12.76),	0.204 (1.58),	
Pol C:	0.675 (2.83),	2.543 (16.80),	0.801 (4.70)
	1.661 (9.46),	2.850 (17.58),	
Pol D:	0.496 (1.31),	1.667 (5.44),	0.495 (1.68)
	0.829 (2.80),	1.636 (5.22)	
Backed samples			
Pol A:	0.127 (3.91),	0.825 (25.62)	
	0.070 (3.61),	0.690 (21.70)	
Pol B:	0.143 (2.03),	0.302 (2.66),	0.149 (1.19)
	0.277 (2.32),	1.257 (10.70),	0.847 (9.78)
Pol C:	0.632 (4.20),	0.599 (4.27),	0.718 (4.58)
	0.620 (4.40),	1.159 (7.25),	1.942 (12.39)
Pol D:	0.207 (1.12),	0.385 (1.46),	1.010 (3.42)
	0.505 (1.92),	0.291 (0.90),	0.722 (2.32)

for each case (calculated as described in section 7.1). The energy lost in plastic bending per unit area  $W_b$  can be now expressed as a percentage of P. The results of that simple calculation for each of the E.V.A. copolymers are averaged and shown in table (7-10). Considering that they represent samples with a wide range of thickness (1.22 to 1.90 mm) and three substrates of different topography giving rise to a wide range of peel loads (0.90 to 6.54 N.mm<sup>-1</sup> for the unbacked and 1.10 to 14.20 N.mm<sup>-1</sup> for the backed samples) table (7-10) suggests that the scatter is only due to experimental errors. The important observation is that the value of  $W_b$  remains constant for each polymer. This is reminiscent of a similar conclusion reached for the stretching energy per unit area  $W_s$  of the unbacked samples. A direct comparison of table (7-6) with table (7-10) shows that the two major energy loss mechanisms studied for the unbacked samples account for the absorption of about 95% of the total input energy per area debonded, at least when the polymer thickness is between 1.50 and 1.70 mm.

A second important remark on table (7-10) is that for both unbacked and backed samples the contribution of  $W_b$  to the total energy increases as the polymer becomes tougher. The reasons for that trend are that :

- (a) A tougher polymer has generally higher yield stress and lower yield strain and:

TABLE 7-10

$W_b$  for three substrates as a percentage of the total input energy  $P$  per unit area debonded. In parenthesis are the number of experiments for each category. (95% confidence limits are indicated).

	Unbacked Samples	Backed Samples
Polymer A	4.34 $\pm$ 0.06 (6)	2.78 $\pm$ 0.83 (4)
Polymer B	13.05 $\pm$ 0.93 (5)	10.52 $\pm$ 2.27 (6)
Polymer C	23.82 $\pm$ 2.01 (5)	15.07 $\pm$ 0.89 (6)
Polymer D	37.82 $\pm$ 1.86 (5)	27.50 $\pm$ 6.95 (6)

(b) For the same thickness and peel load the R value is multiplied by a smaller yield strain and the dominant term:

$$\frac{t}{2R e_y}$$

in equation (2-7) becomes larger.

The combination of the above two effects increases the overall value of  $w_b$  as the vinyl acetate content decreases.

A third observation in table (7-10) is that generally the backed samples have smaller proportions of their total energy dissipated in bending than the unbacked samples. That is consistent with the residual curvature for the two categories which was clearly more profound for the unbacked samples.

Another noticeable difference between the unbacked and backed samples is the somewhat larger experimental scatter in the latter case. The explanation can be the possibility of errors in the accurate measurement of the radius of curvature from the peel profile. When the fabric backing was used the more ductile polymers showed a distinct lip of highly extended polymer in the peel front profile. That geometry complicated the normal measurement of R and in some cases made it impossible.

7.5 INDEPENDENT MEASUREMENT OF  $W_b$

In order to have an independent determination of the bending losses in a fabric supported strip a simple experiment was designed so that the validity of the  $W_b$  values calculated from equation (2-7) could be checked. The experimental set up is shown in figure (7-4). It consists of a metal rod of radius  $r$  which corresponds to  $(r - \frac{t}{2})$  for the peeling test. A fabric backed

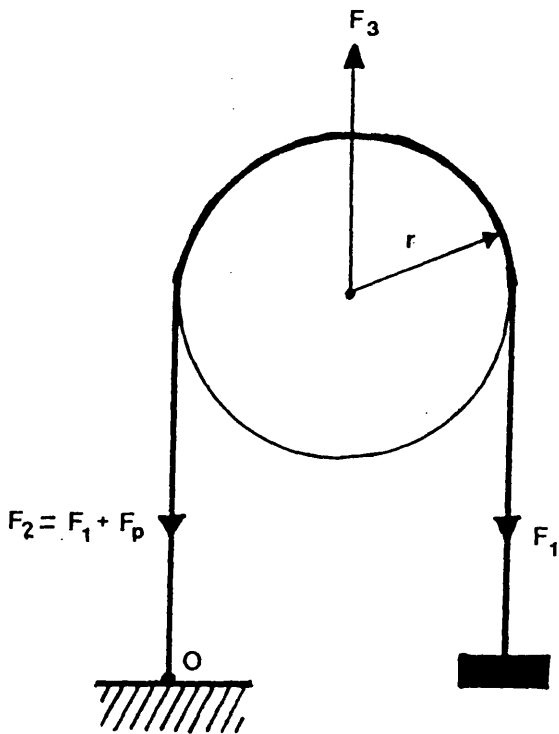


FIGURE 7-4: Experimental set up for measuring energy losses in plastic bendings.

strip of the same width as in the peel test is fixed at point O

and a load  $F_1$  is attached to the other end. The rod is capable of rotating and is connected to the load cell of an Instron tensile machine. When the cross-head moves a distance  $x$  the force  $F_3$  measured by the machine does work  $F_3 \cdot x$ . At the same time the weight has moved a distance  $2x$  and required work  $F_1 \cdot 2x$ . If a part  $F_p$  of force  $F_3$  is used to supply the work done in plastic bending on the left hand side of the strip then for the initial distance  $x$  it requires work  $F_p \cdot x$ . Assuming no other losses and considering the work balance we have:

$$F_3 \cdot x = F_1 \cdot 2x + F_p \cdot x \text{ or} \tag{7-5}$$

$$F_3 = 2F_1 + F_p$$

Also, from figure (7-4) is obvious that:

$$F_2 = F_1 + F_p \tag{7-6}$$

The forces in figure (7-4) can be correlated to those in a peel test. If they are expressed as force per unit width of the strip they also represent energy per unit area. So,  $F_2$  corresponds to the input energy which is available for fracture (or peel energy) per area debonded and  $F_p$  corresponds to the energy expended in plastic bending per area debonded. If it is assumed that the strip in this model undergoes plastic bending and there are no losses due to stretching, by increasing the dead load  $F_1$  a series of  $F_2$

and  $F_p$  values can be calculated from equations (7-5) and (7-6). If  $F_2$  is plotted against  $F_p$  for varying rod diameters we can have a set of lines (one for each rod radius) from which we can then directly obtain  $w_b$  for any value of P.

Although it is tedious to generate the data that this model requires it should prove useful. However, there were a lot of practical problems. The first condition was to use rods of small diameter to create bending of similar curvature to the peel test. The dead load  $F_1$ , necessary to represent a typical peel energy was at least 5 Kgf and it is obvious that the higher the peel energy the smaller the required diameter of the rod. It was proved impossible to machine such a rod; the one with the smallest radius of 0,794 mm could hardly support 2 Kgf. In any case the minimum theoretical value of  $r$  is  $\frac{t}{2}$  and has no meaning

for this model. The second requirement was no other energy losses but bending. That also proved difficult to meet; friction introduced significant errors. The use of bearings for the rotation of the rod and lubricant for the inner part of the strip reduced that problem but has not eliminated it. Therefore the results obtained from the experiments were subject to large errors.

If an improved design can avoid the above experimental problems it is suggested that the proposed model can produce a meaningful independent measurement of the energy expended in plastic bending.



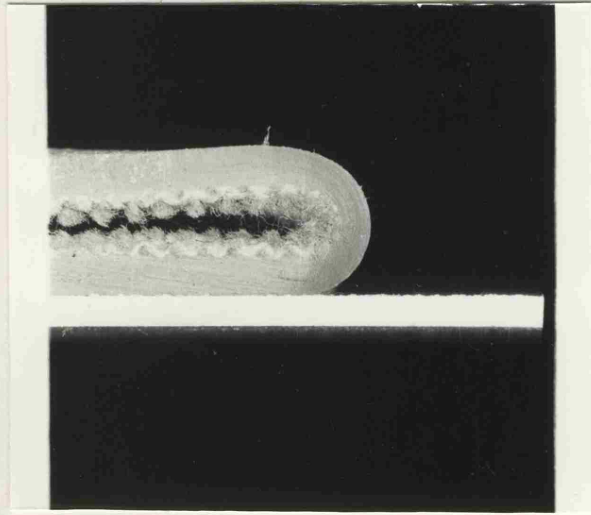
## 7.6 OTHER LOSS MECHANISMS

As it is mentioned in chapter 2 the peel front profile of the backed samples is in some cases different from that for the unbacked samples. A distinct lip of highly extended polymer is following the peel front of the backed strip; there is no such lip formed during the peel testing of unbacked strips.

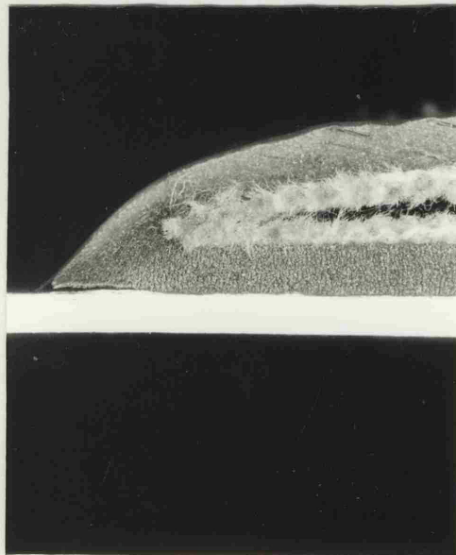
Photographs (7-1) and (7-2) show the peel front profile of two backed specimens while they are peeled from chlorite oxidised copper. It can be seen that the polymer D strip in (7-1) appears to curve tangentially to the substrate in contrast to the polymer A strip in (7-2). Even between all the backed specimens there is difference in the extent of stretching for the four polymer. A second and important observation was that the substrate affects to a significant degree the size of the lip. The substrate that produced the maximum stretching was chlorite oxidised copper. It is interesting to note that the combination of the most ductile polymer (polymer A) and the above substrate recorded also the highest peel loads.

The visual and photographic evidence in the present work suggested that the extension of the polymer in the peel front profile of the backed samples constituted a major energy dissipation mechanism.

(7-1)



(7-2)



PHOTOMICROGRAPHS (7-1) and (7-2): Pictures of the peel front profile of (7-1) polymer D and (7-2)A, peeling from chlorite oxidised copper.

The main reason for that is the very high deformation rate a relatively small volume of polymer is subjected to at the peel front. For example, for the standard crosshead speed of  $50 \text{ mm min}^{-1}$  used in the present project the corresponding peel rate for the backed samples was  $25 \text{ mm min}^{-1}$ . Thus the deformation rate for a strip with an average thickness of  $1.6 \text{ mm}$  is  $15.6 \text{ min}^{-1}$  which is much faster than the deformation rates achieved in chapter 5. In addition to that each layer ( $dt$ ) of the polymer's thickness experiences at the peel front a loading - unloading cycle up to different stresses. For example, the layer close to the metal could be stressed up to the failing tensile stress whereas the layer close to the fabric backing experiences a significantly lower stress. The mechanical equivalent of that energy dissipation mechanism is a hysteresis test (chapter 2) and the energy lost per unit area  $W_1$  is given by:

$$W_1 = \int_0^{t_1} H(t) dt \quad (7-7)$$

where  $t_1$  is the maximum that the polymer thickness reaches and  $H(t)$  is the hysteresis energy lost in tension in a layer inside the polymer and at a distance  $t$  from the substrate. To use equation (7-7) for the determination of  $W_1$ , the exact gradient of stress within the polymer's thickness must be firstly established. Then, the hysteresis values from tensile tests up to stresses corresponding to those at the polymer lip can be used to define  $H(t)$  and hence  $W_1$ .

From the one cycle loading tests described in chapter 5 it was calculated that the variation of the hysteresis energy H per unit volume with the preset stress limit is approximately described by the following relationships:

$$\text{Polymer A: } H_A = -4.84 + 2.10 \sigma \quad (7-8)$$

$$\text{Polymer B: } H_B = -9.93 + 2.49 \sigma \quad (7-9)$$

$$\text{Polymer C: } H_C = -11.64 + 2.94 \sigma \quad (7-10)$$

$$\text{Polymer D: } H_D = -6.98 + 1.32 \sigma \quad (7-11)$$

In equations (7-8) to (7-11) if  $\sigma$  is replaced by any value above the yield stress of the corresponding polymer and at the equal deformation rate of  $0.27 \text{ min}^{-1}$  a positive value of H is obtained. For any such stress the calculated hysteresis energies follow the trend shown in table (7-3). As a consequence the integration of these terms (equation 7-7) will give  $W_1$  values still following the same trend. Thus, although the exact distribution of stresses is not known the above treatment can justify the order of the peel energies required for peeling the four E.V.A. copolymers.

The presence of the backing not only prevents the extension of the freed strip but also transfers the load needed for steady peeling to the interface in a way that the "legging" is elevated to a significant energy loss mechanism. Substrates capable of holding back this polymer lip and/or polymers exhibiting large hysteresis losses in general, obviously dissipate more energy per unit volume resulting in a higher peel load.

In conclusion to obtain an accurate value for the energy lost per unit area  $W_1$  by the "legging" mechanism factors that must be taken into account are:

- (a) The magnitude of the extension at the peel front.
- (b) The rate of polymer deformation for the particular peeling rate and coating thickness.
- (c) The stress gradient along the extended polymer lip and:
- (d) The relationship describing the hysteresis losses with the stress level in a one cycle tensile test carried out at the deformation rate described in (b).

## 7.7 SYNTHESIS OF THE ENERGY DISSIPATION TERMS

The work done by the peeling force has been calculated for backed and unbacked samples from the peel loads and extension ratios presented in chapter 4. The method followed to analyse the input energy was based on the energy balance approach, ie the fact that this energy  $P$  is equal to the sum of all the energy loss terms  $W$  via mechanisms  $i, j, k, \dots$  so generally we have:

$$P = W_i + W_j + W_k + \dots \quad (7-12)$$

Some of these mechanisms were identified and the contribution of each term to the total energy  $P$  has been examined separately. One energy term for both backed and unbacked samples in the right hand side of equation (7-12) is the thermodynamic surface energy required for detachment, which in this case is the thermodynamic work of cohesion  $W_c$  because of the failure modes observed after peeling. This energy term  $W_c$  would represent the total energy  $P$  if during the peeling test the polymer strip was deformed reversibly without any dissipation of mechanical energy. The energy of cohesion  $W_c$  was not determined experimentally but its value was calculated. The contribution that  $W_c$  makes in the general equation (7-12) is insignificant since the total energy term  $P$  is several orders of magnitude larger than  $W_c$ . Other implications due to the term  $W_c$  are discussed in chapter 8.

For the rest of the energy loss terms the use of the inextensible fabric backing distinguished the dissipation terms between backed and unbacked samples and made it necessary to examine these samples separately. Let us deal first with the unbacked samples. The strain energy expended in the detached strip was first calculated from its total extension and by simulating that situation to the strain energy needed in a simple tensile test up to the same extension. It must be noted that stretching during peeling changes also the distance that the peel force is moving and hence the input energy  $P$ . The strain energy per area debonded due to stretching  $W_s$  was found to account for a significant proportion of  $P$ , and in the case of polymer A for about 90%. For a wide range of peel loads arising from different substrates each of the four polymers provided a similar contribution of  $W_s$  to the corresponding input energy  $P$ . This is not surprising considering the method of calculating  $W_s$ . It is however a significant observation showing that the above mechanism is affected by the polymer properties. The substrate, as far as stretching of the peeled strip is concerned, is only reducing the advance of the fracture to different extents and thus causes large or small extension of the strip.

The second energy term examined for the unbacked samples was that expended in plastic bending when the polymer strip traverses the highly bent region in the peeling front. That energy  $W_b$  was calculated from a formula based on elementary bending theory and used by Gent and Hamed (84). The absolute values of  $W_b$

are somewhat smaller than  $W_s$  and so was their contribution to P. This contribution was again proved to depend on the particular polymer rather than the substrate from which it is being peeled. Therefore the energy lost in plastic bending again reflects upon the mechanical properties of the polymers (in this case the yield properties). For the purpose of the bending analysis the substrate can influence the observed peel load only by imposing the degree of bending, ie the radius of curvature R.

It is suggested that the above two mechanisms are the major energy dissipation patterns for the unbacked samples. The experimental results indicate that as the vinyl acetate content is increasing from polymer D to A so does the contribution of  $W_s$  to P whereas at the same time the contribution of  $W_b$  to P is decreasing. The sum of the two accounts for about 95% of the total energy.

The remaining energy available for fracture for the unbacked samples is approximately 5.2, 8.6, 10.5 and 2.0 percent of the total input energies shown in table (7-2) for polymers A, B, C and D respectively. The absolute value of that remaining energy obviously varies for the three substrates. It is suggested that at least a part of this energy is lost in extending the polymer at a small zone close to the fracture plane. The dimensions of that highly stressed zone can be estimated from the thickness by which the strain energy density to failure (table 5-1) must be multiplied to yield the required values of the remaining fracture energy per



unit area. Such estimates produced zones of 10, 19, 28 and 5  $\mu\text{m}$  for polymers A, B, C and D which are consistent with the order of magnitude of the extended polymer filaments seen in the scanning electron micrographs of the fractured surfaces in chapter 6 and also measured as residual polymer thickness.

Let us now consider the backed samples.

For the backed samples the energy expended in plastic bending was also calculated from the previously mentioned equation and its contribution to P was found smaller than the corresponding contribution for the unbacked samples. In addition, less energy is dissipated by that mechanism as the vinyl acetate content increases and a similar explanation as for the unbacked samples is suggested for that trend.

For the polymer-substrate combinations that give high peel loads (eg oxidised copper and polymers A or C) the peel profile showed that a "lip" of highly drawn polymer is formed and in extreme cases that makes the measurement of the radius of curvature impossible. It is suggested that this mechanism dissipates large amounts of energy inside the bulk of the polymer.

The remaining energy available for fracture is approximately 97.2, 89.5, 85.0 and 72.5 percent of the total input energies shown in table (7-3) for polymers A, B, C and D respectively. The absolute

value of that remaining energy also varies for the three substrates but generally polymer/substrates combinations producing large "lip" extensions required larger amounts of input energy for peeling eg oxidised copper and polymer A.

Finally, it has been shown by an approximate treatment that the energy lost per unit area in the polymer lip  $W_1$  will follow the general trend shown in the input energies of table (7-3), ie a decrease from polymer A to polymer D with a peak for polymer C.

## CHAPTER 8

### DISCUSSION AND CONCLUSIONS

#### 8.1 EFFECT OF SUBSTRATE ON THE PEEL LOAD

It was one of the objectives of this work to examine the influence of the metal substrate and its topography on the peel performance of ethylene vinyl acetate copolymers applied as hot-melts. It is well established that the pretreatment of metals generally affects not only the initial adhesion levels but also the durability of adhesive joints. That effect is better understood if the processes taking place at the interface are examined in some detail. The morphology of the substrate can impose the failure mode while its surface chemistry affects decisively the wetting or it can introduce chemical changes to the polymer in contact.

For each ethylene vinyl acetate copolymer the three substrates used in this project recorded a different peel load. However, the order of these loads for any particular polymer remained the same, even when a backing was used; chlorite oxidised copper gave the highest peel loads, chemically polished copper the lowest with intermediate values for etched steel.

This order is reminiscent of results for the adhesion of low

density polyethylene peeled from similarly prepared substrates.

(128) In that study it was also shown that for the case of oxidised copper the growth of the oxide layer as controlled by the substrate oxidation time had a critical effect on the peel adhesion of the polyethylene coating. Let us consider oxidised copper as the first substrate. As regards the chemical changes at the interface it has been suggested before that no significant polymer oxidation occurs when copper is the substrate (141) (148). Experimental results for the E.V.A. copolymer surface released from oxidised copper also point to that direction (see section 6.2). It is clear that polymer oxidation by the chlorite oxide remains an unlikely mechanism to account for the observed high peel loads associated with that substrate. Instead it is suggested that the fibrous topography is the most significant factor leading to improved adhesion. The failure mechanism from a fibrous substrate can be compared to that of a single fibre pulling out of a matrix in a composite material (74). The magnitude of the interfacial shear strength ( $\tau$ ) developed determines the debonding between the fiber and the matrix and is given by: (149)

$$\tau = \frac{\sigma_f d}{2l}$$

where  $\sigma_f$  is the tensile strength of the fibre,  $d$  its diameter and  $l$  its length.

In the present work there is no evidence of any breaking of fibres and failure was proved to occur within the polymer itself. However, the examination of the polymer side of fracture in the scanning electron microscope suggested a failure mechanism based on composite theory and described in detail by Wang et al (74) and Evans et al (128); the stress needed to propagate peeling is transferred through the polymer to the fibre-polymer interface. Shear stresses are then building up around the fibre ends and involve a considerable mass of polymer to plastic deformation. The stress needed to pull out the oxide fibre is not surpassed, so fracture proceeds within the bulk of the polymer. At the same time, shear stresses are building up around oxide fibres still inside the polymer and close to the peel front until fracture occurs, and so forth. Evidence supporting that mechanism comes:

(a) from the microscopic examination of both fractured sides of the bond where the polymer is heavily drawn (pictures 13, 14, 15 and 16) and;

(b) from the peel load-time lines for oxidised copper where the above described sequence is reflected as slip-stick behaviour.

Let us now consider the effect that etched steel had on the observed peel loads. In the as received state etched steel was

significantly rougher than copper (section 3.3). Subsequent etching in hydrochloric acid for 30 seconds did not remove that roughness completely although the topography as seen in a scanning electron microscope was relatively smooth compared to oxidised copper. The debonding stress necessary for steady peeling is again transferred to the interface through the detached strip and has its maximum at the line of detachment. This stress is passed on to the undeformed polymer without significant fluctuation and failure occurs cohesively very close to the interface. The load-time line in the case of etched steel is relatively steadier suggesting the above mechanism. Some peaks in that line correspond to the peel front passing along the machining lines which are the only visible large discontinuities on the bare metal seen in the scanning electron microscope (photomicrograph 3-1). The fracture process for etched steel clearly involved less polymer in plastic deformation than the one for oxidised copper. Evidence for that is provided by fractography (pictures 9 and 10) as well as by a reduction in the difference between the peel loads for the four polymers as compared to oxidised copper.

The latter observation suggests that the maximum stresses before failure at an E.V.A. copolymer/etched steel interface are such that the stresses transferred into the bulk of the polymer are such that the significance of the properties of the particular polymer deformed

is diminished, ie a change in polymer does not alter the peel load as dramatically as oxidised copper.

In addition to the proposed fracture mechanism, etched steel affects the measured peel loads by introducing chemical changes at the interface. The results from X.P.S. show an increased oxygen content on the surface of the four polymers after being soaked off the above substrate. The same effect has been observed by other authors (128) (141) (148) for polyethylene and it has been proposed that steel catalyses the oxidation of the polymer at the interface. It is suggested that a similar reaction takes place at the interface under consideration. Although its exact contribution to the peel load remains unknown, oxidation is likely to improve adhesion:

(a) through the introduction of more polar groups at the interface or/and;

(b) by strengthening mechanically a polymer layer close to the interface.

The third substrate, chemically polished copper, had also an effect on the peel load. The differences between the peel loads of the four E.V.A. copolymers were further reduced and the adhesion level for any particular polymer was the lowest amongst the three substrates. The measurement of the contact angles between three liquids and polished copper after peeling showed cohesive failure

within the bulk of the polymer. The fact that the polymer side of the fracture is a replica of the metal structure as well as the absence of any extensive polymer drawing suggests that the residual polymer film is very thin ie less than approximately 1  $\mu\text{m}$  which was the thickness for oxidised copper. Working with polyethylene Bright et al (141) suggested that copper actually inhibits any polymer oxidation. If that argument is employed for the four ethylene vinyl acetate copolymers of the present work - or at least to the hydrocarbon segments in their macromolecule - the interface reinforcement mechanism proposed for etched steel does not apply for polished copper and that may explain the low peel adhesion of that substrate.

In conclusion, it is beyond doubt that the metal substrate and its surface topography affect the measured peel load to a great extent. The failure mechanism and fracture path are mainly dictated by the substrate. The proposed mechanisms for the E.V.A. copolymers are similar to those shown to be valid for polyethylene peeled from identical substrates.

The experimental evidence from this work in support of these arguments comes from:

- (a) surface analysis of the fractured surfaces by M.I.R. infra-red spectroscopy and X.P.S.;



(b) the line on the peel load/time graph;

(c) examination of the fractured surfaces by scanning electron microscopy and;

(d) the fact that the order of increasing peel load for a particular E.V.A. copolymer is identical to low density polyethylene ie polished copper, etched steel and chlorite oxidised copper.

## 8.2 EFFECT OF BACKING ON THE PEEL LOAD

By comparing the peel loads in figures (4-2) and (4-4) it is obvious that the use of the fabric backing increases the peel load dramatically. By adopting the energy balance approach the major mechanisms of energy absorption have been identified and their contribution has been assessed. Obviously, different mechanisms operate depending upon the use or not of the fabric support. It is proposed that the difference in the dissipation processes can account for the dramatic increase of the peel strength. Such a change is inevitable since for example the backing prevents any elongation of the freed strip and also involves more polymer in local deformation close to the peel front.

It is interesting to note that the trend for the peel loads of the four polymers remains broadly the same for both cases. That observation suggests that although the patterns of energy dissipation change, it is the polymers response to deformation (by any mechanism) that is accountable for the measured peel load.

### 8.3 EFFECT OF POLYMER ON THE PEEL LOAD

It is clear that the adhesion of E.V.A. copolymers to the metals employed for this work as measured by the peeling test depends strongly upon the polymer being peeled. (See the results in chapter 4.) The fluctuations in peel strength from polymer A to polymer D are in fact larger than those obtained by altering the substrate. Thus the role of the substrate is confined to its ability to transfer stresses of a certain level from the interface to the polymer by one of the mechanisms described in section 8.1 and it is the properties of the particular polymer that dominate the measured peel strength.

The first obvious change in the four E.V.A. copolymers is their vinyl acetate content. If the separation from the metals was purely adhesive the existence of more polar groups at the interface would be an important factor during debonding. However, the separation was cohesive and also it is clear from figures (4-2) and (4-4) that the adhesion does not decrease monotonically from polymer A to polymer D. Therefore the interpretation becomes more complex.

The main pattern in the peel loads of the four polymers was a decrease from high values for A to low for D with a peak at polymer C. Some mechanical properties of the polymers like yield stress, yield strain and elastic modulus change monotonically

with the vinyl acetate content. Significantly though, other properties follow the trend of the peel loads.

One mechanical test showing a similar trend was the "trousers" type tear test (figure 5-8). Ahagon et al (150) argued that the tear path is sometimes wider than the thickness of the uncut sheet used to calculate the tear energy because it propagates at an angle to the principal tensile stress. Visual examination of the torn surfaces showed that this was the case for the E.V.A. copolymers. But even if the tear energy values are reduced by the proposed (150) forty percent the trend remains the same.

A second polymer property which from polymer A to D followed a trend reminiscent of the peel loads is the strain energy density to failure (table 5-1). The capacity of the polymers to absorb strain energy when stressed to failure in a tensile mode shows decreasing values from polymer A to polymer D with a peak for polymer C. Although the absolute values of table (5-1) have to be adjusted for the true deformation rate during peeling it is worth noting that the trend remains unchanged for the three test rates used. It has been shown in chapter 7 that the stretching energy term  $W_s$  in the case of unbacked samples constitutes a major part of the input energy. That in conjunction to the results of table (5-1) can explain the trend in the peel loads, at least for the unbacked samples.

The basic energy dissipation mechanism in the case of the backed samples was that associated with losses at the peel front.

The stress distribution in that zone has been recently studied by Niesiolowski and Aubrey (151). They peeled at 90° a polybutyl acrylate adhesive backed by a polyester tape from glass and photographed the peeling profile. By considering the stresses developed close to the peel front they concluded that the force required for peeling may be very significantly affected by filamentation. Although the peel angle in the present work is 180° the energy analysis approach to the same phenomenon leads to a similar conclusion; large amounts of energy available for fracture have been ascribed to the above mechanism. It is interesting that as with the stretching energy of the unbacked samples, the energy dissipated in the "legging" mechanism has been directly correlated to the mechanical response of the coating which in this case is the hysteresis loss in one cycle. It was gratifying to see that the hysteresis losses measured independently for polymer A to polymer D follow the same trend as the peel energy.

It is today well established that the behaviour of a peel joint depends strongly upon the mechanical properties of the peeling member. The evidence for ethylene vinyl acetate copolymers peeled from copper and steel reinforces this argument further by relating the energy dissipation mechanisms studied to particular properties of the polymers. The same input energy required for peeling can

be also analysed by following the generalised fracture mechanics approach used by Andrews and Kinloch (86) (87) and discussed in chapter 2. The idea that their treatment implies is that the total energy of peeling  $P$  can be expressed as the product of the thermodynamic work of cohesion  $W_c$  (for the failure modes observed in the present investigation) and an energy dissipation function  $f$  to account for the viscoelastic losses in the adhesive. The values of  $W_c$  as determined by contact angle measurements have an insignificant contribution to the total energy compared with other mechanisms. They also increase from about  $67 \text{ mJ.m}^{-2}$  for polymer D to about 98 for polymer A (table 7-4). This difference however is magnified when it is multiplied by the viscoelastic loss function  $f$  which is expected to be much larger.

The rheological losses incorporated in the function are expected to depend upon the test temperature and rate which were constant in the present work. Also, if the energy dissipation mechanism are considered separately, the function is expected to depend upon the polymer characteristics which are important for the particular process, ie the yield values for the bonding mechanism. That suggestion was verified by the results of this investigation; for at least two mechanisms (bending and stretching) it has been shown that their relative contribution to a wide range of input energies was virtually unchanged for the same polymer. A similar suggestion has been reported by Aubrey et al (152). They associated the observed peel strength of a poly (butyl acrylate) based

adhesive to glass with the change in strain within the adhesive, a parameter expected to be greater for an adhesive of low modulus than for adhesive of high modulus. That change in strain was reflected in the filamentation process during peeling.

In conclusion the effect that the four different E.V.A. copolymers have on the observed peel loads can be explained by considering the energy dissipated in deformation processes within the polymers. The principle on which the generalised theory of fracture mechanics is based was shown to be consistent with the experimental results at least when the rheological losses were considered separately for each dissipation mechanism.

#### 8.4 CONCLUSIONS

The 180° peel adhesion of four E.V.A. copolymers with varying vinyl acetate content peeled from steel and copper has been analysed by considering the energy balance during peeling.

The surface topography of the metal substrate influences the energy required for peeling by dictating the fracture mechanism (different for microfibrinous and conventional substrate topographies). Also, the substrate affects the polymer in contact by causing chemical changes to different extents depending upon the particular metal.

The peel energy was also influenced by the use or not of an inextensible fabric backing. The backing manifested its influence by altering the processes through which the input energy was dissipated in the system.

Finally, a change in polymer also affect the peel energy significantly. That phenomenon can be better understood by considering the various energy dissipation mechanisms. For the unbacked samples the major contributions to the peeling energy come from stretching the freed strip and plastic bending. For the backed samples energy is lost in plastic bending and in the "legging" mechanisms. All the mechanisms studied are related to specific mechanical properties of the polymers the values of which justify the trend



observed in the input energy of the four polymers. In addition the experimental results of this work are consistent with the idea of the peel energy being a product of the interfacial and rheological losses.

- (1) S S VOYUTSKII  
"Autohesion and adhesion of high polymers"  
(Interscience, New York, 1963)
- (2) R M VASENIN  
Vys. Soed. Vol 2 (1960) p.851
- (3) B V DERYAGUIN, N A KROTOVA, V V KARASSEV, Y M KIRILLOVA,  
I N ALEINIKOVA  
"Proceedings of second international congress on  
surface activity - II"  
(Butterworths, London, 1957) p.417
- (4) B V DERYAGUIN  
Research, Vol 8 (1955) p.70
- (5) H KRUPP, W SCHNABEL  
J. of Adhesion, Vol 5 (1973) p.269
- (6) C T H STODDART, D R CLARKE, C J ROBBIE  
J. of Adhesion, Vol 2 (1970) p.241
- (7) A D ROBERTS  
"Adhesion - 1" Ed. K W Allen  
(Applied Science Publishers, London, 1977) p.207
- (8) H SCHONHORN  
"Adhesion: Fundamentals and practice"  
(Ministry of Technology, Maclaren, London, 1969) p.12
- (9) J W McBAIN, D G HOPKINS  
Second Report of the Adhesives Research Committee  
HMSO, London (1926)
- (10) W C WAKE, E M BORROFF  
Trans. Inst. Rub. Ind., Vol 25 (1949) p.199
- (11) B M HAINES  
"Aspects of adhesion - 3" Ed. D J Alner  
(University of London Press, London, 1967) p.40
- (12) J R G EVANS, D E PACKHAM  
J. of Adhesion, Vol 10 (1979) p.39

- (13) C W JENNINGS  
J. of Adhesion, Vol 4 (1972) p.25
- (14) K W ALLEN, H S ALSALIM  
J. of Adhesion, Vol 6 (1974) p.229
- (15) J R HUNTSBERGER  
"Treatise on adhesion and adhesives" Ed. R L Patrick  
(Marcel Dekker, New York, 1967) Vol 1, p.119
- (16) D TABOR  
Report on the Progress of Applied Chemistry, Vol 36  
(1951) p.621
- (17) R J GOOD  
"Treatise on adhesion and adhesives" Ed. R L Patrick  
(Marcell Dekker, New York, 1967) Vol 1, p.9
- (18) L PAULING  
"The nature of the chemical bond" 3rd Eddition  
(Cornell University Press, New York, 1960)
- (19) D K OWENS  
J. of Applied Polymer Science, Vol 19 (1975) p.265
- (20) D K OWENS  
J. of Applied Polymer Science, Vol 19 (1975) p.3315
- (21) A R BLYTHE, D BRIGGS, C R KENDALL, D G RANCE,  
V J I ZICHY  
Polymer, Vol 19 (1978) p.1273
- (22) F M FOWKES  
"Recent advances in adhesion" Ed L H Lee  
(Gordon and Breach, London, 1973) p.39
- (23) D K OWENS, R C WENDT  
J. of Applied Polymer Science, Vol 13 (1969) p.1741
- (24) J L KOENIG, P T K SHIN  
J. of Colloid and Interface Sci, Vol 36 (1971)  
p.247

- (25) R BAILEY, J CASTLE  
J. of Materials Science, Vol 12 (1977) p.2049
- (26) M GETTINGS, A J KINLOCH  
J. of Materials Science, Vol 12 (1977) p.2511
- (27) A W WHITE, L M GOWDIN, T WOLFRAM  
J. of Adhesion, Vol 9 (1978) p.238
- (28) M G SIMONSEN, R V COLEMAN, P K HANSMA  
J. of Chemical Physics, Vol 61 (1974) p.3789
- (29) J J BIKERMAN  
"The science of adhesive joints"  
(Academic Press, New York, 1961)
- (30) J J BIKERMAN  
J. of Adhesion, Vol 3 (1972) p.333
- (31) R J GOOD  
J. of Adhesion, Vol 4 (1972) p.133
- (32) H SCHONHORN  
J. of Polymer Science, A-1 (1963) p.2343
- (33) E D PLUEDEDEMAN  
J. of Adhesion, Vol 2 (1970) p.184
- (34) J R HUNTSBERGER  
J. of Polymer Science, A-1 (1963) p.1339
- (35) D BRIGGS, D M BREWIS, M B KONIECZO  
J. of Materials Science, Vol 11 (1976) p.1270
- (36) M GETTINGS, F S BAKER, A J KINLOCH  
J. of Applied Polymer Science, Vol 21 (1977) p.2375
- (37) W D BASCOM, C O TIMMONS, R L JONES  
J. of Materials Science, Vol 10 (1975) p.1037
- (38) L H SHARPE  
J. of Adhesion, Vol 4 (1972) p.51

- (39) W E HANFORD  
US Patent 23967 (1946)
- (40) R H BEEMAN, G E SMEDBERG  
Tappi, Vol 50(4) (1967) p.164
- (41) S d'ADOLF  
Rubber World, June 1964, p.80
- (42) G E J REYNOLDS  
J. of Oil Colour Chem Assoc, Vol 53 (1970) p.399
- (43) M H EDSER  
Paint Manufact, December 1967, p.25
- (44) C A FINCH  
Chemistry and Industry, Vol 42 (1971) p.1187
- (45) R J LITZ  
Adhesives Age, August 1971, p.32
- (46) L W BLIGHT, D C SUTHERLAND  
Modern Packaging, July 1961, p.134
- (47) "The hot melts -1"  
Modern Packaging, Vol 38(2) (1964) p.113
- (48) "The hot melts -2"  
Modern Packaging, Vol 38(3) (1965) p.125
- (49) G W GILBY  
"Developments in rubber technology" Ed. A Wheelan and  
K S Lee  
(Applied Science Publishers, London, 1982) Chapter 4
- (50) I O SALYER, A S KENYON  
J. of Polymer Science, Vol 9 (1971) p.3083
- (51) T FUJIKI, M UEMURA, Y KOSAKA  
J. of Applied Polymer Science, Vol 12 (1968) p.267

- (52) M SAITO, H TADA, Y KOSAKA  
J. of Polymer Science, Vol 8 (1970) p.2255
- (53) W H SMAROOK, S BONOTTO  
Polymer Engineering and Science, Vol 8(1) (1968)  
p.41
- (54) H NOBUHIRO, K HITOSHI, U MARARU  
Toyo Soda Kenkyu Hokoku, Vol 18(1) (1974) p.9
- (55) V V VAGANOV, N Z EVTYUKOV, A D YAKOVLEV, Y A MULIN,  
A L COLDENBERGG  
Plast Massy, Vol 3 (1978) p.71
- (56) G C LEE, M H EDSEER  
Polymers Paint and Colour Journal, May 1973, p.478
- (57) M HIROSHI, H YASUMORI  
Mokuzai Gakkaishi, Vol 25(4) (1979) p.288
- (58) P J HINE, D E PACKHAM, S EL-MUDDARIS  
J. of Adhesion, Vol 17 (1984) p.207
- (59) R S RIVLIN  
Paint Technology, Vol 9 (1944) p.215
- (60) T HATA  
Chemistry of High Polymers (Japan), Vol 4 (1947) p.67
- (61) B V DERYAGUIN, N A KROTOVA  
Doklady Akad. Nauk., Vol 61 (1948) p.849
- (62) G J SPIES  
Aircraft Engineering, Vol 25 (1953) p.64
- (63) J J BIKERMAN  
J. of Applied Physics, Vol 28 (1957) p.1484
- (64) J J BIKERMAN  
J. of Applied Polymer Science, Vol 2 (1959) p.216
- (65) D H KAEUBLE  
Transactions of the Soc. of Rheology, Vol 4 (1960) p.45

- (66) D H KAELBLE  
Transactions of the Soc. of Rheology, Vol 9 (1965) p.135
- (67) A N GENT, G R HAMED  
Polymer Eng. and Science, Vol 17 (1977) p.462
- (68) J L GARDON  
J. of Applied Polymer Science, Vol 7 (1963) p.625
- (69) J L GARDON  
J. of Applied Science, Vol 7 (1963) p.643
- (70) C JOUWERSMA  
J. of Polymer Science, Vol 45 (1960) p.253
- (71) T K M WONG  
PhD Thesis, CNA A 1970
- (72) A D CROCOMBE, R D ADAMS  
J. of Adhesion, Vol 12 (1981) p.127
- (73) A D CROCOMBE, R D ADAMS  
J. of Adhesion, Vol 13 (1982) p.241
- (74) T T WANG, H N VAZIRANI  
J. of Adhesion, Vol 4 (1972) p.353
- (75) A A GRIFFITH  
Phil. Transactions of the Royal Soc. A221 (1920) p.163
- (76) R S RIVLIN, A G THOMAS  
J. of Polymer Science, Vol 10 (1953) p.291
- (77) P B LINDLEY  
J. of the I.R.I, Vol 5 (1971) p.243
- (78) K KENDAL  
J. of Physics: Appl. Physics, Vol 8 (1975) p.1449
- (79) A J DUKE  
J. of Applied Polymer Science, Vol 18 (1974) p.3019

- (80) A J DUKE, R P STANDBRIDGE  
J. of Applied Polymer Science, Vol 12 (1968) p.1487
- (81) A N GENT, G R HAMED  
J. of Adhesion, Vol 7 (1975) p.91
- (82) F YAMAMOTO, S YAMAKAWA, S TSURU  
J. of Polymer Science, Physics Ed., Vol 18 (1980) p.1847
- (83) M D CHANG, K L DEVRIES, M L WILLIAMS  
J. of Adhesion, Vol 4 (1972) p.221
- (84) A N GENT, G R HAMED  
J. of Applied Polymer Science, vol 21 (1977) p.2817
- (85) D W AUBREY, G N WELDING, T WONG  
J. of Applied Polymer Science, Vol 13 (1969) p.2193
- (86) E H ANDREWS, A J KINLOCH  
J. of Polymer Science, Symposium 46 (1974) p.1
- (87) E H ANDREWS, A J KINLOCH  
Proc. Royal Society, A332 (1973) p.385
- (88) A N GENT, J SCHULTZ  
J. of Adhesion, vol 3 (1972) p.281
- (89) A N GENT, R P PETRICH  
Proceedings of the Royal Soc. vol A-310 (1969) p.433
- (90) H E BAIR, S MATSUOKA, R G VADIMSKY, T T WANG  
J. of Adhesion, Vol 3 (1971) p.89
- (91) T IGARASHI  
J. of Appl. Pol. Science, Physics Ed., vol 13 (1975) p.2129
- (92) R J KOOPMANS, R Van der LINDEN, E F VANSANT  
Polymer Engineering and science, Vol 22 (1982) p.878
- (93) N GRASSIE  
Transactions of the Faraday Soc., vol 48 (1952) p.379



- (94) D H GRANT, N GRASSIE  
Transactions of the Faraday Soc., Vol 52 (1960) p.445
- (95) R J KOOPMANS, R Van der LINDEN, E F VANSANT  
J. of Adhesion, Vol 11 (1980) p.191
- (96) R J KOOPMANS  
J. of Adhesion, vol 15 (1983) p.117
- (97) H T CHEN, M E LEWIS  
Analytical Chemistry, vol 36 (1964) p.1394
- (98) K NAKAO  
J. of Adhesion, Vol 4 (1972) p.95
- (99) J L KARDOS  
J. of Adhesion, Vol 5 (1973) p.119
- (100) H J SCHONHORN  
J. of Polymer Science: Polym. Letters, Vol 2 (1964) p.465
- (101) P M KAMATH, R W WAKEFIELD  
J. of Applied Polymer Science, Vol 9 (1965) p.3153
- (102) B W CHERRY, S EL MUDDARIS  
J. of Adhesion, Vol 2 (1970) p.42
- (103) H J SCHONHORN, H L FRISCH, T K KWEI  
J. of Applied Physics, Vol 37 (1966) p.4967
- (104) J R G EVANS, D E PACKHAM  
J. of Adhesion, Vol 9 (1978) p.267
- (105) F EGAN, D SATAS  
Adhesives Age, Vol 9(8) (1966) p.22
- (106) J JOHNSTON  
Adhesives Age, Vol 11(4) (1968) p.20
- (107) D PERETZ, O ISHAI  
J. of Adhesion, Vol 10 (1980) p.317

- (108) G R HAMED  
J. of Adhesion, Vol 16 (1983) p.31
- (109) Technical data for "EVATANE" Resins (Ethylene Vinyl Acetate)  
ICI, Paper EV501, August 1980
- (110) Grade Selection Guide, "ELVAX" Resins (Ethylene Vinyl  
Acetate), Du Pont de Nemours, Paper E15467, Switzerland
- (111) A N GENT, C T R PULFORD  
"Wear and tear of rubber" Ed. E H Andrews  
(Applied Science Publishers, London, 1979) p.155
- (112) L MULLINS  
Transactions of the IRI, Vol 35 (1959) p.213
- (113) H W GREENSMITH, A G THOMAS  
J. of Polymer Science, Vol 18 (1955) p.189
- (114) "Handbook of Plastics Test Methods"  
Ed. R P Brown (G Godwin Ltd, Bath, 1981) p.151
- (115) D E PACKHAM, J R G EVANS, P R DAVIES  
J. of Adhesion Vol 13 (1981) p.29
- (116) W L BAUN  
"Applications of surface science - 4"  
(North Holland Publishing Company, 1980) p.291
- (117) D B ARNOLD  
"Developments in adhesives - 2" Ed. A J Kinloch  
(Applied Science Publishers, London, 1981) p.231
- (118) D H BUCKLEY  
"Surface effects in adhesion, friction, wear and lubrication"  
(Elsevier Scientific Publ., Amsterdam, 1981) p.19
- (119) S WISCHNITZER  
"Introduction to electron microscopy"  
(Pergamon Press, 1970) p.105
- (120) E H ANDREWS  
"Fracture in Polymers"  
(Oliver and Roud, London and Edinburgh, 1968) p.177

- (121) W D BASCOM, S T GADONSKI, C M HENDERSON, R L JONES  
J. of Adhesion, Vol 8 (1977) p.213
- (122) A J KINLOCH, N R SMART  
J. of Adhesion, Vol 12 (1981) p.23
- (123) T SMITH  
J. of Adhesion, Vol 14 (1982) p.145
- (124) D R MULVILLE, R N VAISHNAV  
J. of Adhesion, Vol 7 (1975) p.215
- (125) R L PATRICK, J A BROWN, L E VERHOEVEN, E J RIPLING,  
S MOSTOVOY  
J. of Adhesion, Vol 1 (1969) p.136
- (126) F S BAKER  
J. of Adhesion, Vol 10 (1979) p.107
- (127) R L PATRICK, W G GEHMAN, L DUNBAR, J A BROWN  
J. of Adhesion, Vol 3 (1971) p.165
- (128) J R G EVANS, D E PACKHAM  
J. of Adhesion, Vol 10 (1979) p.177
- (129) H N VAZIRANI  
J. of Adhesion, Vol 1 (1969) p.208
- (130) R G AZRAK  
J. of Colloid and Interface Sci., Vol 47(3) (1974) p.779
- (131) D BRIGGS  
"Surface analysis and pretreatment of plastics and metals"  
Ed. D M Brewis  
(Applied Science Publishers, London, 1982) p.73
- (132) D T CLARK, W J FEAST, W K R MUSGRAVE, I RITCHIE  
J. of Polymer Science, Vol 13 (1975) p.857
- (133) F YAMAMOTO, S YAMAKAWA  
J. of Applied Polymer Science, Vol 25 (1980) p.2479
- (134) D BRIGGS, D M BREWIS, M B KONIECZKO  
J. of Materials Science, Vol 12 (1977) p.429

- (135) D W DWIGHT, W M RIGGS  
J. of Colloid and Interface Sci., Vol 47 (1974) p.650
- (136) A J KINLOCH  
"Adhesion - 6" Ed. K W Allen  
(Applied Science Publishers, London, 1982) p.95
- (137) N J HARRICK  
J. of Physical Chemistry, Vol 64 (1960) p.1110
- (138) J P LUONGO, H SCHONHORN  
J. of Polymer Science, Vol 6 (1968) p.1649
- (139) H A WILLIS, V J I ZICHY  
"Polymer Surfaces" Ed. D T Clark and W J Feast  
(Willey, London, 1978) p.287
- (140) R N WENZEL  
Industrial and Engineering Chemistry, Vol 28(8)  
(1936) p.988
- (141) K BRIGHT, B W MALPASS  
European Polymer Journal, Vol 4 (1968) p.431
- (142) K BRIGHT, B W MALPASS, D E PACKHAM  
British Polymer Journal, Vol 3, (1971) p.205
- (143) "Handbook of x-ray photoelectron spectroscopy"  
ED. C D Wagner, W M Riggs, L E Davies, J F Moulder  
(Perkin Elmer, 1979)
- (144) M P SEAH  
"Practical surface analysis by Auger and x-ray  
Photoelectron Spectroscopy" Ed. D Briggs and M P Seah  
(John Wiley and Sons, 1983) p.181
- (145) F M FOWKES  
Ind. Eng. Chemistry, Vol 56(12) (1964) p.40
- (146) D H KAEUBLE  
J. of Adhesion, Vol 2 (1970) p.66
- (147) D G RANCE  
"Surface analysis and pretreatment of plastics and  
metals" Ed. D M Brewis  
(Applied Science Publishers, London, 1982) p.121

- (148) J M SYKES, T P HOAR  
J. of Polymer Science, Vol 7, A-1 (1969) p.1385
- (149) L T DRZAL, M J RICH, M F KOENIG, P F LLOYD  
J. of Adhesion, Vol 16 (1983) p.133
- (150) A AHAGON, A N GENT, H J KIM, Y KUMAGAI  
Rubber Chemistry and Technology, Vol 48 (1975) p.896
- (151) F NIESIOLOWSKI, D W AUBREY  
J. of Adhesion, Vol 13 (1981) p.87
- (152) D W AUBREY, S GINOSATIS  
J. of Adhesion, Vol 12 (1981) p.189